Università degli Studi di Ferrara

DOTTORATO DI RICERCA IN
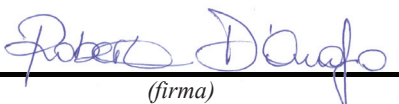### Scienze della Terra e del Mare

CICLO XXIX

COORDINATORE Ch.mo Prof. Massimo Coltorti

PLANKTIC FORAMINIFERAL RESPONSE TO THE EARLY EOCENE CLIMATIC PERTURBATIONS: THE POST-PETM HYPERTHERMALS AND THE EECO EVENT

Settore Scientifico Disciplinare GEO/01

Dottorando	**Tutore**
Roberta D'Onofrio	Ch.ma Prof.ssa Valeria Luciani
(firma)	*(firma)*

Co-Tutori

Ch.mo Prof. Gerald Dickens (Rice University, USA)

Ch.ma Prof.ssa Bridget Wade (University College of London, UK)

Anni 2014/2016

Abstract

The early Paleogene is one of the most climatically dynamic intervals of the Earth's history being characterized by both long- and short-term perturbations generally related to profound variations on the global carbon cycle and paleoceanographic conditions. The study of these perturbations is particularly intriguing since they represent natural experiments to test the resilience of different Earth's systems, included the biosphere, to the past extreme climate changes allowing the evaluation of the consequent reassessments.

The main goal of this research project was to investigate some extreme warming episodes characterizing the early Eocene climate at different time-scale mainly through the planktic foraminiferal record. Planktic foraminifera are among the most important marine calcifiers of recent and past oceans and major contributors of the carbonate pump which acts in buffering high atmospheric pCO$_2$. Moreover, they are widely employed in the study of past environments as they record the effects of major upper water-column perturbations both in the chemistry of their tests and changes within the assemblages. Environmental stress due to anthropogenic burning of fossil fuels and concomitant warming pose outstanding questions regarding environmental change and biotic responses. A more complete comprehension of planktic foraminiferal changes during past extreme warming episodes therefore presents a fascinating focal point for study. Nonetheless, the early Eocene climate have been recently investigated and characterized mainly in terms of temperature anomalies and oceanographic changes. The effects of the climatic and carbon cycle perturbations on biotic communities are much less constrained.

The first object of study was the early Eocene interval recording some short-lived events of intense global warming known as "hyperthermals". Although they have different magnitudes, hyperthermals share several key characteristics beyond evidence for excess warmth, most notably negative carbon isotope (δ^{13}C) excursions (CIEs) and evidence for dissolution of deep-sea carbonate. The most extreme and studied hyperthermal is the Paleocene/Eocene Thermal Maximum (PETM) at ~56 Ma. Specifically, this project is focused on three post-PETM hyperthermals that are less constrained especially regarding the impact on planktic foraminferal assemblages: the H1 or Eocene Thermal Maximum 2 (ETM2, ~54 Ma), the H2 and I1 events.

A second object of this research was the long-lasted Early Eocene Climatic Optimum (EECO). The EECO is a loosely defined interval of peak Cenozoic warmth (from approximately 53 to 49 Ma) when atmospheric pCO$_2$ was probably considerably high and mean global temperatures were the warmest of the last 90 Myr, likely exceeding those of present day by at least 10 °C. A series of short-term CIEs have been recently recognized in superposition to the EECO. Interestingly, minor attention has been dedicated to the EECO and the long-lasting impacts of this extraordinary global warmth, especially in terms of planktic foraminiferal response.

To pursue the research aims of this thesis, three early Eocene deep-sea successions were appropriately selected from different paleoceanographic settings such as the low-latitude central western Tethyan Terche section (northeastern Italy; Belluno Basin, Venetian Southern Alps), the western Atlantic Ocean Drilling Project (ODP) Site 1051 (Blake Nose, Leg 171 B), from the northern hemisphere, and the mid-latitudes eastern Atlantic ODP Site 1263 (Walvis Ridge, Leg 208) from the southern hemisphere. These case studies were approached with integrated micropaleontological analysis and multi-proxy methods (mainly oxygen and carbon stable-isotopes, dissolution proxies) in order to provide a more comprehensive and reliable interpretation of possible biotic and environmental disruptions.

Results from the high-resolution investigation of three post-PETM hyperthermals, the ETM2, H2 and I1 events at the Tethyan Terche section highlight that significant changes occurred in planktic foraminiferal and calcareous nannofossil assemblages across these events, although the recorded changes were transient and more intense during the ETM2. Each of these events coincides with

lithological anomalies consisting in significantly reduction in calcium carbonate content (marly units, MUs). The MUs are interpreted as mainly linked to increased terrigenous dilution, as dissolution proxies do not display significant variations. Modifications within calcareous plankton suggest increase in surface-water eutrophication with respect to the pre-event conditions, coupled with a weakening of the upper water-column thermal stratification. Higher nutrient discharge was related to intensified hydrological cycle as a consequence of the warmer climate. Interestingly, the observed perturbed conditions persisted during the early CIE recovery, implying slower recovery rates for the environment and biota than for the carbon cycle.

The analysis of the selected Atlantic sites encompassing the EECO reveals that major changes occurred in planktic foraminiferal assemblages across this long-lasted perturbation. The most prominent change is documented at the EECO beginning when the relative abundance of *Morozovella* permanently decreased up to two thirds, along with a progressive decrease in the number of species. Concomitantly, the genus *Acarinina* almost doubled its abundance and diversified within the EECO. Besides the north western Atlantic low-latitudes Site 1051 and south eastern mid-latitudes Site 1263, here analysed, this significant overturn between two important calcifiers of tropical-subtropical early Paleogene oceans was previously documented in other low-latitude locations from different paleoceanographic settings, such as the central western Tethyan Farra and Possagno sections, the Pacific Deep Sea Drilling Project (DSDP) Site 577 and the Contessa section for central Italy. The new high-resolution data from Site 1051, here provided, allow us to precisely locate such variation at the CIE known as J event, recently proposed as the EECO basal boundary, whereas it was delayed by ~165 kyr at Site 1263, the sole mid-latitude record from the southern hemisphere investigated to date. Being almost concomitant and geographically widespread, the *Morozovella* decline represents a global response to the paleoenvironmental disruptions induced by the EECO rather than by local factors, even though the triggering mechanisms for this striking change remain elusive. Possible causes to explain this permanent change are manifold and may include the sustained elevated temperature, prolonged high level of pCO$_2$ and the possibly related surface-waters acidification, loss of photo-symbionts (bleaching) or even interactions with other microplankton groups. A test on *Morozovella* species from Site 1051 was consequently performed to verify the bleaching hypothesis through analysis of the δ^{13}C signal in specimens from restricted size-fractions, through the established relationship between test size and δ^{13}C in fossil planktic foraminifera. Evidences of loss in photosymbionts relationship and test-size reduction were actually documented in a number of *Morozovella* species just above the J event. Nonetheless, the bleaching signal was transient and it involved the acarininids as well, that increased their abundance concomitantly, thus invalidating this hypothesis as the most probable mechanism to explain the *Morozovella* permanent drop at the EECO onset. Interestingly, some species of *Morozovella* never recover their maximum test-size, even after having restored the photo-symbiotic relationship. Decrease in planktic foraminiferal test-size can be related to crossing the ecological optimum threshold due to the occurrence of different types of environmental stressors, in addition to the bleaching.

The planktic foraminiferal response to the EECO at Site 1263 includes, beside the morozovellids decline, the virtual disappearance of the biserial chiloguembelinids, commonly considered as inhabiting the oxygen minimum zone, and a certain reduction in abundance of the thermocline-dweller subbotinids, both recorded at the initial EECO phase. These evidences are interpreted as a result of ecological niches contraction probably related to weakening of the upper water-column thermal stratification. The whole aforementioned signals emphasize the striking effect of the long-lasted EECO perturbation that superimposed and prevailed on the ephemeral changes linked to the early Eocene hyperthermals.

Transient changes in planktic foraminferal assemblages consist of marked increases in *Acarinina* abundance and drop in morozovellids and subbotinids mainly coinciding with the CIEs at all the investigated locations. The fluctuations in abundance of *Acarinina* and *Morozovella* are out of phase at

the examined sites as also observed in other locations during the early Eocene. These evidences, together with minor differences in the stable-isotope record, imply some dissimilarity in the ecological behaviour that induced competition within the mixed-layer habitat shared by the two genera.

An intriguing planktic foraminiferal morphological feature, the coiling direction, was also examined in the morozovellid population at both the Atlantic Site 1051 and Site 1263. The coiling direction of trochospiral planktic foraminifera is a widely investigated morphological feature in living species and in upper Quaternary sediment whereas this morphological trait remains scarcely documented in older marine sediments. The true causes of coiling direction changes remain however a stimulating problem. In recent assemblages these changes are mainly interpreted as reflecting ecological adaptation especially to temperature but several studies indicate that other factors might influence this feature (e.g., salinity, seasonal effects, water density, increased surface-water eutrophy, reproductive strategy). Most of the recent sinistral and dextral mortphotypes are actually genetically differentiated although criptic species clearly show adaptation to different water-masses having different ecological preferences. Therefore, planktic foraminiferal morphotypes with different coiling direction can be used for stratigraphic correlation and palaeoenvironmental interpretations even though they may represent criptic speciation. The analysis of this interesting morphological character from Site 1051 and Site 1263 demonstrates that morozovellids display a dominant dextral preference during the interval preceding the EECO at both the studied sites. However, all species show a first, prominent flip to sinistral coiling mode starting slightly above the J event. This switch from dextral to sinistral coiling became permanent for most of the *Morozovella* species slightly above the K/X event. Temporary but significant switches towards sinistral coiled morphotypes also occurred during several pre-EECO hyperthermals. This record sheds new light on the coiling direction preferences of early Paleogene planktic foraminifera. Previous interpretations favour genetic explanations for coiling flips rather than ecological responses. Our present data cannot validate or disprove the former idea, but should stimulate renewed thought on the latter idea.

The dataset here presented provide new insight on the impact of early Eocene climate on planktic foraminferal asssemblages. Results demonstrate that planktic foraminifera were extremely sensitive to the warm and dynamic climate context of the early Eocene and that their response was somewhat proportioned with both the time-extent and the magnitude of the early Eocene perturbations. Actually, the major and permanent changes resulted from the long-lasted EECO interval that prevailed on the ephemeral variations linked to the early Eocene hyperthermals.

Riassunto

Il Paleogene inferiore rappresenta uno degli intervalli climaticamente più dinamici della storia della Terra essendo stato caratterizzato da perturbazioni sia di breve sia di lungo periodo generalmente associate a profonde variazioni del ciclo del Carbonio e delle condizioni paleooceanografiche. Queste perturbazioni climatiche sono particolarmente interessanti in quanto rappresentano esperimenti naturali per testare la resilienza dei diversi sistemi del pianeta Terra, biosfera inclusa, alle variazioni climatiche estreme permettendo di valutare i conseguenti riassestamenti.

L'obiettivo primario di questo progetto di ricerca è stato quello di investigare alcuni episodi di riscaldamento estremo che hanno caratterizzato il clima dell'Eocene inferiore a differenti scale temporali principalmente attraverso l'analisi a foraminiferi planctonici. I foraminiferi planctonici sono tra i più importanti calcificatori degli oceani passati ed attuali e maggiori contributori della pompa dei carbonati che agisce nel mitigare gli elevati livelli di $p\text{CO}_2$ atmosferica. Inoltre, questi organismi sono ampiamente utilizzati nello studio delle condizioni ambientali del passato in quanto registrano gli effetti delle maggiori perturbazioni verificatesi nella porzione superiore della colonna d'acqua, sia nella chimica dei loro gusci sia tramite variazioni nelle associazioni.

Lo stress ambientale causato dalla combustione antropica delle risorse fossili e il concomitante riscaldamento globale pongono quesiti ancora irrisolti riguardo i cambiamenti ambientali e la possibile risposta biotica ad essi. Una più completa comprensione delle variazioni registrate dai foraminiferi planctonici durante gli episodi di riscaldamento estremo del passato rappresenta quindi un fondamentale punto di riferimento per gli studi futuri. Nonostante ciò, il clima dell'Eocene inferiore è stato, ad oggi, principalmente investigato e caratterizzato in termini di anomalie di temperatura e variazioni oceanografiche. Gli effetti delle perturbazioni climatiche e del ciclo del Carbonio sulle comunità biotiche rimangono, al contrario, ancora poco definiti.

Il primo oggetto di studio è stato un intervallo dell'Eocene inferiore contenente alcuni eventi d'intenso riscaldamento globale e breve durata noti come "ipertermali". Sebbene presentino magnitudo differenti, gli ipertermali condividono molteplici caratteristiche chiave, oltre alle evidenze di un eccessivo riscaldamento, in particolare escursioni negative degli isotopi del Carbonio (*Carbon Isotope Excursions*, CIEs) ed evidenze di dissoluzione dei carbonati di mare profondo. L'ipertermale più intenso e maggiormente studiato è il *Paleocene/Eocene Thermal Maximum* (PETM) verificatosi ~56 Ma fa. Nello specifico, questo progetto è incentrato su tre ipertermali post-PETM che sono stati meno caratterizzati del PETM, specialmente per quel che riguarda l'impatto sulle associazioni a foraminiferi planctonici: gli eventi H1 o *Eocene Thermal Maximum* 2 (ETM2, ~54 Ma), H2 e I1.

Un secondo oggetto di ricerca è stato l'evento di lunga durata noto come *Early Eocene Climatic Optimum* (EECO). L'EECO è un intervallo i cui limiti non sono ancora chiaramente definiti (si estende approssimativamente da 53 a 49 Ma) e coincide con il picco del trend di riscaldamento di lungo periodo del Cenozoico, quando i livelli di $p\text{CO}_2$ atmosferica erano notevolmente alti e le temperature medie globali erano le più calde degli ultimi 90 Ma. Una serie di rapide escursioni negative nella curva degli isotopi del Carbonio sono state recentemente riconosciute anche in sovrapposizione dell'EECO. È interessante notare che è stata dedicata solo un'attenzione marginale all'EECO e agli effetti a lungo termine prodotti da questo straordinario evento di riscaldamento globale, soprattutto per quel che riguarda la risposta dei foraminiferi planctonici.

Per perseguire gli obiettivi di ricerca proposti, sono state opportunamente selezionate tre successioni di mare profondo dell'Eocene inferiore da diversi contesti paleoceanografici, tra cui le sezioni del Terche dalla Tetide centro-occidentale (Bacino di Belluno, Italia nord-orientale, Alpi del Sud Venete) e del *Site* dell'*Ocean Drilling Project* (ODP) 1051 (Blake Nose, Leg 171 B) dall'Atlantico occidentale, entrambe site nella fascia delle basse latitudini dell'emisfero boreale, e la sezione del *Site* ODP 1263 (Walvis Ridge, Leg 208) dall'Atlantico sud-orientale, posta nella fascia delle medie latitudini dell'emisfero australe. Questi casi di studio sono stati affrontati integrando l'analisi micropaleontologica con altri *proxy* (principalmente isotopi stabili dell'ossigeno e del carbonio e indicatori di dissoluzione), al fine di fornire un'interpretazione quanto più completa ed attendibile delle perturbazioni biotiche ed ambientali.

I risultati delle indagini ad alta risoluzione dei tre ipertermali post-PETM, gli eventi ETM2, H2 e I1, presso la sezione tetidea del Terche hanno evidenziato rilevanti cambiamenti nelle associazioni a foraminiferi planctonici e nannofossili calcarei durante questi eventi, sebbene le variazioni registrate

siano state transitorie e più intense durante l'ETM2. Ognuno di questi eventi coincide con delle anomalie litologiche che sono l'espressione sedimentologica di una marcata riduzione nel contenuto in carbonato di calcio (unità marnose o *Marly Units*, MUs). Le MUs sono state interpretate come principalmente riconducibili ad un aumento della diluizione terrigena, in quanto gli indicatori di dissoluzione non mostrano variazioni significative. Le variazioni all'interno del plancton calcareo suggeriscono un aumento dell'eutrofizzazione delle acque superficiali, rispetto alle condizioni pre-evento, associato ad un indebolimento della stratificazione termica nella porzione superiore della colonna d'acqua. Il maggiore input di nutrienti è stato attribuito a un intensificazione del ciclo idrologico, risultato del forte riscaldamento climatico. È interessante notare che le condizioni di perturbazione osservate persistono anche durante la fase di recupero delle CIE, implicando dei tassi di recupero più lenti per l'ambiente ed il biota rispetto al ciclo del carbonio.

L'analisi dei *Site* atlantici selezionati e comprendenti l'intervallo dell'EECO ha rivelato che una serie di marcati cambiamenti si sono verificati nelle associazioni a foraminiferi planctonici in concomitanza di questa perturbazione di lunga durata. Il cambiamento più significativo è documentato all'inizio dell'EECO, quando le abbondanze relative di *Morozovella* diminuiscono in modo permanente di circa due terzi in parallelo ad una progressiva riduzione del numero di specie. Al contempo, il genere *Acarinina* quasi raddoppia la sua abbondanza e si diversifica all'interno dell'EECO. Oltre ai *Site* atlantici qui analizzati, il *Site* 1051 delle basse latitudini nell'atlantico nord-occidentale a il *Site* 1263 delle medie latitudini nell'atlantico sud-orientale, questo significativo turnover tra due importanti calcificatori degli oceani tropicali-subtropicali del Paleogene inferiore è stato precedentemente documentato in altre località delle basse latitudini poste in diversi contesti paleooceanografici, come ad esempio le sezioni della Tetide centro-occidentali di Farra e Possagno, il *Site Deep Sea Drilling Project* (DSDP) 577 (Shatsky Rise) nel Pacifico occidentale e la sezione Tetidea della Contessa nell'Italia centrale. I nuovi dati ad alta risoluzione qui forniti per il *Site* 1051 hanno permesso di posizionare con precisione tale variazione in corrispondenza della CIE nota come evento J, recentemente proposto come il limite basale dell'EECO, mentre risulta ritardata di ~165 mila anni al *Site* 1263, l'unico record dalle medie latitudini dell'emisfero australe indagato fino ad oggi. Essendo quasi concomitante e geograficamente diffuso, il declino del genere *Morozovella* sembra rappresentare dunque una risposta globale alle perturbazioni paleoambientali indotte dall'EECO piuttosto che una risposta a fattori locali, sebbene i meccanismi d'innesco di questo sorprendente cambiamento rimangano elusivi. Le possibili cause per spiegare questo cambiamento permanente sono molteplici e possono includere la temperatura elevata, i prolungati alti livelli di pCO$_2$ atmosferica e l'eventuale acidificazione delle acque superficiali, la perdita di foto-simbionti (*bleaching*) o anche interazioni con altri gruppi del microplancton. È stato conseguentemente eseguito un test su varie specie di *Morozovella* dal *Site* 1051 al fine di verificare l'ipotesi del *bleaching* attraverso l'analisi del segnale del δ^{13}C in esemplari provenienti da frazioni granulometriche ristrette, dato il ben definito rapporto esistente tra la dimensione dei gusci ed il δ^{13}C nei foraminiferi planctonici fossili portatori di simbionti. Evidenze di una certa riduzione nel rapporto con i foto-simbionti e nella dimensione dei gusci sono state effettivamente documentate in alcune specie di *Morozovella* poco sopra l'evento J. Tuttavia, il segnale di bleaching registrato nei morozovellidi è risultato transitorio ed ha interessato anche gli acarininidi la cui abbondanza, al contrario, aumenta durante l'EECO, invalidando così questa ipotesi come uno dei meccanismi più probabili per spiegare il calo permanente di *Morozovella* alla base dell'EECO. È interessante notare come alcune specie di *Morozovella* non recuperino la dimensione massima del guscio anche dopo il ripristino del rapporto foto-simbiotico. La diminuzione nelle dimensioni dei gusci dei foraminiferi planctonici può essere associata al superamento della soglia di optimum ecologico causata dal verificarsi di diversi tipi di stress ambientali oltre al bleaching.

La risposta dei foraminiferi planctonici all'EECO nel Site 1263 include, oltre al declino dei morozovellidi, la scomparsa virtuale del gruppo dei biseriali, i chiloguembelinidi, comunemente considerato adatto a proliferare nella zona del minimo di ossigeno, nonché una certa riduzione nell'abbondanza dei subbotinidi, che proliferano nella fascia del termoclino. Entrambe le variazioni sono state documentate nella fase iniziale dell'EECO. Queste testimonianze sono state interpretate come riconducibili ad una contrazione delle nicchie ecologiche probabilmente correlata all'indebolimento della stratificazione termica nella porzione superiore della colonna d'acqua. La totalità dei segnali sopra menzionati sottolineano che il sorprendente effetto della perturbazione di lunga durata indotta dall'EECO si è sovrapposto ed ha prevalso sui cambiamenti effimeri legati agli ipertermali dell'Eocene inferiore.

Le variazioni a carattere transitorio nelle associazioni e foraminiferi planctonici consistono generalmente in un marcato aumento nell'abbondanza di *Acarinina* e un parallelo calo di morozovellidi e subbotinidi e sono registrate principalmente in coincidenza delle CIE in tutti i luoghi indagati. Le fluttuazioni di abbondanza di *Acarinina* e *Morozovella* sono generalmente fuori fase nei *Site* esaminati così come osservato anche in altre località durante l'Eocene inferiore. Queste evidenze, insieme a piccole differenze nel record degli isotopi stabili di *Acarinina* e *Morozovella*, implicano una certa diversità nel comportamento ecologico che può aver indotto una certa competizione all'interno dell'habitat del *mixed-layer* condiviso dai due generi.

È stata inoltre esaminata un'interessante caratteristica morfologica dei foraminiferi planctonici, la direzione di avvolgimento, nella popolazione dei morozovellidi provenienti da entrambi i *Site* atlantici 1051 e 1263. La direzione di avvolgimento nei foraminiferi planctonici trocospirali è una caratteristica morfologica ampiamente investigata nelle specie viventi e nelle forme provenienti dai sedimenti del Quaternario superiore, sebbene questo carattere rimanga ancora scarsamente documentato nei sedimenti più antichi. Le vere cause che innescano variazioni nella direzione di avvolgimento rimangono, in ogni caso, un'incognita stimolante. Nelle associazioni attuali questi cambiamenti sono stati principalmente interpretati come un adattamento ecologico essenzialmente alla temperatura. Diversi studi indicano, tuttavia, che altri fattori possono influenzare questa caratteristica morfologica come, ad esempio, la salinità, effetti stagionali, la densità dell'acqua, incrementi nell'eutrofia delle acque superficiali, strategie riproduttive. Inoltre, la maggior parte dei morfotipi sinistrorsi e destrorsi degli oceani attuali sono, in realtà, geneticamente differenziati sebbene le specie criptiche mostrino chiaramente un adattamento a diverse masse d'acqua avendo delle differenti preferenze ecologiche. Pertanto, i morfotipi di foraminiferi planctonici con diversa direzione d'avvolgimento possono essere utilizzati sia per correlazioni biostratigrafiche sia per interpretazioni paleoambientali, pur rappresentando specie criptiche. L'analisi di questo interessante carattere morfologico nei *Site* 1051 e 1263 dimostra che i morozovellidi presentano, in entrambi i siti studiati, una preferenza dominante nell'avvolgimento destrorso durante l'intervallo che precede l'EECO. Tuttavia, ciascuna specie mostra una prima marcata, seppur transitoria, inversione nella modalita di avvolgimento sinistrorso a partire da un livello leggermente al di sopra dell'evento J. Questo passaggio da avvolgimento destrorso a sinistrorso diviene permanente per la maggior parte delle specie di *Morozovella* poco al di sopra dell'evento K/X. Delle inversioni temporanee ma significative verso morfotipi ad avvolgimento sinistrorso si sono verificate anche nel corso di diversi ipertermali pre-EECO. Questo record, per la prima volta correlato con le curve degli isotopi stabili del carbonio, pone dunque nuove prospettive sulle preferenze nelle direzioni di avvolgimento dei foraminiferi planctonici del Paleogene inferiore. Le interpretazioni dei precedenti lavori prediligono una spiegazione genetica per le inversioni nella direzione di avvolgimento piuttosto che una risposta ecologica. I nuovi dati qui ottenuti non possono convalidare o negare la prima ipotesi, ma stimolano una rinnovata considerazione della seconda.

In conclusione, la raccolta dei dati presentati in questa tesi fornisce nuove evidenze sull'impatto del clima dell'Eocene inferiore sulle associazioni a foraminiferi planctonici. Tali risultati dimostrano come i foraminiferi planctonici siano estremamente sensibili al dinamico contesto climatico di riscaldamento dell'Eocene inferiore e che la loro risposta sia stata in qualche modo proporzionata sia alla durata che all'intensità delle perturbazioni eoceniche inferiori. Infatti, i cambiamenti maggiori e con effetto permanente sono stati innescati dall'intervallo di lunga durata dell'EECO che ha prevalso sulle variazioni effimere legate agli ipertermali dell'Eocene inferiore.

Table of Contents

Chapter III

Major perturbations in the global carbon cycle and photosymbiont-bearing planktic foraminifera during the early Eocene   **67**

Chapter IV

Testing photosymbiont bleaching in planktic foraminifera at the start of the Early Eocene Climatic Optimum   **117**

Chapter V

Planktic foraminiferal response to early Eocene carbon cycle perturbations in the
Southeast Atlantic Ocean (ODP Site 1263)

Chapter VI

Change from dominant dextral to sinistral coiling in planktic foraminifera
Morozovella during the Early Eocene Climatic Optimum

A Gloria

CHAPTER I

General Introduction:

Reserch context and aims

---

1. General Introduction

1.1. Early Paleogene Climate and Carbon Cycle

The early Paleogene is one of the most intriguing intervals of the Earth's history on a climatic perspective for two main reasons. The first reason is that the early Paleogene climate was extremely dynamic and complex in terms of long-term changes and short-term extreme warming episodes that were both related to profound variations of the global carbon cycles and paleoceanographic conditions. The second reason is connected to the fact that the early Paleogene warming events represent natural experiments to test how the different component of Earth's systems, included the biosphere, reacted to extreme climate changes and consequent reassessments.

A long-term warming started in the Late Cretaceous and reached its maximum in coincidence of the interval known as Early Eocene Climatic Optimum (EECO, Zachos et al., 2001, 2008) (Fig. 1). During the EECO, atmospheric pCO$_2$ was probably considerably high and mean global temperatures were the warmest of the last 90 Myr (Zachos et al., 2001; Hyland and Sheldon, 2013), likely exceeding those of present day by at least 10 °C (Zachos et al., 2008; Bijl et al., 2009; Huber and Caballero, 2011; Hollis et al., 2012; Pross et al., 2012; Inglis et al., 2015). The isotope record based on benthic foraminifera documents that following the EECO deep sea temperatures became progressively cooler (e.g. Zachos et al., 2001). This cooling trend led to the onset of an icehouse regime with the emplacement of permanent ice-sheets in Antarctica at Eocene-Oligocene transition, 34 Ma (Hambrey et al., 1991; Zachos et al., 1992) (Fig. 1).

Superimposed to the long-term trend, several transitory events of intense global warming have been identified and associated with negative shifts in stable carbon isotopes (e.g. Cramer et al., 2003; Lourens et al., 2005; Röhl et al., 2005; Thomas et al., 2006; Nicolo et al., 2007; Agnini et al., 2009; Coccioni et al., 2012; Lauretano et al., 2015, 2016; Westerhold et al., 2015) (Fig. 1). These events were firstly defined as "hyperthermals" by Thomas et al. (2000) and are currently known to be paced by orbital oscillations, in particular by short (100 kyr) and long (405 kyr) eccentricity cycle, with the exception of the Paleocene/Eocene Thermal maximum (PEM), the most extreme and extensively studied hyperthermal occurred at ~56 Ma (e.g., Kennett and Stott, 1991; Cramer et al., 2003; Zachos et al., 1993; Lourens et al., 2005; Westerhold et al., 2007, 2008, 2015; Galeotti et al., 2010; Zachos et al., 2010; McInerney and Wing, 2011; Littler et al., 2014; Lauretano et al., 2015; 2016).

Considerable scientific interest has been focused on understanding the early Paleogene hyperthermals, especially the most prominent PETM. This is because several of the hyperthermals were clearly associated with massive input of carbon to the ocean and atmosphere, as well as profound turnovers in various biotic ecosystems (e.g. Kelly et al., 1996, 1998; Thomas, 1998; Crouch et al., 2001; Gingerich 2001, 2003; Sluijs et al., 2006; Raffi and De Bernardi, 2008; Scheibner and Speijer, 2008; Self-Trail et al., 2012; Yamaguchi and Norris, 2012; Clyde et al., 2013; Agnini et al., 2014). Indeed, for these reasons, the PETM is often suggested as the best past analogue for current and future climate change (e.g., Pagani et al., 2006; O'Connor et al., 2010; McInerny and Wing, 2011; Zeebe and Zachos, 2013). The magnitude of the PETM carbon isotope excursion (CIE>–3‰) in marine carbonates, the duration (~170–230 kyr) and the intensity (5–8°C) of global warming (e.g., McInerney and Wing, 2011) are unmatched among the other hyperthermals. This suggests indeed that an extraordinary amount of ^{13}C-depleted carbon was rapidly injected into the ocean-atmosphere system at the PETM time causing significant variations in oceanic and atmospheric circulation. However, the source of this carbon input and the mechanisms activating such emission are still matter of debate (e.g., Pagani et al., 2006; Sluijs et al., 2007; Zeebe et al., 2009; Dickens, 2011; Lunt et al., 2011; Sexton et al., 2011; De Conto et al., 2012; Kirtland-Turner et al., 2014). In deep-sea sediments, major hyperthermals are generally marked by distinct clay layers associated with pronounced peaks in magnetic susceptibility (e.g., Lourens et al., 2005; Zachos et al., 2005, Coccioni et al., 2012). These clay intervals have been mainly attributed to carbonate dissolution and interpreted as the results of deep-water acidification relate to high concentration in atmospheric CO_2 that caused significant shoaling of the lysocline and carbonate compensation depth (CCD) (e.g. Zachos et al., 2005; Stap et al., 2009). Acceleration of the hydrological cycle and weathering are as well documented during a number of hyperthermals (Bowen et al., 2004; Giusberti et al., 2007; Pagani et al., 2006; Zachos et al., 2006; Agnini et al., 2009; Slotnick et al 2012). At least two other Eocene warming events have been recognized as proper hyperthermals such as the Eocene Thermal Maximum 2 (ETM2, or H1) occurred at ~54.1Ma (Fig. 1) (δ^{13}C shift ~1‰ in marine carbonates, evidence of 3.5 °C in surface water warming, e.g., Cramer et al., 2003; Lourens et al., 2005; Nicolo et al., 2007; Sluijs et al., 2009; Stap et al., 2009, 2010b, Slotnick et al., 2012; D'haenens et al., 2012; Lauretano et al., 2015) and the K/X or ETM3 event occurred at ~52.8 Ma (δ^{13}C shift ~1‰ in marine carbonates, evidence of ~4 °C warming in the tropical Atlantic sea-floor, e.g., Cramer et al., 2003; Röhl et al., 2005; Sexton et al., 2006; Thomas et al., 2006; Agnini et al., 2009; Coccioni etal., 2012). Several others minor CIEs (~0.5‰) punctuated the

long-term warming culminated at the EECO and are believed to occur later in the middle Eocene (e.g., Cramer et al., 2003; Sexton et al., 2011; Coccioni et al., 2012; Kirtland-Turner et al., 2014; Luciani et al., 2016).

Less attention has been however dedicated to the EECO and the long-lasting impacts of extraordinary global warmth, especially in terms of biotic response. In fact, even a formal definition of EECO, first widely introduced by Zachos et al. (2001), remains problematic. Recent work (Slotnick et al., 2015; Lauretano et al., 2015; Luciani et al., 2016) has tried to resolve the terminology and stratigraphic issues by defining the EECO as the interval comprised between a significant carbon cycle perturbation known as the "J event" (Cramer et al., 2003) and the appearance of *Discoaster sublodoensis*, a well-calibrated and easily recognizable calcareous nannofossil biohorizon. The EECO thus spans from approximately 53 to 49 Ma, and its beginning occurred near the boundary of polarity chrons C24n.2r and C24n.3n. Significant plant and mammal turnovers occurred indeed on land during the EECO (Wing et al., 1991; Zonneveld et al., 2000; Wilf et al., 2003; Falkowski et al., 2005; Woodburne et al., 2009; Figueirido et al., 2012). In the marine realm, evolutionary turnover happened as well, in particular the origin of modern calcareous nannofossil community structure (Agnini et al., 2006, 2014; Schneider et al., 2011; Shamrock et al., 2012) and possibly of diatoms (Sims et al., 2006; Oreshkina, 2012). These observations, both from continents and the oceans, support a hypothesis that long-term climate change during the EECO may have forced biotic evolution (Ezard et al., 2011). Nevertheless, detailed records of planktic foraminiferal assemblages across this interval remain scarce.

The Paleogene climate variability has attracted in the last decades great scientific attention, as aforementioned, in terms of temperature anomalies and geochemical changes characterization, however the effects of the climatic perturbations on biotic communities still remain largely unexplored.

1.2 Modern Climate and Insights from the Fossil Record

There are several points of similarities between the early Eocene warming episodes and the direction in which is forced to evolve the modern climate. Starting from the industrial revolution our planet is indeed experiencing a progressive increase into the atmosphere concentration of greenhouse gases. Such emissions, mainly consisting of carbon dioxide (CO_2) and methane (CH_4), are related to the anthropogenic burning of fossil-fuels and, at lesser extent, to the cement manufacturing which both drastically are rising in particular
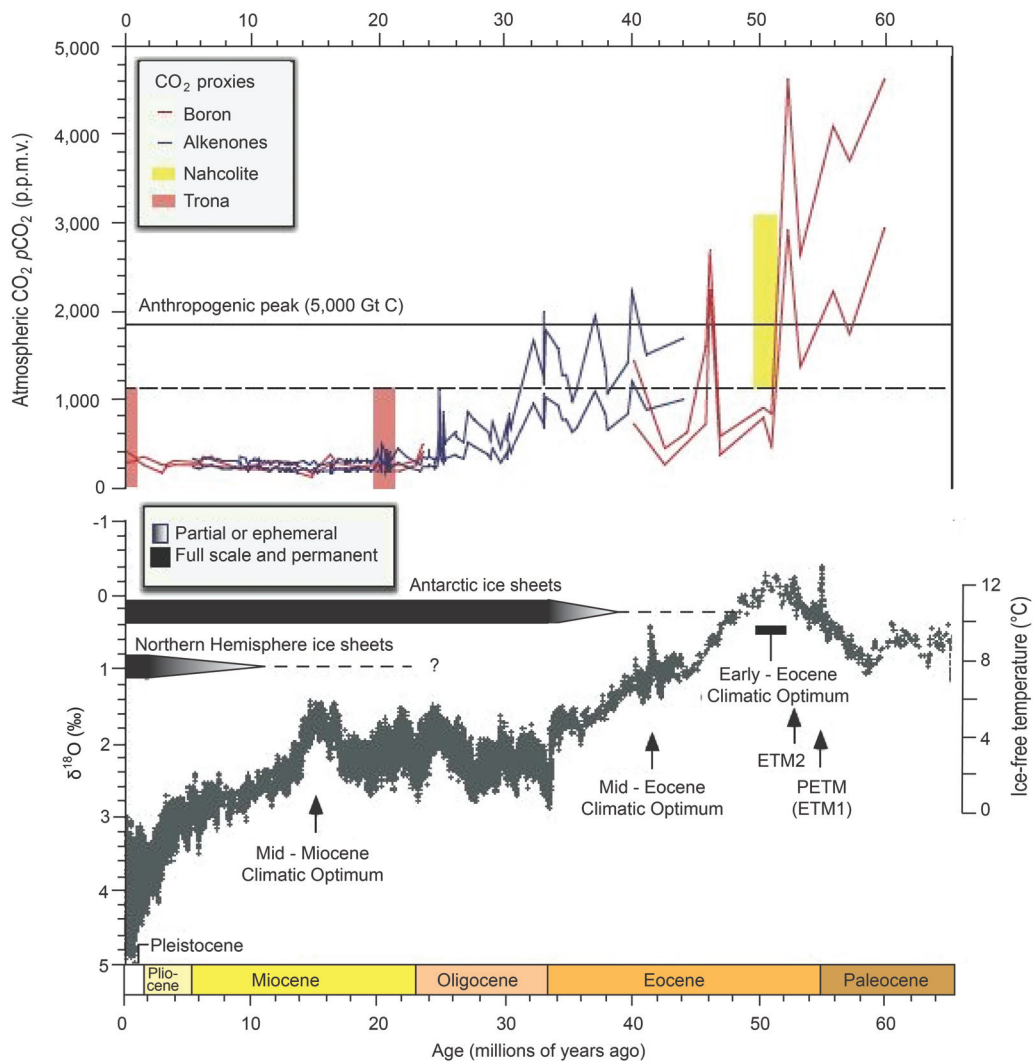
Figure 1. Image from Zachos et al. (2008) illustrating the atmospheric CO_2 levels and the global climate history across the last 65 Ma. Upper graph shows a compilation of pCO_2 reconstructions from different proxies. The horizontal dashed line represents the maximum pCO_2 for the Neogene (Miocene to present) and the minimum pCO_2 for the early Eocene (1,125 p.p.m.v.). Lower graph shows the stacked benthic foraminiferal $\delta^{18}O$ (‰, VPDB) from Deep Sea Drilling Project and Ocean Drilling Program sites. Note the multi-million year-long Early Eocene Climatic Optimum, the more transient Mid-Eocene Climatic Optimum, and the very short-lived early Eocene hyperthermals such as the PETM (also known as Eocene Thermal Maximum 1, ETM1) and Eocene Thermal Maximum 2 (ETM2; also known as ELMO).

during the last decades (e.g., Pepper et al., 1992; Pachauri et al., 2014, and reference therein). The most recent report referred to the CO_2 level in the atmosphere from the Mauna Loa Observatory (Hawaii, USA) is dated to the October 5th 2016 and is quite alarming since during the last years CO_2 concentrations have repetitively exceeded the 400 parts per million (ppm) and are expected to grow in the next future with a rate of 2.11 ppm per year. The primary effect of a rapid rising in atmosphere CO_2 levels is a global increase in Earth's average surface temperature (e.g., Solomon et al., 2007; Pagani et al., 2010; Stoker et al., 2013; Pachauri et al., 2014). A second impact is the ocean acidification that can irreversibly

affect the marine calcifier organisms (Raven et al., 2005; Field et al., 2011; Gattuso and Hansson, 2011). Global temperatures of the past decade have not yet exceeded the peak interglacial values but are warmer than during the ~75% of the Holocene (Solomon et al., 2007; Stoker et al., 2013). Projections for 2100 provided by the United States Intergovernmental Panel on Climate Change model (Solomon et al., 2007; Stoker et al., 2013) underline that Earth's surface temperature are expected to rise under all the possible greenhouse-gas emission scenario thus exceeding the Holocene temperatures (Marcott et al., 2013). Without mitigation of the present-day greenhouse gases emission, the atmospheric CO_2 concentration could exceed 1000 ppm at the end of the 21st century. Along with these dramatic forecasts it is very likely that heat waves will occur more often and last longer, that extreme precipitation events will become more intense and frequent in many regions, that the ocean will continue to warm and acidify, and global mean sea level to rise (Stoker et al., 2013; Pachauri et al., 2014). The time required to restore the climatic and geochemical pre-emission conditions are estimated to be in the order of 10^4-10^5 years (Archer et al., 2009) whereas biota might need millions of years to recover (Alroy, 2008). However, due to the potential effect of positive feedback mechanisms, these responses can be nonlinear thus timing and magnitude of climatic effects can be puzzling (e.g., Zachos et al., 2008).

In light of these next-future developments, the scientific community is increasingly addressed to investigate possible past analogues episodes of extreme warming linked to massive emissions of CO_2 into the ocean-atmosphere system (e.g., Pagani et al., 2006; O'connor et al., 2010; McInerny and Wing, 2011; Zeebe and Zachos, 2013). On this perspective, the early Eocene sediments offers an exceptional natural laboratory to study time intervals in which pCO_2 and temperatures were rapidly changing and probably becoming even much higher than today (e.g., Zachos et al., 2008). In the last decades, the study of sedimentary successions encompassing the early Eocene and the so-called "hyperthermals", greatly improved our knowledge about the climate dynamics of the greenhouse world of the early Paleogene.

My research project was developed following this line of researches and aimed to investigating early Eocene climatic perturbations at different time-scales such as the short-term post-PETM hyperthermals and the relatively long-term EECO interval. Specifically, this Ph.D. thesis is focused on the study of planktic foraminifera that represent an excellent group of organisms in which to examine links between past climate and evolution as they are abundant in many marine sediment records (e.g., Corfield, 1987; Kelly et al., 1996, 1998; Quillévéré and Norris, 2003, Schmidt et al., 2004; Ezard et al., 2011; Fraass et al., 2015;

Luciani et al., 2016). Furthermore, they are widely employed in the study of environments as they record effects of the major perturbations both in the chemistry of their tests and in changes within the assemblages. Modern planktic foraminifera are responsible for at least a quarter of global carbonate production and greatly contribute to the so-called 'carbonate pump' e.g., the biotic calcium carbonate production and transport to the deep ocean acting as a buffer of huge pCO$_2$ (e.g., Berner and Raiswell, 1983; Sigman et al., 2010). The response of the marine carbon cycle to changes in atmospheric CO$_2$ concentrations will be therefore governed, at least to some extent, by the response of calcifying organisms to global change. Understanding the effects of C-cycle perturbation on early Eocene planktic foraminifera is crucial to better evaluate the possible resilience of the recent planktic foraminifera to the ongoing climatic and oceanographic scenario.

One of the major issues emerging from the studies of early Paleogene climate is that paleoclimatic perturbations have been so far essentially characterised in terms of geochemical, sedimentological and stable-isotope variations whereas their impact on long and short-term repercussion on biota remain largely unconstrained. The final aim of my Ph.D. project is to gain a deeper understanding on which degree the selected global carbon cycle perturbations and related climate changes affected the Eocene planktic foraminifera and to reconstruct the impacts on paleoenvironmental and paleoceanographic modifications.

The selected case studies were approached by integrating diverse quantitative micropaleontological analyses and geochemical proxies. The latter include mainly the carbon and oxygen stable-isotope characterization of the intervals analyzed. Proxies to evaluate deep-water carbonate dissolution and planktic foraminiferal productivity were also examined. Specifically, in the first case-study, the response to planktic foraminifera to three post-PETM hyperthermals from a Tethyan succession (Terche section, Fig. 2) is integrated with the study of calcareous nannoplankton, bulk-stable isotopes and magnetostratigraphy with the purpose to better evaluate changes in surface-water environments. Dissolution proxies helped to evaluating possible taphonomic bias from the studied record.

In the second case, repercussions on planktic foraminifiera associated with the EECO are investigated on two Atlantic Ocean Drilling Project (ODP) Sites, Site 1051 and Site 1263 (Fig. 2). Data on planktic foraminifera include, besides quantitative information on population changes, also modifications in selected morphological characters such as test-size and morozovellids coiling direction. These records are coupled with geochemical analyses both on bulk sediments and on planktic foraminiferal tests in order to enclose the faunal results within a paleoceanographic context and provide reconstructions as detailed as possible.

2. Materials

This research project has been focused on three early Eocene hemipelagic and pelagic sediments appropriately selected from low and temperate latitude locations (1) the central-western Tethyan Terche section (Belluno, northeastern Italy), (2) the northwtesern Atlantic succession of the ODP Site 1051 (Blake Nose, Leg 171 B) and (3) the southeastern Atlantic ODP Site 1263 (Walvis Ridge, Leg 108) (Fig. 2).

The Terche section is located into the Valbelluna area from Venetian region of northeastern Italy. This region has been extensively studied in the past decades (e.g. Giusberti et al., 2007; Luciani et al., 2007, 2010; Agnini et al., 2009, 2014; Boscolo Galazzo et al., 2013) since it is characterized by extremely well exposed Late Cretaceous-early Paleogene successions with high sedimentation rates and good recovery of different microfossil record (e.g. calcareous nannofossils, planktic and benthic foraminifera). The Terche section was deposited on a marginal-marine basin, the Belluno Basin, in the central-western Tethys. The Belluno Basin is a Mesozoic-Cenozoic paleogeographic unit of the Southern Alps (e.g., Bosellini, 1989). The interest on the Terche section is related to the occurrence of three expanded marly units that interrupt the predominantly carbonate sedimentation. These lithological anomalies represent the sedimentary expression of early Eocene hyperthermals, the ETM2 (or H1), the H2 and I1 (e.g. Cramer et al., 2003; Lourens et al., 2005). The Terche section has therefore offered the opportunity to study the planktic foraminferal response to these three early Eocene hyperthermals, not yet explored in this critical Tethyan area.

The ODP Site 1051 was cored in the northwestern Atlantic on the Blake Nose, a gentle ramp extending from 1000 to 2700 m water depth east of Florida (Norris et al., 1998). Many features make this succession an appropriate sub-tropical site for this study. The Site 1051 is located at 30° 03.2' N, 76° 21.5' W and was positioned slightly to the south during the early Eocene (Ogg and Bardot, 2001; Van Hinsbergen et al., 2015). The interval here studied (hole 1051 A) is from 452.24 to 353.10 mbsf, and presents high sedimentation rate and good sediment recovery except for the interval between 382 and 390 mbsf, which contains significant chert and hiatus (Shipboard Scientific Party, 1998). Previous studies provide the calcareous plankton biostratigraphy (Norris et al., 1998; Mita, 2001; Luciani and Giusberti, 2014) and a revised designation to the polarity chrons (Luciani et al., 2016) thus ensuring that this site is a very good location for examining foraminiferal assemblages through the onset of the EECO. The depth during the late Paleocene and middle Eocene has been estimated as above the CCD, precisely lower bathyal (1000–2000 m) through benthic foraminiferal
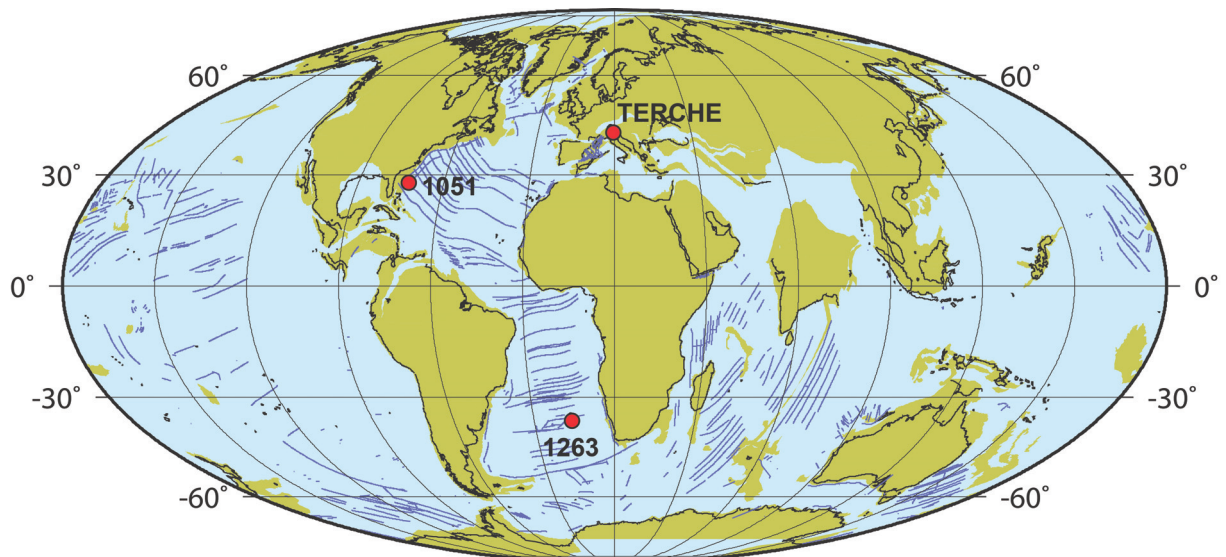
Figure 2. Earth at ~50 Ma showing the approximate location of the sites focus of this Thesis. Base map is from http://www.odsn/de/services/paleomap.html with paleolatitudes modified for Sites 1051 and 1263 according to www.paleolatitude.org model version 1.2 (Van Hinsbergen et al., 2015). Terche paleolatitude is based on the http://www.odsn.de/odsn/services/paleomap/adv_map.html model since it is not yet available at www.paleolatitude.org.

assemblages (Norris et al., 1998) or 2200 m at ca 50 Ma through subsidence and sedimentation rate calculations to Bohaty et al. (2009).

The ODP Site 1263 is located near the crest of the Walvis Ridge flank, in the south-eastern Atlantic (28°32 S, 2°47 E). The present water depth of 2717 m is significantly higher than the estimation for the early Eocene of ~1500 m (Zachos et al. 2004). Latitude was as well considerably different in the early Eocene, being positioned southward of ~10° (Van Hinsbergen et al., 2015). This implies that during the early Eocene the Site 1263 sediments were deposited in a fully-bathyal depositional environment of a temperate open-ocean paleoceanographic setting of the southern hemisphere. Site 1263 has a good sedimentary recovery yielding a complete early Eocene sequence that mainly consists of nannofossil ooze, and chalk. The early Eocene at Walvis Ridge was largely studied during the last years with efforts mainly devoted to collect geochemical, isotopic and cyclostratigraphic data (e.g. Lourens et al., 2005; Westerhold et al., 2007, Stap et al. 2009, 2010a, 2010b; Lauretano et al., 2016). Nonetheless, biotic record at this Site is restricted to the hyperthermals ETM2, H2, I1 and I2 (e.g. Dedert et al., 2012, 2014; Gibbs et al., 2012; D'Haenens et al., 2014). The purpose to generate a continuous planktic foraminiferal dataset across the EECO for the Site 1263 is therefore particularly relevant.

As abovementioned all the selected successions have a record complete enough to investigate the early Eocene climatic perturbations. These localities provide therefore an ideal combination for studying and correlate the post-PETM hyperthermals and EECO repercussions on the surface marine ecosystem from different paleooceanographic settings.

3. Thesis Outline

An integrated approach was used in **Chapter II** by adopting multiple biotic and abiotic proxies to characterize the Terche section. The aim is to document the environmental impact and biotic repercussion of three successive C-cycle perturbations such as the ETM2, the H2 and the I1 events in the crucial area of central-western Tethys. Specifically, this study represents the first attempt to integrate the response of two different plankton groups, the planktic foraminifera and the calcareous nannofossils, across the investigated events, coupled with stable isotope data and several dissolution proxies. This approach allows a more comprehensive and reliable interpretation of the biotic and environmental disruption occurred in the upper water column in coincidence with the aforementioned C-cycle perturbations. The solid bio-magneto-stratigraphic framework permits to correlate the Terche abiotic record to those from the Atlantic ODP Site 1258 (Demerara Rise) and 1263 (Walvis Ridge) thus providing a comparable age model for the Terche section. In light of the pervasive dissolution of deep-sea carbonate sediments globally detected during the early Paleogene carbon isotope excursion events, a consistent part of this study was devoted to analyse the most useful proxies to evaluating possible carbonate dissolution. Dissolution proxies, derived from both foraminifera and calcareous nannofossils, allowed us to evaluate that biotic results were mostly unbiased by taphonomic effects. The calcareous nannofossil dataset was provided by Eliana Fornaciari and Sonia Telch from the Padua University (Italy).

My personal contribute to the **Chapter III** is referred to the quantitative planktic foraminiferal analysis presented for the early to earlier middle Eocene sediments from the ODP Site 1051. In this chapter the comparison between planktic foraminiferal record and C-cycle variations is shown across three early Eocene successions encompassing the EECO, the crucial interval when Earth surface temperatures reached their Cenozoic maximum. Besides the Atlantic ODP Site 1051, **Chapter III** presents data from the central-western Tethyan Possagno section (northeastern Italy) and from the Pacific Deep Sea Drilling Project (DSDP) Site 577, Shatsky Rise, north-western Pacific. The correlation between planktic foraminiferal and isotopic record generated for these sequences located in different paleo-oceanographic settings of low-latitudes, allows the identification of a major variations in planktic

foraminifera assemblages. This variation consists in a drastic and permanent decline in abundances of the *Morozovella* genus (Luciani et al., 2016), one of most important calcifiers of the early Paleogene tropical and sub-tropical oceans. The marked *Morozovella* decline occurred close to the CIE referred to as J event and related to one of the "hyperthermals" characterizing the early Paleogene climate (e.g., Cramer et al., 2003). For the Possagno section the quantitative analyses on planktic foraminiferal assemblages, fragmentation index (*F index*) and weight-percent coarse fraction (*WPCF*) were performed by Valeria Luciani. Planktic foraminiferal data from the DSDP Site 577 are from Lu (1995) and Lu and Keller (1995).

Chapter IV was dedicated to explore one of the possible reasons for the outstanding symbiont-bearing *Morozovella* decline, occurred at low-latitudes during one of the most intriguing climatic interval of the early Paleogene, the EECO. Actually, even whether in Chapter III the low-latidude widespread drop in abundance of the early Eocene morozovellids is documented, no possible causes to explain such variation has been demonstrated. Key records were generated across the EECO at Site 1051 in the northwest Atlantic. This is one of the sites where the morozovellid decline has been documented (Luciani et al., 2016), although not in fine detail. The timing of *Morozovella* decline was therefore refined and then was explored a possible reason: the loss of photosymbionts, known as 'bleaching' from the loss of the coloured algal symbionts. The symbiotic relationship with photosynthetic algae is a key strategy adopted by many modern planktic forminiferal species as it is advantageous in foraminiferal longevity and calcification processes, allowing the host to succeed in low-nutrient environments (e.g., Be´ 1982; Be´ et al. 1982; Hemleben et al., 1989). We can therefore expect detrimental consequences for photosymbiotic-bearing foraminifera populations if environmental changes affect algal endosymbiosis. Firstly, quantitative analyses of the *Morozovella* species was generated across the EECO in order to evaluate whether the permanent drop in abundance involved the whole *Morozovella* population or was restricted to selected species. Since the bleaching may affect the rate of planktic foraminiferal growth and test calcification, we can expect test-size reduction whether it occurred (Bé et al., 1982; Caron et al., 1982; Edgar et al., 2012). We provide therefore also a quantitative record of test-size variations among the larger (≥300 μm) *Morozovella* species.

The bleaching test was performed through the analyses of the established relationship that links test-size variations with $\delta^{13}C$ value in fossil planktic foraminifera, i.e. increase in test-size coincides to progressively ^{13}C enriched tests (e.g. Berger et al., 1978; Pearson et al., 1993; Spero and Lea, 1993; D'Hondt et al., 1994; Norris, 1996). These analyses were carried

out running monospecific specimens of most of the *Morozovella* species recorded at Site 1051, mono-generic specimens of the mixed-layer dweller *Acarinina* genus and of the thermocline-dwellers *Subbotina*. All specimens were selected and picked into restricted size-fraction. A higher resolution record with respect to Luciani et al. (2016, Chapter III) of planktic foraminiferal relative abundances of the main genera from Site 1051 is as well presented in Chapter IV. The detailed micropaleontological record is presented here alongside to a bulk carbon and oxygen isotopic framework, previously absent for the EECO interval at Site 1051. This new data integrate the curve from Cramer et al. (2003) that ends at the J event. We are aware that significant warming represents one of the most important stressors that may induce inhibition of the photosymbiont activity (e.g., Douglas et al., 2003). We tried therefore to generate a high-resolution record on paleotemperatures across the J event through two geochemical tools widely employed in paleoceanographic and paleoclimatic reconstructions, such as the TEX_{86} and the $\delta^{18}O$ proxies.

The **Chapter V** presents and discusses the results of a study conducted across the EECO interval on planktic foraminiferal assemblages at the southeastern Atlantic ODP Site 1263, Walvis Ridge. A detailed characterization in terms of ciclostratigraphy and stable isotopes has been recently provided for this Site (Lauretano et al., 2015; 2016). These works provide a robust temporal framework for long- and short-term variability in the C-cycle during the early Eocene (~ 49– 54 Ma). The astronomically tuned age model for the early Eocene further confirms the link between large-scale carbon release and climate response to orbital forcing, in particular to short- and long-eccentricity cycles (Lauretano et al., 2015; 2016). Nonetheless, we provide our bulk carbon and oxygen stable isotope curves. As for the Site 1051, planktic foraminifera have been studied through both qualitatively (biostratigraphic investigation) and quantitatively (main changes in planktic formainferal population). Dissolution (*F index*) and paleoproductivity proxies (*CF)* foraminiferal-based are as well provided.

An intriguing planktic foraminiferal morphological feature, the coiling direction of early Paleogene morozovellids, was examined in **Chapter VI**. This feature is widely investigated in the modern and Pleistocene planktic foraminiferal polulations but still insufficiently explored in the fossil record. This aspect has great potential applications for stratigraphic correlation and paleoclimatic-paleoceanographic studies. The interest on possible changes in *Morozovella* coiling direction is within the goal to examine possible modifications underwent within this important group of planktic foraminifera that suffered a profound crisis during the EECO. Of particular interest is the fact that switches in planktic foraminiferal coiling direction can be largely influenced by changes in water–masses properties (e.g. Morard et al., 2016 and

references therein). Coiling direction data were collected for each *Morozovella* species across the interval spanning the EECO at Site 1051 and for the *Morozovella* genus at Site 1263. Results are interpreted in the context of the paleoceanographic and paleoclimatic background discussed in Chapter III and IV.

References

Agnini, C., G. Muttoni, D. V. Kent, and D. Rio (2006), Eocene biostratigraphy and magnetic stratigraphy from Possagno, Italy: The calcareous nannofossil response to climate variability, Earth Planet. Sci. Lett., 241, 815–830, doi:10.1016/j.epsl.2005.11.005.

Agnini, C., J. Backman, H. Brinkhuis, E. Fornaciari, L. Giusberti, V. Luciani, D. Rio, and A. Sluijs (2009), An early Eocene carbon cycle perturbation at ~52.5 Ma in the Southern Alps: Chronology and biotic response, Paleoceanography, 24, PA2209, doi:10.1029/2008PA001649.

Agnini, C., E. Fornaciari, I. Raffi, R. Catanzariti, H. Pälike, J. Backman, and D. Rio (2014), Biozonation and biochronology of Paleogene calcareous nannofossils from low and middle latitudes, Newslett. Stratigr., 47(2), 131–181, doi:10.1127/0078-0421/2014/0042.

Alroy, J., (2008), Dynamics of origination and extinction in the marine fossil record, Proc. Natl. Acad. Sci., USA, 105, 11.536–11.542, doi:10.1073/pnas.0802597105).

Archer, D., M. Eby, V. Brovkin, A. Ridgwell, L. Cao, U. Mikolajewicz, K. Caldeira, K. Matsumoto, G. Munhoven, A. Montenegro, and K. Tokos (2009), Atmospheric lifetime of fossil fuel carbon dioxide, Annu. Rev. Earth Planet. Sci., 37, 117–134, doi:10.1146/annurev.earth.031208.100206.

Bé, A.W. H. (1982), Biology of planktonic foraminifera, in: Foraminifera: notes for a short course, Broadhead T., Stud. Geol., 6, Univ. Knoxville, Tenn., 51–92.

Bé, A.W. H., Spero, H. J., and O. R. Anderson (1982), Effects of symbiont elimination and reinfection on the life processes of the planktonic foraminifer *Globigerinoides sacculifer*, Mar. Biol., 70, 73–86.

Berger, W. H., J. S. Killingley, and E. Vincent (1978), Sable isotopes in deep-sea carbonates-box core erdc-92, west equatorial pacific, Oceanologica Acta, 1(2), 203-216.

Berner, R. A., and R. Raiswell (1983), Burial of organic carbon and pyrite sulfur in sediments over Phanerozoic time: a new theory, Geochimica et Cosmochimica Acta, 47(5), 855-862.

Bijl, P. K., S. Schouten, A. Sluijs, G.-J. Reichart, J. C. Zachos, and H. Brinkhuis (2009), Early Paleogene temperature evolution of the southwest Pacific Ocean, Nature, 461, 776–779, doi:10.1038/nature08399.

Bohaty, S. M., J. C. Zachos, F. Florindo, and M. L. Delaney (2009), Coupled greenhouse warming and deep-sea acidification in the middle Eocene, Paleoceanography, v. 24 (2), doi:10/1029/2008PA001676.

Bosellini, A. (1989), Dynamics of Tethyan carbonate platform, in Controls on Carbonate Platform and Basin Platform, Soc. Sediment. Geol. (SEPM) Spec. Publ., edited by P. D. Crevello et al., 44, 3–13, Univ. of California, Berkeley.

Boscolo Galazzo, F., L. Giusberti, V. Luciani, and E. Thomas (2013), Paleoenvironmental changes during the Middle Eocene Climatic Optimum (MECO) and its aftermath: The benthic foraminiferal record from the Alano section (NE Italy), Palaeogeography, Palaeoclimatology, Palaeoecology, 378, 22–35.

Bowen, G. J., D. J. Beerling, P. L. Koch, J. C. Zachos, and T. Quattlebaum (2004), A humid climate state during the Palaeocene/Eocene thermal maximum, Nature, 432(7016), 495–499.

Caron, D. A., A. W. H. Bé, and O. R. Anderson (1982), Effects of variations in light intensity on life processes of the planktonic foraminifer *Globigerinoides sacculifer* in laboratory culture: Journal of the Marine Biological Association of the United Kingdom, v. 62, p. 435–451, doi:10.1017/S0025315400057374.

Clyde, W. C., P. D. Gingerich, S. L. Wing, U. Röhl, T. Westerhold, G. Bowen, K. Johnson, A. A. Baczynski, A. Diefendorf, F. McInerney, D. Schnurrenberger, A. Noren, K. Brady, and the BBCP Science Team (2013), Bighorn Basin Coring Project (BBCP): a continental perspective on early Paleogene hyperthermals, Sci. Dril., 16, 21–31, doi:10.5194/sd-16-21-2013.

Coccioni, R., G. Bancalà, R. Catanzariti, E. Fornaciari, F. Frontalini, L. Giusberti, L. Jovane, V. Luciani, J. Savian, and M. Sprovieri (2012), An integrated stratigraphic record of the Palaeocene-lower Eocene at Gubbio (Italy), New insights into the early Palaeogene hyperthermals and carbon isotope excursions, Terra Nova, 24, 380–386, doi:10.1111/j.1365-3121.2012.01076.x.

Corfield, R. M. (1987), Patterns of evolution in Palaeocene and Eocene planktonic foraminifera, Micropalaeontology of carbonate environments, Ellis Horwood, Chichester, England, 93-110.

Cramer, B. S., D. V. Kent, and M.-P. Aubry (2003), Orbital climate forcing of excursions in the late Paleocene–early Eocene (chrons C24n–C25n), Paleoceanography, 18(4), 1097, doi:10.1029/2003PA000909.

Crouch, E. M., C. Heilmann-Clausen, H. Brinkhuis, H. E. G. Morgans, K. M. Rogers, H. Egger, and B. Schmitz (2001), Global dinoflagellate event associated with the late Paleocene thermal maximum, Geology, 29, 315–318.

De Conto, R. M., S. Galeotti, M. Pagani, D. Tracy, K. Schaefer, T. Zhang, D. Pollard, and D. J. Beerling (2012), Past extreme warming events linked to massive carbon release from thawing permafrost, Nature, 484, 87–91, doi:10.1038/nature10929.

Dedert, M., H. M. Stoll, D. Kroon, N. Shimizu, K. Kanamaru, and P. Ziveri (2012), Productivity response of calcareous nannoplankton to Eocene Thermal Maximum 2 (ETM2), Clim. Past, 8(3), 977–993, doi:10.5194/cp-8-977-2012.

Dedert, M., H. Stoll, S. Kars, J. R. Young, N. Shimizu, D. Kroon, L. Lourens, and P. Ziveri (2014), Temporally variable diagenetic overgrowth on deep-sea nannofossil carbonates across Palaeogene hyperthermals and implications for isotopic analyses, Mar. Micropaleontol., 107, 18–31.

D'haenens, S., A. Bornemann, P. Stassen, and R. P. Speijer (2012), Multiple early Eocene benthic foraminiferal assemblage and $\delta^{13}C$ fluctuations at DSDP Site 401 (Bay of Biscay-NE Atlantic), Mar. Micropaleontol., 88–89, 15–35, doi:10.1016/j.marmicro.2012.02.006.

D'haenens, S., A. Bornemann, P. Claeys, U. Röhl, E. Steurbaut, and R. P. Speijer (2014), A transient deep-sea circulation switch during Eocene Thermal Maximum 2, Paleoceanography, 29, 370–388, doi:10.1002/2013PA002567.

D'Hondt, S., J. C. Zachos, and G. Schultz (1994), Stable isotopic signals and photosymbiosis in Late Paleocene planktic foraminifera, Paleobiology, 20, 391–406.

Dickens, G. R. (2011), Down the rabbit hole: Toward appropriate discussion of methane release from gas hydrate systems during the Paleocene-Eocene thermal maximum and other past hyperthermal events, Clim. Past, 7(3), 831–846, doi:10.5194/cp-7-831-2011.

Douglas, A. E. (2003), Coral bleaching—How and why?, Mar. Pollut. Bull., 46, 385–392.

Edgar, K. M., S. M. Bohaty, S. J. Gibbs, P. F. Sexton, R. D. Norris, and P. A. Wilson (2012), Symbiont "bleaching" in planktic foraminifera during the Middle Eocene Climatic Optimum, Geology, 41, 15–18, doi:10.1130/G33388.1.

Ezard, T. H. G., T. Aze, P. N. Pearson, and A Purvis (2011) Interplay between changing climate and species' ecology drives macroevolutionary dynamics, Science, 332, 349–351.

Falkowski, P. G., M. E. Katz, A. J. Milligan, K. Fennel, B. S. Cramer, M. P. Aubry, R. A. Berner, M. J. Novacek, and W. M. Zapol (2005), Mammals evolved, radiated, and grew in size as the concentration of oxygen in Earth's atmosphere increased during the past 100 million years, Science, 309, 2202–2204.

Field, C. B., V. Barros, T. F. Stocker, D. Qin, K. J. Mach, G.-K. Plattner, M. D. Mastrandrea, M. Tignor and K. L. Ebi (2011), Workshop Report of the Intergovernmental Panel on Climate Change (2011), Workshop on Impacts of Ocean Acidification on Marine Biology and Ecosystems, IPCC, 2011: Contribution of Working Group II Technical Support Unit, Carnegie Institution, Stanford, CA, USA, 164 pp.

Figueirido, B., C. M. Janis, J. A. Pérez-Claros, M. De Renzi, and P. Palmqvist (2012), Cenozoic climate change influences mammalian evolutionary dynamics, P. Natl. Acad. Sci. USA, 109, 722–727.

Fraass, A. J., D. K. Kelly, and S. E. Peters (2015), Macroevolutionary history of the planktic foraminifera, Annu. Rev. Earth Pl. Sc., 43, 139–66, doi:10.1146/annurev-earth-060614-105059.

Galeotti, S., S. Krishnan, M. Pagani, L. Lanci, A. Gaudio, J. C. Zachos, S. Monechi, G. Morelli, and L. J. Lourens (2010), Orbital chronology of Early Eocene hyperthermals from the Contessa Road section, central Italy, Earth Planet. Sci. Lett., 290(1–2), 192–200, doi:10.1016/j.epsl.2009.12.021.

Gattuso, J.-P., and L. Hansson (2011), Ocean acidification: history and background, in Ocean acidification edited by Gattuso, J.-P., and L. Hansson, 1–20, Oxford University Press, Oxford, UK.

Gibbs, S. J., P. R. Bown, B. H. Murphy, A. Sluijs, K. M. Edgar, H. Pälike, C. T. Bolton, and J. C. Zachos (2012), Scaled biotic disruption during early Eocene global warming events, Biogeosciences, 9(11), 4679–4688, doi:10.5194/bg-9-4679-2012.

Gingerich, P. D. (2001), Rates of evolution on the time scale of the evolutionary process, Genetica, 112–113, 127–144.

Gingerich, P. D. (2003), Mammalian response to climate change at the Paleocene–Eocene boundary: Polecat Bench record in the northern Bighorn Basin, Wyoming, Geol. Soc. Am. Spec. Pap., 369, 463–478.

Giusberti, L., D. Rio, C. Agnini, J. Backman, E. Fornaciari, F. Tateo, and M. Oddone (2007), Mode and tempo of the Paleocene–Eocene thermal maximum in an expanded section from the Venetian pre-Alps, Geol. Soc. Am. Bull., 119, 391–412, doi:10.1130/B25994.1.

Hambrey, M. J., W. U. Ehrmann, and B. Larsen (1991), Cenozoic glacial record of the Prydz Bay continental shelf, East Antarctica, in Proceedings of the Ocean Drilling Program, Scientific results, edited by Barron, J., B. Larsen, et al., College Station, Texas, Ocean Drilling Program, 119, 77–132.

Hemleben, C., Spindler, M., and O. R. Anderson (1989), Modern planktonic foraminifera, edited by Hemleben, C., Spindler, M., and O. R. Anderson, Springer-Verlag, New York, ISBN-13: 9780387968155, 1–363.

Hollis, C. J., K. W. R. Taylor, L. Handley, R. D. Pancost, M. Huber, J. B. Creech, B. R. Hines, E. M. Crouch, Morgans, H. E. G., J. S. Crampton, S. Gibbs, P. N. Pearson, and J. C. Zachos (2012), Early Paleogene temperature history of the Southwest Pacific Ocean: Reconciling proxies and models, Earth Planet. Sc. Lett., 349–350, 53–66, doi:10.1016/j.epsl.2012.06.024.

Huber, M. and R. Caballero (2011), The early Eocene equable climate problem revisited, Clim. Past, 7, 603–633, doi:10.5194/cp-7-603-2011.

Hyland, E. G., and N. D. Sheldon (2013), Coupled CO2-climate responseduring the Early Eocene Climatic Optimum, Palaeogeogr.Palaeocl., 369, 125–135.

Kelly, D.C., T. J. Bralower, J. C. Zachos, I. Premoli Silva, and E. Thomas (1996), Rapid diversification of planktonic foraminifera in the tropical Pacific (ODP Site 865) during the late Paleocene thermal maximum, Geology, 24, 423–426, doi:10.1130/0091-7613(1996)024<0423:RDOPFI>2.3.CO;2.

Kelly, D. C., T. J. Bralower, and J. C. Zachos (1998), Evolutionary consequences of the latest Paleocene thermal maximum for tropical planktonic foraminifera, Palaeogeography, Palaeoclimatology, Palaeoecology, 141, 139–161, doi:10.1016/S0031-0182(98)00017-0.

Kennett, J. P., and L. D. Stott (1991), Abrupt deep-sea warming, palaeoceanographic changes and benthic extinctions at the end of the Palaeocene, Nature, 353, 225–229.

Kirtland-Turner, S., P. F. Sexton, C. D. Charles, and R. D. Norris (2014), Persistence of carbon release events through the peak of early Eocene global warmth, Nat. Geosci., 12, 1–17, doi:10.1038/ngeo2240.Inglis et al., 2015

Inglis, G. N., A. Farnsworth, D. Lunt, G. L. Foster, C. J. Hollis, M. Pagani, P. E. Jardine, P. N. Pearson, P. Markwick, A. M. J. Galsworthy, L. Raynham, K. W. R. Taylor, and R. D. Pancost (2015), Descent toward the icehouse: Eocene sea surface cooling inferred from GDGT distributions, Paleoceanography, 30, 100–1020, doi:10.1002/2014PA002723.

Lauretano, V., K. Littler, M. Polling, J. C. Zachos, and L. J. Lourens (2015), Frequency, magnitude and character of hyperthermal events at the onset of the Early Eocene Climatic Optimum, Clim. Past, 11, 1313–1324, doi:10.5194/cp-11-1313-2015.

Lauretano, V., F. J. Hilgen, J. C. Zachos and L. J. Lourens (2016), Astronomically tuned age model for the early Eocene carbon isotope events: A new high-resolution δ^{13}C benthic record of ODP Site 1263 between~ 49 and~ 54 Ma, Newsletters on Stratigraphy, 49(2), 383-400.

Littler, K., U. Röhl, T. Westerhold, and J. C. Zachos (2014), A high-resolution benthic stable isotope record for the South Atlantic: Implications for orbital-scale changes in late Paleocene–early Eocene climate and carbon cycling, Earth Planet. Sc. Lett., 401, 18–30, doi:10.1016/j.epsl.2014.05.054.

Lourens, L. J., A. Sluijs, D. Kroon, J. C. Zachos, E. Thomas, U. Röhl, J. Bowles, and I. Raffi (2005), Astronomical pacing of late Palaeocene to early Eocene global warming events, Nature, 435, 1083–1087.

Lu, G. (1995), Paleocene-Eocene transitional events in the ocean: Faunal and isotopic analyses of planktic foraminifera, PhD Thesis, Princeton University, Princeton, 1–284.

Lu, G., and G. Keller (1995), Planktic foraminiferal faunal turnovers in the subtropical Pacific during the late Paleocene to early Eocene, J. Foramin. Res., 25, 97–116.

Luciani, V. and L. Giusberti (2014), Reassessment of the early–middle Eocene planktic foraminiferal biomagnetochronology: new evidence from the Tethyan Possagno section (NE Italy) and Western North Atlantic Ocean ODP Site 1051, J. Foramin. Res., 44, 187–201.

Luciani, V., L. Giusberti, C. Agnini, J. Backman, E. Fornaciari, and D. Rio (2007), The Paleocene–Eocene Thermal Maximum as recorded by Tethyan planktonic foraminifera in the Forada section (northern Italy), Mar. Micropaleontol., 64(3), 189–214, doi:10.1016/j. marmicro.2007.05.001.

Luciani, V., L. Giusberti, C. Agnini, E. Fornaciari, D. Rio, D. J. A. Spofforth, and H. Pälike (2010), Ecological and evolutionary response of Tethyan planktonic foraminifera to the middle Eocene climatic optimum (MECO) from the Alano section (NE Italy), Palaeogeography, Palaeoclimatology, Palaeoecology, 292, 82–95.

Luciani, V., G. R. Dickens, J. Backman, E. Fornaciari, L. Giusberti, C. Agnini, and R. D'Onofrio (2016), Major perturbations in the global carbon cycle and photosymbiont-bearing planktic foraminifera during the early Eocene, Clim. Past, 12, 981–1007, doi:10.5194/cp-12-981-2016.

Lunt, D. J., A. Ridgwell, A. Sluijs, J. C. Zachos, S. Hunter, and A. Haywood (2011), A model for orbital pacing of methan hydrate destabilization during the Paleogene, Nat. Geosci., 4, 775–778, doi:10.1038/ngeo1266.

Marcott, S. A., J. D. Shakun, P. U. Clark, and A. C. Mix (2013), A Reconstruction of Regional and Global Temperature for the Past 11,300 Years, Science, 339, 1198-1201.

McInerney, F. A., and S. L. Wing (2011), The Paleocene-Eocene Thermal Maximum: A perturbation of carbon cycle, climate, and biosphere with implications for the future, Annu. Rev. Earth Planet. Sci., 39(1), 489–516, doi:10.1146/annurev-earth-040610-133431.

Mita, I. (2001), Data Report: Early to late Eocene calcareous nannofossil assemblages of Sites 1051 and 1052, Blake Nose, Northwestern Atlantic Ocean, in Proc. Ocean Drill. Progr., Sci. Results, 171B, edited by Kroon, D., R. D. Norris, and A. Klaus, 1–28, Available from World Wide Web: <http://www-odp.tamu.edu/publications/171B_SR/chap_07/chap_07.htm>.

Morard, R., M. Reinelt, C. M. Chiessi, J. Groeneveld, and M. Kucera (2016), Tracing shifts of oceanic fronts using the cryptic diversity of the planktonic foraminifera Globorotalia inflate, Paleoceanography, 31(9), 1193–1205.

Nicolo, M. J., G. R. Dickens, C. J. Hollis, and J. C. Zachos (2007), Multiple early Eocene hyperthermals: Their sedimentary expression on the New Zealand continental margin and in the deep sea, Geology, 35(8), 699–702.

Norris, R. D. (1996), Symbiosis as an evolutionary innovation in the radiation of Paleocene planktic foraminifera, Paleobiology, 22(4), 461–480.

Norris, R. D., D. Kroon, and A. Klaus (1998), Proceedings of the Ocean Drilling Program, Initial Reports, Proc. Ocean Drill. Progr., Sci. Results, 171B, 1–749.

O'Connor, F. M., O. Boucher, N. Gedney, C. D. Jones, G. A. Folberth, R. Coppell, W. J. Collins, J. Chappellaz, J. Ridley, and C. E. Johnson (2010), Possible role of wetlands, permafrost, and methane hydrates in the methane cycle under future climate change: A review, Reviews of Geophysics, 48(4).

Ogg, J. G. and L. Bardot (2001), Aptian through Eocene magnetostratigraphic correlation of the Blake Nose Transect (Leg 171B), Florida continental margin, Proc. Ocean Drill. Progr., Sci. Results, 171B, 1–58, doi:10.2973/odp.proc.sr.171B.104.2001.

Oreshkina, T. V. (2012), Evidence of late Paleocene–early Eocene hyperthermalevents in biosiliceous sediments of Western Siberia andadjacent areas, Aust. J. Earth Sci., 105, 145–153.

Pachauri, R. K., M. R. Allen, V. R. Barros, J. Broome, W. Cramer, R. Christ, J. A. Church, L. Clarke, Q. Dahe, P. Dasgupta, N. K. Dubash, O. Edenhofer, I. Elgizouli, C. B. Field, P. Forster, P. Friedlingstein, J. Fuglestvedt, L. Gomez-Echeverri, S. Hallegatte, G. Hegerl, M. Howden, K. Jiang, B. Jimenez Cisneroz, V. Kattsov, H. Lee, K. J. Mach, J. Marotzke, M. D. Mastrandrea, L. Meyer, J. Minx, Y. Mulugetta, K. O'Brien, M. Oppenheimer, J. J. Pereira, R. Pichs-Madruga, G. K. Plattner, H. O. Pörtner, S. B. Power, B. Preston, N. H.

Ravindranath, A. Reisinger, K. Riahi, M. Rusticucci, R. Scholes, K. Seyboth, Y. Sokona, R. Stavins, T. F. Stocker, P. Tschakert, D. van Vuuren, and J. P. van Ypserle (2014), Climate change 2014: Synthesis Report. Contribution of Working Groups I, II and III to the Fifth Assessment Report of the Intergovernmental Panel on Climate Change, edited by Pachauri, R., and L. Meyer, Geneva, Switzerland, IPCC, 151, ISBN: 978-92-9169-143-2.

Pagani, M., K. Caldeira, D. Archer, and J. C. Zachos (2006), An ancient carbon mystery, Science, 314, 1556–57, doi:10.1126/science.1136110.

Pagani, M., Z. Liu, J. LaRiviere, and A. C. Ravelo (2010), High Earth-system climate sensitivity determined from Pliocene carbon dioxide concentrations, Nature Geosciences, 3, 27–30.

Pearson, P. N., N. J. Shackleton, and M. A. Hall (1993), Stable isotope paleoecology of middle Eocene planktonic foraminifera and multispecies isotope stratigraphy, DSDP Site 523, South Atlantic, J. Foraminiferal Res., 23, 123-140, doi:10.2113/gsjfr.23.2.123.

Pepper W. J., J. Leggett, R. Swart, J. Wasson, J. Edmonds, and I. Mintzer (1992), Emissions scenarios for the IPCC. An update: assumptions, methodology, and results, Support document for ch. A3, in Climate Change 1992: Supplementary Report to the IPCC Scientific Assessment, edited by Houghton, J. T., B. A. Callandar, and S. K. Varney, pp. 69–96. Cambridge, UK: Cambridge University Press.

Pross, J., L. Contreras, P. K. Bijl, D. R. Greenwood, S. M. Bohaty, S. Schouten, J. A. Bendle U. Röhl, L. Tauxe, J. I. Raine, E. Claire, C. E. Huck, T. van de Flierdt, S. R. Stewart, S. S. R. Jamieson, C. E. Stickley, B. van de Schootbrugge, C. Escutia, and H. Brinkhuis (2012), Persistent near-tropical warmth on the Antarctic continent during the early Eocene Epoch, Nature, 488, 73–77, doi:10.1038 /nature11300.

Quillévéré, F., and R. D. Norris (2003), Ecological development of acarininids (planktonic foraminifera) and hydrographic evolution of Paleocene surface waters, Special Papers-Geological Society Of America, 223-238.

Raffi, I., and B. De Benardi (2008), Response of calcareous nannofossils to the Paleocene-Eocene Thermal Maximum: observations on composition, preservation and calcification in sediments from ODP Site 1263 (Walvis Ridge-SW Atlantic), Mar. Micropal. 69, 119–138, doi:10.1016/j.marmicro.2008.07.002)

Raven, J., K. Caldeira, H. O. Elderfield, P. L. Hoegh-Guldberg, U. Riebesell, J. Shepherd, C. Turley, A. Watson (2005), Ocean acidification due to increasing atmospheric carbon dioxide, 60, London, UK, The Royal Society.

Röhl, U., T. Westerhold, S. Monechi, E. Thomas, J. C. Zachos, and B. Donner (2005), The third and final early Eocene Thermal Maximum: Characteristics, timing, and mechanisms of the "X" event, Geol. Soc. Am. Abstr. Program, 37(7), 264.

Scheibner, C., and R. P. Speijer (2008), Late Paleocene–early Eocene Tethyan carbonate platform evolution—a response to long-and short-term paleoclimatic change, Earth-Science Reviews, 90(3), 71-102.

Schmidt, D. N., H. R. Thierstein, and J. Bollmann (2004), The evolutionaryhistory of size variation of planktic foraminiferal assemblagesin the Cenozoic, Palaeogeogr. Palaeocl., 212, 159–180,doi:10.1016/j.palaeo.2004.06.002.

Schneider, L. J., T. J. Bralower, and L. J. Kump (2011), Response ofnannoplankton to early Eocene ocean destratification, Palaeogeogr.Palaeocl., 310, 152–162.

Self-Trail, J. M., D. S. Powars, D. K. Watkins, and G. A. Wandless (2012), Calcareous nannofossil assemblage changes across the Paleocene–Eocene Thermal Maximum: Evidence from a shelf setting, Marine Micropaleontology, 92, 61-80.

Sexton, P. F., R. D. Norris, P. A. Wilson, H. Pälike, T. Westerhold, U. Röhl, C. T. Bolton, and S. J. Gibbs (2011), Eocene global warming events driven by ventilation of oceanic dissolved organic carbon, Nature, 471(7338), 349–352, doi:10.1038/nature09826.

Sexton, P. F., P. A. Wilson, and P. N. Pearson (2006), Microstructural and geochemical perspectives on planktic foraminiferal preservation: 'Glassy' versus 'Frosty', Geochemistry Geophysics Geosystems, 7, Q12P19, doi:10.1029/2006GC001291.

Shamrock, J. L., D. K. Watkins, and K. W. Johnston (2012), Eocene biogeochronology of ODP Leg 122 Hole 762C, Exmouth Plateau (northwest Australian Shelf), Stratigraphy, 9, 55–76.

Shipboard Scientific Party (1998), Site 1051, in Proc. ODP, Init. Repts., 171B, edited by Norris, R. D., D. Kroon, A. Klaus, et al., College Station, TX (Ocean Drilling Program), 171–239. doi:10.2973/odp.proc.ir.171b.105.1998.

Sigman, D. M., M. P. Hain, and G. H. Haug (2010), The polar ocean and glacial cycles in atmospheric CO_2 concentration, Nature, 466(7302), 47-55.

Sims, P. A., D. G. Mann, and L. K. Medlin (2006), Evolution of the diatoms:insights from fossil, biological and molecular data, Phycologia,45, 361–402.

Slotnick, B. S., G. R. Dickens, M. J. Nicolo, C. J. Hollis, J. S. Crampton, and J. C. Zachos (2012), Large-amplitude variations in carbon cycling and terrestrial weathering during the latest Paleocene and earliest Eocene: The record at Mead Stream, New Zealand, J. Geol., 120(5), 487–505, doi:10.1086/666743.

Slotnick, B. S., G. R. Dickens, C. J. Hollis, J. S. Crampton, P. S. Strong, and A. Phillips (2015), The onset of the Early Eocene Climatic Optimum at Branch Stream, Clarence River valley, New Zealand, New Zeal. J. Geol. Geop., 58, 1–19, doi:10.1080/00288306.2015.1063514.

Sluijs A, S. Schouten, M. Pagani, M. Woltering, H. Brinkhuis, J. S. Sinninghe Damsté, G. R. Dickens, M. Huber, G.-J. Reichart, R. Stein, J. Matthiessen, L. J. Lourens, N. Pedentchouk, J. Backman, K. Moran and the Expedition 302 Scientists (2006), Subtropical Arctic Ocean temperatures during the Palaeocene/Eocene Thermal Maximum, Nature 441, 610–613, doi:10.1038/nature04668.

Sluijs, A., G. J. Bowen, H. Brinkhuis, L. J. Lourens, and E. Thomas (2007), The Paleocene–Eocene thermal maximum super greenhouse:biotic and geochemical signatures, age models and mechanismsof global change, in Deep-Time Perspectives on ClimateChange, edited by Williams, M., A. M. Haywood, F. J. Gregory, and D. N. Schmidt, Micropalaeont. Soc. Spec. Publ., GeologicalSociety, London, 323–350.

Sluijs, A., S. Schouten, T. H. Donders, P. L. Schoon, U. Röhl, G.-J. Reichart, F. Sangiorgi, J. H. Kim, J. S. Sinninghe Damsté, and H. Brinkhuis (2009), Warm and wet conditions in the Arctic region during Eocene Thermal Maximum 2, Nat. Geosci., 2(11), 1–4, doi:10.1038/ngeo668.

Solomon, S., D. Qin, M. Manning, M. Marquis, K. Averyt, M. M. B. Tignor, H. LeRoy Miller Jr., and Z. Chenet (2007), Climate Change 2007: The Physical Science Basis, Contribution of Working Group I to the Fourth Assessment Report of the Intergovernmental Panel on Climate Change, Cambridge University Press, Cambridge, United Kingdom and New York, NY, USA, 129–385.

Spero, H. J., and D. W. Lea (1993), Intraspecific stable isotope variability in the planktic foraminifera *Globigerinoides sacculifer*: Results from laboratory experiments, Marine Micropaleontology, v. 22, p. 221–234, doi:10.1016/0377 -8398(93)90045-Y.

Stap, L., A. Sluijs, E. Thomas, and L. J. Lourens (2009), Patterns and magnitude of deep sea carbonate dissolution during Eocene Thermal Maximum 2 and H2, Walvis Ridge, Southeastern Atlantic Ocean, Paleoceanography, 24, PA1211, doi:10.1029/2008PA001655.

Stap, L., L. J. Lourens, E. Thomas, A. Sluijs, S. Bohaty, and J. C. Zachos (2010a), High-resolution deep-sea carbon and oxygen isotope records of Eocene Thermal Maximum 2 and H2, Geology, 38, 607–610, doi:10.1130/G30777.1.

Stap, L., L. J. Lourens, A. van Dijk, S. Schouten, and E. Thomas (2010b), Coherent pattern and timing of the carbon isotope excursion and warming during Eocene Thermal Maximum 2 as recorded in planktic and benthic foraminifera, Geochem. Geophys. Geosyst., 11, Q11011, doi:10.1029/2010GC003097.

Stocker, T. F., D. Qin, G.-K. Plattner, M. Tignor, S. K. Allen, J. Boschung, A. Nauels, Y. Xia, V. Bex and P. M. Midgley, Climate Change 2013: The Physical Science Basis, Contribution of Working Group I to the Fifth Assessment Report of the Intergovernmental Panel on Climate Change, Cambridge University Press, Cambridge, United Kingdom and New York, NY, USA, 1–27, doi:10.1017/CBO9781107415324.031.

Thomas, E. (1998), Biogeography of the late Paleocene benthic foraminiferal extinction, in Late Paleocene-early Eocene climaticand biotic events in the marine and terrestrial Records, edited by Aubry, M.-P., S. Lucas, and W. A. Berggren, Columbia University Press, New York, 214–243.

Thomas, E., J. C. Zachos, and T. J. Bralower (2000), Deep-sea environments on a warm earth: latest Paleocene–early Eocene, in Warm Climates in Earth History, edited by B. Huber, K. MacLeod, and S. Wing, 132–160, Cambridge Univ. Press, Cambridge, U. K.

Thomas, E., H. Brinkhuis, M. Huber, and U. Röhl (2006), An ocean view of the early Cenozoic greenhouse world, Oceanography, 19, 63–72.

Van Hinsbergen, D. J. J., L. V. de Groot, S. J., van Schaik, W. Spakman, P. K. Bijl, A. Sluijs, C. G. Langereis, and H. Brinkhuis (2015), A Paleolatitude Calculator for Paleoclimate Studies, PLoS ONE, 10, e0126946, doi:10.1371/journal.pone.0126946.

Westerhold, T., U. Röhl, J. Laskar, I. Raffi, J. Bowles, L. J. Lourens, and J. C. Zachos (2007), On the duration of magnetochrons C24r and C25n and the timing of early Eocene global warming events: Implications from the Ocean Drilling Program Leg 208 Walvis Ridge depth transect, Paleoceanography, 22, PA2201, doi:10.1029/2006PA001322.

Westerhold, T., U. Röhl, I. Raffi, E. Fornaciari, S. Monechi, V. Reale, J. Bowles, and H. F. Evans (2008), Astronomical calibration of the Paleocene time, Palaeogeogr. Palaeoclimatol. Palaeoecol., 257, 377–403, doi:10.1016/j.palaeo.2007.09.016.

Westerhold, T., U. Röhl, T. Frederichs, S. M. Bohaty, and J. C. Zachos (2015), Astronomical calibration of the geological timescale: Closing the middle Eocene gap, Clim. Past, 11(9), 1181–1195, doi:10.5194/cp-11-1181-2015.

Wilf, P., R. N. Cúneo, K. R. Johnson, J. F. Hicks, S. L. Wing, and J. D. Obradovich (2003), High plant diversity in Eocene South America:evidence from Patagonia, Science, 300, 122–125.

Wing, S. L., T. M. Bown, and J. D. Obradovich (1991), Early Eocene biotic and climatic change in interior western North America, Geology, 19, 1189–1192.

Woodburne, M. O., G. F. Gunnell, and R. K. Stucky (2009), Climate directly influences Eocene mammal faunal dynamics in North America, P. Natl. Acad. Sci. USA, 106, 13399–13403.

Yamaguchi, T., and R. D. Norris (2012), Deep-sea ostracode turnovers through the Paleocene-Eocene thermal maximum in DSDP Site 401, Bay of Biscay, North Atlantic, Mar. Micropaleontol., 86–87, 32–44.

Zachos, J. C., J. R. Breza, and S. W. Wise (1992), Early Oligocene ice-sheet expansion on Antarctica: Stable isotope and sedimentological evidence from Kerguelen Plateau, southern Indian Ocean. Geology, 20(6), 569-573.

Zachos, J. C., K. C. Lohmann, J. C. Walker, and S. W. Wise (1993), Abrupt climate change and transient climates during the Paleogene: A marine perspective, The Journal of Geology, 101(2), 191-213.

Zachos, J. C., M. Pagani, L. Sloan, E. Thomas, and K. Billups (2001), Trends, rhythms, and aberrations in global climate 65 Ma to present, Science, 292, 686–693, doi:10.1126/science.1059412.

Zachos, J. C., D. Kroon, P. Blum, et al. (2004), Proc. ODP, Init. Repts., 208, College Station, TX (Ocean Drilling Program), doi:10.2973/odp.proc.ir.208.2004.

Zachos, J. C., U. Röhl, S. A. Schellenberg, A. Sluijs, D. A. Hodell, D. C. Kelly, E. Thomas, M. Nicolo, I. Raffi, L. J. Lourens, H. McCarren, and D. Kroon (2005), Rapid acidification of the ocean during the Paleocene-Eocene thermal maximum, Science, 308, 1611–1615, doi:10.1126/science.1109004.

Zachos, J. C., S. Schouten, S. Bohaty, Sluijs A, Brinkhuis H, Gibbs S, Bralower T, and Quattlebaum T. (2006), Extreme warming of mid-latitude coastal ocean during the Paleocene-Eocene Thermal Maximum: inferences from TEX_{86} and isotope data, Geology, 34, 737–740, doi:10.1130/G22522.1.

Zachos, J. C., G. R. Dickens, and R. E. Zeebe (2008), An early Cenozoic perspective on greenhouse warming and carbon-cycle dynamics, Nature, 451(7176), 279-283, doi:10.1038/nature06588.

Zachos, J. C., H. K. McCarren, B. Murphy, U. Röhl, and T. Westerhold (2010), Tempo and scale of late Paleocene and early Eocene carbon isotope cycles: Implications for the origin of hyperthermals, Earth Planet. Sci. Lett., 299, 242–249, doi:10.1016/j.epsl.2010.09.004.

Zeebe, R. E., J. C. Zachos, and G. R. Dickens (2009), Carbon dioxide forcing alone insufficient to explain Palaeocene–Eocene Thermal Maximum warming, Nat. Geosci., 2(8), 576–580, doi:10.1038/ngeo578.

Zeebe, R. E., and J. C. Zachos (2013), Long-term legacy of massive carbon input to the Earth system: Anthropocene versus Eocene, Philosophical Transactions of the Royal Society of London A: Mathematical, Physical and Engineering Sciences, 371(2001), 20120006.

Zonneveld, J. P., G. F.Gunnell, and W. S. Bartels (2000), Early Eocene fossil vertebrates from the southwestern Green River Basin, Lincoln and Uinta Counties, Wyoming, J. Vertebr. Paleontol., 20, 369–386.

CHAPTER II

Environmental perturbations at the early Eocene ETM2, H2, and I1 events as inferred by Tethyan calcareous plankton (Terche section, northeastern Italy)

Roberta D'Onofrio[1], Valeria Luciani[1], Eliana Fornaciari[2], Luca Giusberti[2], Flavia Boscolo Galazzo[2], Edoardo Dallanave[3], Thomas Westerhold[4], Mario Sprovieri[5], and Sonia Telch[2]

[1]Dipartimento di Fisica e Scienze della Terra, Università di Ferrara, Ferrara, Italy,

[2]Dipartimento di Geoscienze, Università di Padova, Padua, Italy,

[3]Department of Earth and Environmental Science, Ludwig Maximilians University of Munich, Munich, Germany,

[4]MARUM - Center for Marine Environmental Sciences, University of Bremen, Bremen, Germany,

[5]Istituto per l'Ambiente Marino Costiero del Consiglio Nazionale delle Ricerche, Campobello di Mazzara, Italy

Abstract

Several early Eocene hyperthermals have been recently investigated and characterized in terms of temperature anomalies and oceanographic changes. The effects of these climatic perturbations on biotic communities are much less constrained. Here we present new records from the Terche section (northeastern Italy) that, for the first time, integrates data on planktic foraminifera and calcareous nannofossils across three post-Paleocene/Eocene Thermal Maximum (PETM) negative carbon isotope excursions (CIEs). The biomagnetostratigraphic framework generated at Terche allows us to confidently relate such CIEs to the Eocene Thermal Maximum 2 (ETM2), H2, and I1 events. Each of these events coincides with lithological anomalies characterized by significantly lower calcium carbonate content (marly units, MUs). We interpret these MUs as mainly linked to an effect of increased terrigenous dilution, as dissolution proxies do not display significant variations. Calcareous plankton assemblages change significantly across these events and radiolarians increase. Observed changes suggest that transient warming and environmental perturbations, though more intense during ETM2, occurred during each of the three investigated perturbations. Variations among calcareous plankton suggest increase in surface-water eutrophication with respect to the pre-event conditions, coupled with a weakening of the upper water-column thermal stratification. Higher nutrient discharge was related to intensification of the hydrological cycle as a consequence of the warmer climate. These conditions persisted during the early CIE recovery, implying slower recovery rates for the environment and biota than for the carbon cycle.

1. Introduction

The early Paleogene climate was characterized by abrupt, short-term global warming events, known as hyperthermals. The term "hyperthermal" was introduced by Thomas et al. (2000) to describe "intervals—during the early Paleogene—of extremely high temperatures and very low latitudinal sea surface temperature gradients during which the deep-intermediate oceans were dominated by waters derived from subtropical latitudes." The most extreme hyperthermal was the extensively studied Paleocene/Eocene Thermal Maximum (PETM or ETM1, e.g., Kennett and Stott, 1991; Zachos et al., 2010; McInerney and Wing, 2011) at ~56 Ma (e.g., Westerhold et al., 2008). Hyperthermals share similar characteristics, though with different magnitudes, such as negative excursions in $\delta^{18}O$ and $\delta^{13}C$ records (e.g., Cramer et

al., 2003; Littler et al., 2014, and references therein) and evidence for dissolution of deep-sea carbonates due to lysocline rise (e. g., Zachos et al., 2005; Leon-Rodriguez and Dickens, 2010; Hönisch et al., 2012). Nonetheless, the magnitude (>–3‰ δ^{13}C excursion in marine carbonates; 5–8°C of global warming, e.g., McInerney and Wing, 2011) and duration (~170–230 kyr, e.g., Giusberti et al., 2007; Röhl et al., 2007) of the PETM were unmatched among the hyperthermals so that it is considered as an exceptional perturbation of the climate and carbon cycle. Orbitally tuned records suggest that most of the early Paleogene hyperthermals and short-lived carbon isotope excursions, with the exception of the PETM, were paced by variations in Earth's orbit, with particular control in the long (405 kyr) and short (100 kyr) eccentricity bands (e.g., Cramer et al., 2003; Lourens et al., 2005; Westerhold et al., 2007, 2008, 2015; Galeotti et al., 2010; Zachos et al., 2010; Littler et al., 2014; Lauretano et al., 2015). Variations in Earth's orbital parameters are believed to have induced repeated emissions of isotopically depleted CO_2 into the ocean-atmosphere system (Lourens et al., 2005; Sexton et al., 2011; Kirtland-Turner et al., 2014), but the ^{13}C-depleted carbon reservoir along with the carbon cycle dynamics allowing such emissions remains uncertain (e.g., Pagani et al., 2006; Zeebe et al., 2009; Dickens, 2011; Lunt et al., 2011; Sexton et al., 2011; De Conto et al., 2012; Kirtland-Turner et al., 2014).

Among extra-PETM carbon isotope excursions (CIEs) the Eocene Thermal Maximum 2 (also referred as ELMO in Lourens et al., 2005; H1 in Cramer et al., 2003) at 54.02 Ma was the most intense, with a ~1‰negative CIE in marine carbonates (e.g., Stap et al., 2009; Galeotti et al., 2010; Leon-Rodriguez and Dickens, 2010; Littler et al., 2014). During the ETM2 ocean sea surface temperature warmed of approximately 3.5°C (Sluijs et al., 2009; Stap et al., 2010b), and precipitations increased at mid latitudes and in the Arctic region (Nicolo et al., 2007; D'haenens et al., 2012, 2014; Slotnick et al., 2012; Krishnan et al., 2014). Smaller negative CIEs, close to ~0.5‰, and with an average duration of 40–60 kyr punctuated the long-term warming trend started in the latest Paleocene and culminated into the Early Eocene Climatic Optimum and continued to occur later in the middle Eocene (e.g., Cramer et al., 2003; Sexton et al., 2011; Kirtland-Turner et al., 2014; Luciani et al., 2016). There is a general consensus to refer the PETM, the ETM2, and the Eocene Thermal Maximum 3 (ETM3 or X/K; at 52.83 Ma, Röhl et al., 2005; Thomas et al., 2006; Westerhold et al., 2015) as proper hyperthermals (e.g., Nicolo et al., 2007; Zachos et al., 2010; Slotnick et al., 2012). However, there is no total agreement whether to extend this designation to the numerous other early Paleogene minima in δ^{13}C (e.g., Zachos et al., 2010; Kirtland-Turner et al., 2014).

Extensive research is being focused on characterizing the early Paleogene succession of extra-PETM negative CIEs in terms of geochemical variations, timing, and magnitude. However, relatively little effort has been devoted to investigate their biotic repercussions, environmental impact, and potential influence on biotic long-term evolution. In particular, the response of marine calcareous plankton to the early Paleogene carbon cycle perturbations is so far largely unconstrained due to the widespread occurrence of carbonate dissolution at deep-sea sites (e.g., Stap et al., 2009; Leon-Rodriguez and Dickens, 2010; Dedert et al., 2012; Gibbs et al., 2012; Jennions et al., 2015). Nonetheless, calcareous plankton plays a crucial role in both the carbon cycle and in reconstruction of paleoceanographic conditions, thanks to the recognized paleoecological affinities of most Eocene genera or species. Only a few scattered oceanic records are available to date (Fig. 1). Most of the calcareous nannofossil assemblages from oceanic sites (Ocean Drilling Program, ODP) are affected by differential dissolution. They record both decrease (North Pacific Site 1209) and increase (South Atlantic, Site 1265) in primary productivity during the ETM2 (Dedert et al., 2012; Gibbs et al., 2012). The sole ETM2 planktic foraminiferal record, published to date, is provided by Stassen et al. (2012) from the shelf setting of the Dababiya section (Egypt), and it shows an increase of acarininids across the event.

Here we add new integrated biomagnetostratigraphic and geochemical data for the ETM2, H2, and I1 events as recorded at the Terche section (northeastern Italy, central western Tethys). We investigate planktic foraminiferal and calcareous nannofossil assemblages across these three subsequent post-PETM events with the aim to increase our understanding of the behavior of marine biota communities during abrupt warming episodes and of their resilience to periodic climate disruptions. We may also achieve insight on correspondences and dissimilarities among the investigated events, considering that they are not unanimously regarded as hyperthermals. Our calcareous plankton records present only minor signs of dissolution across the δ^{13}C minima, possibly representing the most genuine record available to date as regards the assemblages integrity. This study represents the first attempt to integrate and directly compare the responses of the main calcareous plankton groups to multiple post-PETM events of carbon cycle perturbations.
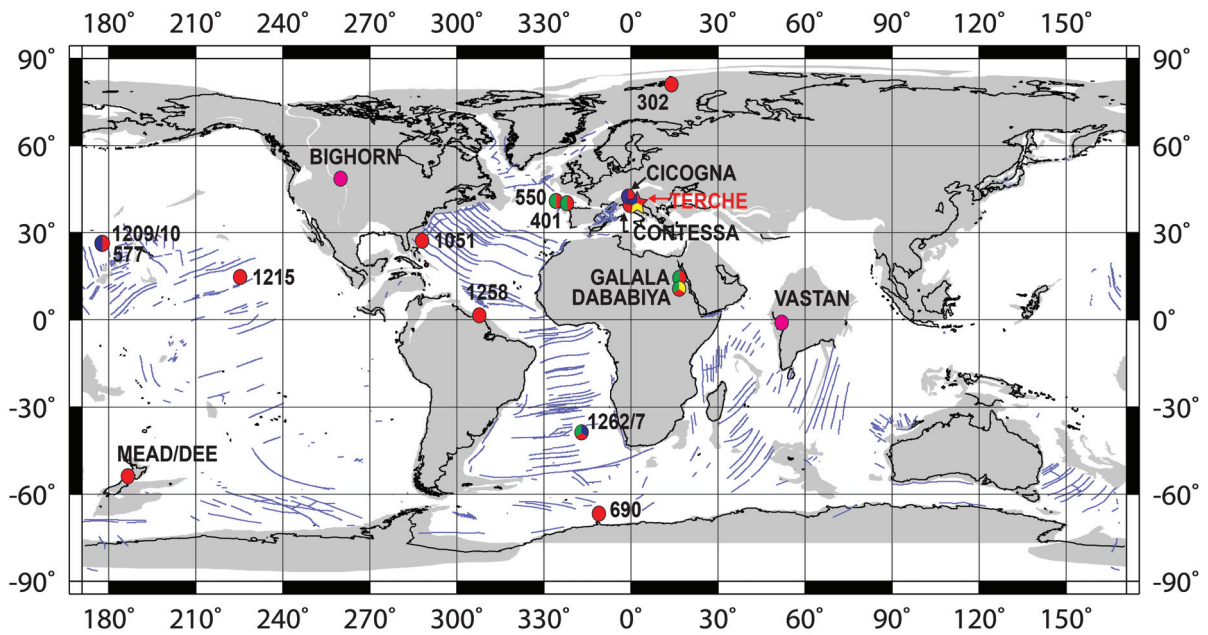
Figure 1. Earth at 54 Ma showing multiple locations where ETM2, H2, and I1 carbon isotope excursions have been documented in bulk carbonate or planktic and benthic foraminifera. These locations include the following: Ocean Drilling Program (ODP) Sites 1262 to 1267, 690, 1051 and Deep Sea Drilling Program (DSDP) sites 401 and 550 from the Atlantic Ocean (Lourens et al., 2005; Cramer et al., 2003; Röhl et al., 2005; Zachos et al., 2005, 2010; Stap et al., 2009, 2010a, 2010b;D'Haenens et al., 2012); Integrated Ocean Drilling Program Site 302 from Artic Ocean (Sluijs et al., 2009; Schoon et al., 2011);ODP sites 1209, 1210, 1215 and DSDP Site 577 from the Pacific Ocean (Dedert et al., 2012; Gibbs et al., 2012; Leon-Rodriguez and Dickens, 2010; Cramer et al., 2003); land sections from Mead and Dee Stream, New Zealand (Hollis et al., 2005; Nicolo et al., 2007; Slotnick et al., 2012); Bighorn Basin, North America (Abels et al., 2012; Chew, 2015); Vastan, India (Clementz et al., 2011); Italy (Contessa section, central Italy, Galeotti et al., 2010; Coccioni et al., 2012; Cicogna sections, northeastern Italy, Agnini et al., 2016); Galala and Dababiya sections from Egypt (Höntzsch et al., 2011; Stassen et al., 2012). Red color: locations where geochemical data are not coupled with biotic data from marine record; blue color: sites with data on calcareous nannofossils; green color: successions showing variations on benthic foraminifera; yellow color: data on planktic foraminifera; and pink color: terrestrial record. Note that the Terche section (star) is the only deep-sea record where the combined response from calcareous nannofossil and planktic foraminifera is given for the three post-PETM hyperthermals. Base map is from http://www.odsn.de/services/paleomap.html, paleolatitudes are modified according to www.paleolatitude.org model version 1.2 (Van Hinsbergen et al., 2015).

2. Settings, Stratigraphy, and Lithology

The Terche section (46°2′43.61″N, 12°4′47.78″E) is located in the Venetian Southern Alps (northeastern Italy), approximately 2 km south of Mel village (Belluno), and outcrops in correspondence of a Terche Creek right tributary (Fig. S1 in the supporting information). Sedimentary rocks exposed in the study area are part of the local Upper Cretaceous-lower Eocene pelagic-hemipelagic succession, deposited in the Belluno Basin, a Mesozoic-Cenozoic paleogeographic unit of the Southern Alps (e.g., Bosellini, 1989). The entire Terche section consists of more than 85 m of pink-reddish to green scaly calcareous marls and marly

27

limestones, locally rhythmically organized, referred to as the Scaglia Rossa Formation. The section splits into two segments, here labelled A and B (Fig. 2), by a tectonized and covered interval occurring at approximately 61m from the base. The segment A is 63m thick and presents in the upper portion a scarcely outcropping package (>3m) of dark red clayey marls corresponding to the clay marl unit (CMU), the regional lithological expression of the PETM main CIE (Giusberti et al., 2007). The segment B (~ 27mthick) is the main focus of this paper and crops out with continuity. It is characterized by the presence of three reddish marly and clayey intervals (marly units, MUs) which thickness varies from 1.1 to 1.5 m. Such lithological anomalies, here labelled as MU1, MU2, and MU3 (from the base to the top), interrupt the predominantly calcareous marl lithology.

3. Methods

3.1. Planktic, Benthic Foraminifera, and Radiolarians

Planktic foraminifera and radiolarians were analyzed on 78 samples spanning the lower Eocene portion of the Terche section containing the three post-PETM MUs (segment B; Fig. 2). The sample spacing was 2–10 cm across the MUs and 40–60 cm below and above. Foraminifera were extracted using different techniques depending on the different lithologies. Specifically, soft marly samples were processed with the hydrogen peroxide method, whereas limestone and indurate marl were treated with the "cold acetolyse" technique of Lirer (2000). For both these methods, 50–100 g of dry sediment was crushed into small fragments of about5mm in diameter. The disintegration is carried out by immersion of the obtained fragments in a solution of hydrogen peroxide (H_2O_2) diluted from 10% to 35% or a solution of acetic acid (CH_3COOH) diluted to 80%. In most cases, additional treatment with pure surface-tension-active chemical products (e.g., neo-Desogen) was required in order to eliminate or reduce clumps of residues or incrustations on the test surface. In some cases a gentle ultrasonic bath (e.g., low frequency at 40 kHz for less than 15 s) further improved the cleaning of the tests. All the samples were washed and sieved using a 63 μm mesh size.

Planktic foraminifera have been analyzed by counting the relative abundance of genera and groups of genera on a population of about 300 specimens in the greater than or equal to 63 μm size fraction on representative splits of washed residues. Counts are expressed in percentage. Groups of genera were combined according to the ecological affinities of the different taxa (Pearson et al., 2006, and references therein). In the *Subbotina* group were

included the genera *Subbotina*, *Parasubbotina*, *Paragloborotalia*, and *Globorotaloides*, while the chiloguembelinids comprise *Chiloguembelina* and *Zeauvigerina*. Foraminiferal taxonomic criteria adopted in this study are from Olsson et al. (1999) and Pearson et al. (2006). Planktic foraminiferal biostratigraphy is according to Wade et al. (2011).

Benthic foraminiferal assemblage was analyzed for paleobathymetric indications between −8 and +11 m (Fig. 2). Analyses were performed on the ≥63 μm size fraction on representative splits of washed residues (obtained using a precision microsplitter) containing a number of benthic foraminifera greater than or equal to 400 specimens.

Radiolarian abundance was estimated as relative percentage with respect to planktic foraminifera on a population of at least 300 specimens.

3.2. Calcareous Nannofossils

Ninety-one samples were prepared from unprocessed material as smear slides and examined using a light microscope at ~1250X magnification. Samples for calcareous nannofossil analysis have been collected both from segment A (at spacing variable from 2.0m to 0.5 m) and B (at spacing variable from 0.5 m to 0.05 m, Table S2) to preliminarily characterize biostratigraphically the entire section and to evaluating the abundance and the state of preservation of the calcareous nannofossil assemblages. The presence or absence of index species was assessed by mean of quantitative and semiquantitive countings following the methods developed by Thierstein et al. (1977), Backman and Shackleton (1983), Rio et al. (1990a), and Gardin and Monechi (1998). Specifically, (1) the abundance of selected species was calculated taking into account at least 300 specimens; (2) a prefixed number of taxonomically related forms was counted, e.g., 100 sphenoliths; (3) index species were counted in a prefixed area (1mm2); and (4) specimens of rare but biostratigraphically useful species (i.e., discoasterids and *Tribrachiatus*) were counted in an area of about 6–7 mm^2, which is roughly equivalent to three vertical traverses.

Calcareous nannofossil zonations are according to Okada and Bukry (1980) and Agnini et al. (2014).

3.3. Magnetostratigraphy

The magnetic mineralogy and rock-magnetic properties of the Paleogene sediments of the Belluno Basin have been extensively investigated by Dallanave et al. (2009, 2010, 2012a, 2012). In particular, detailed paleomagnetic and rock-magnetic study of the lower Eocene

sediments of the Cicogna section (Dallanave et al.,2009, 2010) revealed that the dominant magnetic mineral is detrital hematite, which coexist with minormaghemite. The occurrence of magnetite is limited to gray-greenish levels and spots of early diagenetic origin, commonly associated with bioturbation.

We collected a total of 46 paleomagnetic core samples across 13 stratigraphic meters of the Terche section (Fig. 2, segment B). Samples were drilled with a gasoline-powered drill and oriented with a magnetic compass. From each core we obtained a standard ~11 cm3 specimen for paleomagnetic directional analyses. All the oriented specimens were thermally demagnetized up to 675°C with steps of 50°C, reduced to 25°C from 500°C onward. The natural remanent magnetization (NRM) was measured after each demagnetization stepusing a 2-G Enterprises superconducting magnetometer placed in a shielded room at the Paleomagnetic laboratory of the Ludwig-Maximilians University (Munich, Germany). The component structure of the NRM was examined by means of vector endpoint demagnetization diagrams (Zijderveld, 1967), and the principal component analyses of Kirschvink (1980) have been applied on linear segments of the demagnetization paths to isolate the NRM components. Mean directions and associated confidence limits were calculated using thespherical statistics of Fisher (1953). Directional analyses have been performed with the PaleoMag software compiled by Jones (2002). Scattered magnetic component directions have been generally isolated from room temperature up to ~200°C. After the removal of this spurious component, a characteristic remanent magnetization (ChRM) component of the NRM linearly trending to the origin of the demagnetization axes has been isolated up to 600–675°C in 70% (32/46) of the specimen.

3.4. Stable Isotope and CaCO$_3$ Analyses

Bulk carbon and oxygen stable isotopes and CaCO3 analyses were performed on 150 samples collected from −10.90 m to +11.37 m (segment B; Fig. 2) with a mean spacing of 20 cm. The sample spacing was increased (2–10 cm) across the MUs. Stable isotope analyses were carried out with an automated continuous flow carbonate preparation GasBench II device (Spötl and Vennemann, 2003) and a Thermo Electron Delta Plus XP mass spectrometer at the IAMC-CNR isotope geochemistry laboratory of Naples. The acidification of the samples was performed at 50°C. An internal standard (Carrara Marble with $\delta^{18}O$ = − 2.43‰versus Vienna Pee Dee Belemnite and $\delta^{13}C$ = 2.43‰versus VPDB) was run every six samples, and the NBS19 international standard was measured every 30 samples. Standard deviations of carbon and oxygen isotope measures were estimated to be 0.1 and 0.08‰,

respectively, on the basis of ~200 samples that were measured three times. All of the isotope data are reported in δ‰ versus VPDB.

CaCO₃ content was measured with the electronic gas volumetric GEO-RS Calcimeter (analytical precision of± 0.2%) at the University of Ferrara. All the samples were dried, crushed, and then pulverized. Calcimetric analyses were performed on 0.50 g (±0.001 g) of pulverized samples through the reaction deriving from the treatment with 5ml hydrochloric acid solution (HCl) diluted to 10%. Carbonate weight percentage was obtained as a function of the increase in pressure due to the release of carbon dioxide (CO_2), according to the following relation: $CaCO_3 + 2HCl \rightarrow Ca + 2Cl + H2O + CO_2$. Every 10 determinations the instrument was calibrated using 0.500 g of pure Carlo Erba RPE calcium carbonate powder as standard.

3.5. Dissolution and Calcareous Plankton Preservation Proxies

Hyperthermals are frequently associated with dissolution of deep-sea carbonates due to the rise of the CCD/lysocline (e.g., Zachos et al., 2005; Stap et al., 2009). Planktic foraminiferal tests tend to break into fragments as they dissolve whereas benthic foraminifera are less prone to dissolution (e.g., Berger, 1970, 1973;Bé et al., 1975; Hancock and Dickens, 2005; Leon-Rodriguez and Dickens, 2010; Nguyen and Speijer, 2014). Dissolution can therefore modify the composition of the planktic foraminiferal assemblages (e.g., Berger,1970; Bé et al., 1975; Thunell and Honjo, 1981; Petrizzo et al., 2008; Nguyen et al., 2009, 2011).

In order to assess possible carbonate dissolution effects we adopted here three different proxies based on foraminifera:

1. *The fragmentation index (F index)*. The *F index* was calculated following Berger (1970) and Petrizzo et al.(2008) as the ratio between fragments or partially dissolved planktic foraminiferal tests versus entire tests on ~ 300 individuals. Fragmented foraminifera include specimens showing notable deterioration, missing chambers, and substantial breakage.

2. *The planktic over benthic ratio (P/B)*. The *P/B*, usually adopted with some cautions for paleobathymetric estimations (e.g., Murray, 1976; Van der Zwaan et al., 1990), can be also applied as a dissolution index in absence of significant bathymetric variations. The *P/B* index was calculated on ~300 specimens and is here expressed as 100*P/(P + B).

3. *The weight percent coarse fraction (WPCF)*. The *WPCF* was obtained from the ratio of the dry washed residue (≥38 μm size fraction) to the bulk dry sediment (Hancock and Dickens, 2005). In pelagic sediments not affected by dissolution, the *WPCF* can give

indication about planktic foraminiferal productivity (Hancock and Dickens, 2005). However, the *WPCF* can be largely controlled by dissolution of planktic foraminifera as well, which is strongly coupled to the depth of the regional lysocline (e.g., Berger et al., 1982).

Calcareous nannofossil assemblages can be altered as well by dissolution that can selectively affect the different genera and species (e.g., Adelseck et al., 1973; Bornemann and Mutterlose, 2008; Dedert et al., 2012,2014). The calcareous nannofossil assemblages influenced by dissolution show low number of species accompanied by high abundances of dissolution-resistant taxa (Bornemann and Mutterlose, 2008). The genus *Toweius* is one of the most fragile forms among the early Paleogene taxa (e.g., Dedert et al., 2012). In particular, dissolution first affects the delicate structure of the central area of *Toweius*, thus preventing the identification of the different species. On the contrary, *Discoaster* has been considered as a dissolution-resistant taxon (e.g.,Adelseck et al., 1973; Rio et al., 1990b; Agnini et al., 2007a). A further aspect influencing the calcareous nannofossil preservation is related to the diagenesis that can induce overgrowth (e.g., MacKenzie and Wise, 1983; Dedertet al., 2014).

In order to evaluate the effects of carbonate dissolution and overgrowth on the calcareous nannofossil assemblages at Terche we have applied the following proxies:

1. *The species richness (diversity)*. Species richness is influenced, besides evolution, by both dissolution and overgrowth. Considering that no major turnovers in calcareous nannofossils are documented across the stratigraphic interval here investigated, low number of species can indicate strong dissolution/overgrowth and vice versa.

2. *Qualitative estimate of etching (Q_E) based on the modified scales from Roth and Thierstein (1972) and Roth (1983)*. Here we assess five degrees of etching on the basis of the coccolith outline preservation, the state of delicate structures, and the abundance of small placoliths that are considered as highly dissolution prone (Adelseck et al., 1973) (Table S1.1).

3. *Qualitative estimate of five degrees in overgrowth (Q_O) according to a modified scale from Dedert et al. (2014) (Table S1.2)*. These degrees refer to the specimen thickness and to the differences of the coccolith surfaces from those biogenically sculpted.

4. *The relative percentage of the Toweius species with central area well preserved versus the total Toweius, included the unrecognizable specimens of this genus, i.e., the forms where the central area preservation does not allow the species identification ($T_{species}$)*. High values of the proxy indicate absence of dissolution or slight dissolution. On the contrary, low values suggest strong dissolution.

5. *The relative percentage of Toweius over that of Discoaster (T/D)*. This ratio is introduced here as proxy of dissolution. High values of *T/D* suggest low degree of dissolution and vice versa.

4. Results

4.1. Calcareous Plankton Biostratigraphy

Calcareous plankton is abundant and well diversified in all the samples investigated. Planktic foraminifera at the segment B of Terche are relatively well preserved, though recrystallized and partially filled by calcite, thus allowing the identification at the species level. The main planktic foraminiferal event recorded is the base (B) of *Morozovella formosa* that identifies the boundary between the Zones E3/E4 (Wade et al., 2011) at -4.70 ± 0.40 m (Fig. 2). The zonal marker is quite rare at the level of its appearance. The B of *Morozovella aragonensis* that marks the E4/E5 zonal boundary was not recorded in the studied interval.

All the calcareous nannofossil marker species used to define the zonal boundaries of Okada and Bukry (1980) and Agnini et al. (2014) are present. The entire Terche section encompasses the Zones CNP7 to CNE3 of Agnini et al. (2014) and CP4 to CP10 of Okada and Bukry (1980) (Fig. 2). Nannofossils are generally well diversified, and their preservation ranges from poor to moderate, with variable degrees of overgrowth and recrystallization. Reworked forms are rare, except for the CMU at the Thanetian-Ypresian boundary and for the Ypresian MUs belonging to the segment B where reworked Cretaceous specimens become common to abundant. The segment B of Terche section spans Zones CP8 to CP10 of Okada and Bukry (1980) and Zones CN2 to CN3 pars of Agnini et al. (2014). The main calcareous nannofossil biohorizons are described below in stratigraphic order, from the oldest to the youngest (Fig. 2); their relative abundances are shown in Fig. S2 and Table S2. The relative abundances of species markers of segment A are shown in Fig. S3 and Table S2.
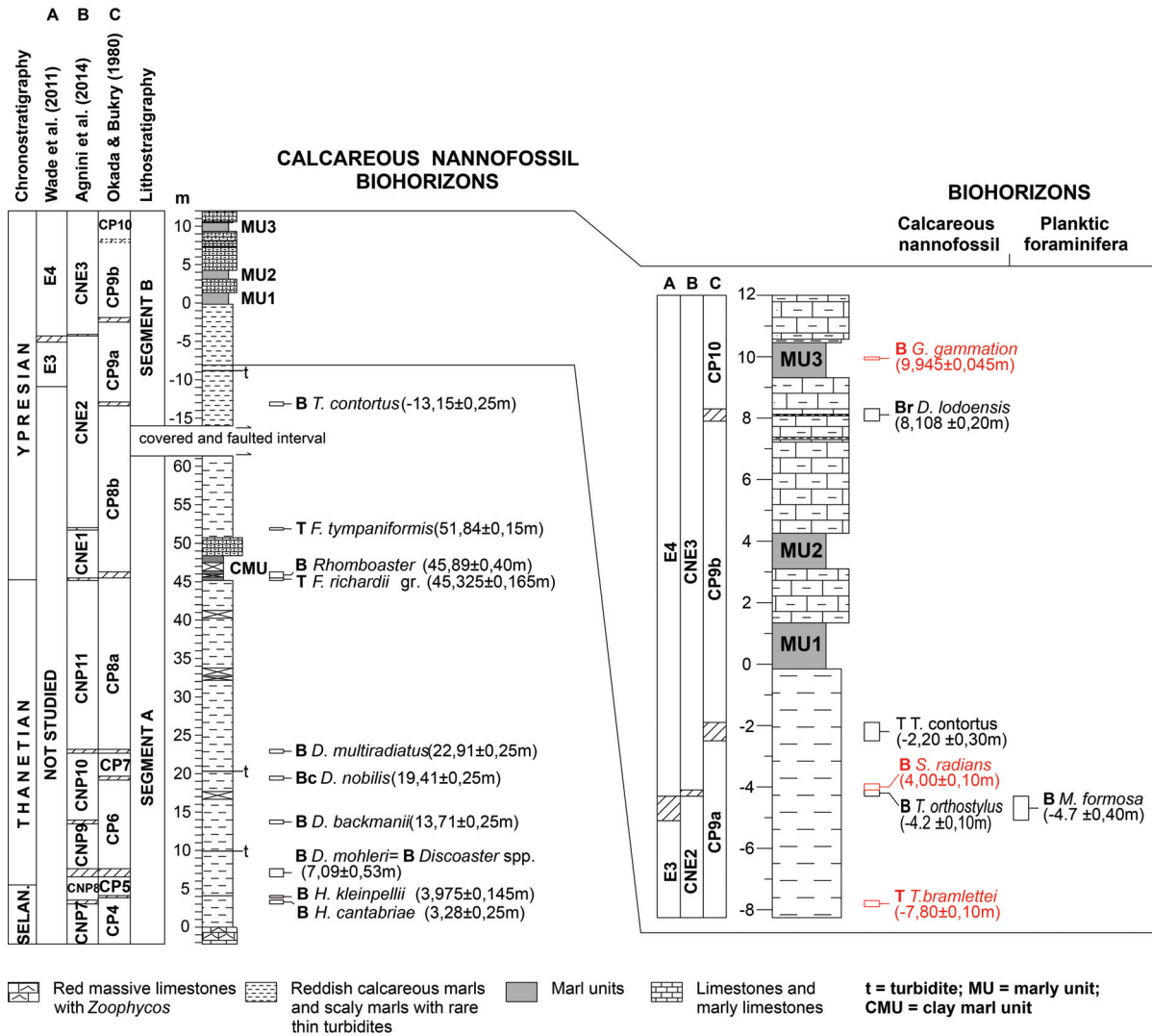
Figure 2. Stratigraphic log of the entire Terche section with the close-up of the segment B focus of this study. Level 0mcorresponds to the level with the lowest CaCO$_3$ value within MU1 (see Fig. 4). Planktic foraminiferal and calcareous nannofossil main (in black) and secondary (in red) biohorizons are shown and discussed in the text, together with the zonal attribution according to Wade et al. (2011), for the former, and Agnini et al. (2014) and Okada and Bukry (1980) for the latter. The unfilled rectangle near the biohorizons indicates the uncertainty derived from the sample spacing. The same uncertainty is represented in the zonal scheme columns by the striped bands. In the next figures representing the studied segment, the zonal boundaries are placed at the middle level between two successive samples. The abundances of calcareous nannofossil zonal markers are given in Figure S2.

1. *Base of Tribrachiatus contortus*. The B of *T. contortus*, at −13.15 ± 0.25 m, defines the lower boundary of Zone CP9a (Okada and Bukry, 1980). *T. contortus* shows a discontinuous distribution, and it is very rare in its initial range. A marked increase in abundance of the species occurs at −10.10 ± 0.10 m.

2. *Base of Tribrachiatus orthostylus* and top (T) of *T. contortus*. The B of *T. orthostylus* marks the lower boundary of Zone CNE3 at −4.2 ± 0.10 m. The increase of this species occurs

concomitantly with the decrease of *T. contortus*, the disappearance of which, at –2.2 ± 0.30 m, identifies the CB9a-CP9b boundary (or base of NP11), consistently with previous data (Agnini et al., 2007, and references therein; Dallanave et al., 2009; Agnini et al., 2014).

3. *Base rare (Br) of Discoaster lodoensis*. The appearance of *D. lodoensis* is used to mark the base of Zones NP12 and CP10 (Martini, 1971; Okada and Bukry, 1980). In the studied material, *D. lodoensis* appears with rare teratological morphotypes (seven and eight-rayed specimens) within Zone CNE3 in agreement with Agnini et al. (2014). This rare presence allows us to determine the Br of *D. lodoensis* that probably corresponds to the B of *D. lodoensis* according to Martini (1971) and Okada and Bukry (1980).

We highlight in Fig. 2 the following supplementary events: T of *Tribrachiatus bramlettei*, B of *Sphenolithus radians*, and B of *Girgisia gammation*. The position of the two first events is in good agreement with previous studies (e.g., Agnini et al., 2006, 2007; Dallanave et al., 2009). In particular, the B of *S. radians* virtually coincides at Terche with the B of *T. orthostylus* at CNE2-CN3 boundary. Our data substantiate that the B of *G. gammation* is a useful event to subdivide Zone CP9b (Agnini et al., 2006, 2007, 2014; Dallanave et al., 2009).

4.2. Magnetostratigraphy

At Terche, the intensity of the NRM ranges from 1.08×10^{-4} to 1.14×10^{-3} Am^{-1}, with an average value of 3.03×10^{-4} Am^{-1} (Fig. 3), in agreement with the data from the coeval part of the Cicogna section (Dallanave et al., 2009, 2010, 2012). The unblocking temperature indicates a magnetization carried by hematite, in agreement with the results obtained from the Cicogna section sediments. The ChRM directions are organized in two modes oriented north down and south up (Fig. 3 and Table 1), which shallow of 19° after correction of a homoclinal 19° bedding tilt dipping 356°E. In tilt corrected coordinates the two modes depart from antipodality of 13.8°, failing the reversal test performed using the procedure of Watson (1983) ($V_w = 12.0$, $V_{critical} = 6.4$). Inverting all ChRM directions to a common north down pointing polarity, we obtained the tilt-corrected mean direction indicated in Table 1.

We determined the virtual geomagnetic pole (VGP) position associated to each ChRM direction. The latitude of the VGPs, relative to the mean paleomagnetic North Pole has been used to interpret the magnetic polarity stratigraphy (Lowrie and Alvarez, 1977; Kent et al., 1995). Positive and negative relative VGP latitudes have been interpreted as reflecting, respectively, normal and reverse magnetic polarity. These data, together with the declination
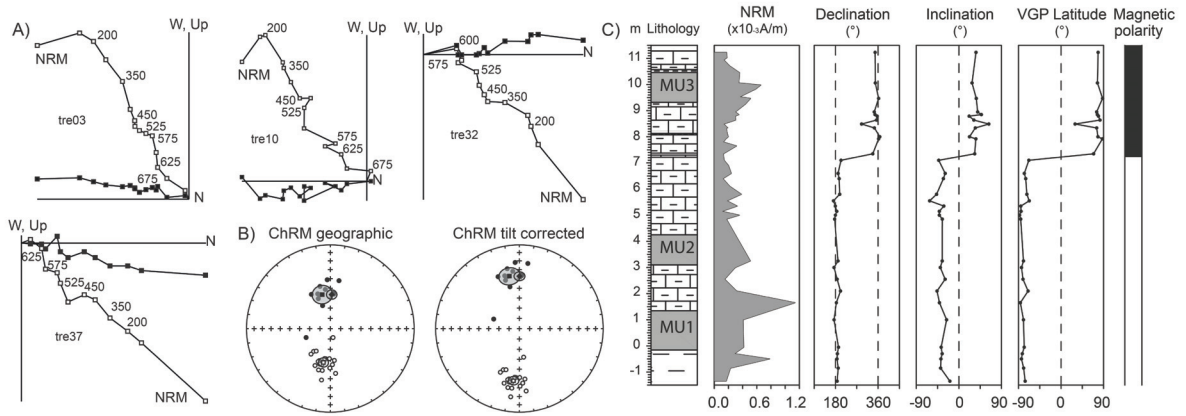
Figure 3. Paleomagnetic results from the Terche section. (a) Representative vector end-point demagnetization diagrams for the Terche specimens, plotted in geographic coordinates. Open (closed) squares represent vector end-point projections onto the vertical (horizontal) plane. Demagnetization steps are in °C. (b) Equal area projection of the characteristic remanent magnetization (ChRM) directions in geographic (left) and tilt-corrected (right) coordinates; black (white) data represent down (up) pointing directions. Black and white squares are average directions plotted with the associated α_{95} cone of confidence. Black diamonds are the average directions, with associated α_{95} cone of confidence, obtained inverting all ChRM directions on a common north pointing polarity. (c) Magnetic polarity stratigraphy of the Terche section. From left to right, lithostratigraphy and thickness, intensity of the natural remanent magnetization (NRM), declination and inclination of the characteristic remanent magnetization (ChRM) directions in tilt-corrected coordinates, virtual geomagnetic poles (VGP) latitude, and derived magnetic polarity stratigraphy; black and white bands represent, respectively, normal and reverse magnetic polarity zones. For lithological symbols see Fig. 2.

Table 1. ChRM directions from the Terche section[a]

N	MAD	Geographic coordinates					Tilt-corrected coordinates			
		k	α_{95}	DEC	INC		k	α_{95}	DEC	INC
		Normal polarity directions								
12	14.1±5.4	20.5	9.4	346.8	55.5		20.7	9.3	349.3	36.2
		Reverse polarity directions								
20	7.3±6.7	49.8	4.7	191.4	-56.0		51.8	4.6	186.5	-37.4
		Reverse and normal polarity directions								
32	9.9±7.0	28.6	4.8	2.3	56.4		29.2	4.8	0.1	37.3

[a]Characteristic remanent magnetization (ChRM) directions from the Terche section. N = number of specimens; MAD = maximum angular deviation (deg); k = Fisher (1953) precision parameter of the mean ChRM direction; α_{95} = Fisher (1953) confidence angle (deg) of the mean ChRM direction; and DEC and INC = declination and inclination of the mean ChRM directions.

and the inclination of the ChRM directions, are shown in Figure 3. The Terche section is characterized by reverse magnetic polarity up to 7.23m and by normal magnetic polarity stratigraphically upward. Integration with biostratigraphic data allows us to correlate this level with the C24r-C24n.3n Chron boundary (Fig. 3).

4.3. CaCO$_3$ and Stable Isotope Record

The CaCO$_3$ Terche record is characterized by a slight increasing trend upward (from mean values of 55% to 64%) interrupted by three major drops corresponding to MUs (Fig. 4 and Table S3). The minimum contents of 21%, 40%, and 37% are reached at +0.08 m, +3.5 m, and +9.43 m, respectively. In parallel with the carbonate drops three negative CIEs are recorded. The stratigraphically lower two shifts (~0.5‰) occur at +0.2 m and +3.8 m in the uppermost part of Chron C24r. The third ~0.5‰CIE is recorded at +9.3 m within the base of sub-Chron C24n.3n (Fig. 4 and Table S3). The δ^{13}C of the studied section records a number of wiggles that are not associated with lithological changes (Fig. 4 and Table S3). By providing a three-point running average of the carbon isotope data, single-overprint outliers are dampened. A rather pronounced negative change of ~0.5‰in the δ^{13}C profile is located at ~ –2.10 m. This shift has been observed at the same stratigraphic position at the nearby Cicogna section (Agnini et al., 2016) and at the ODP Sites 1262 and 1265 (Stap et al., 2010b). The δ^{18}O values widely fluctuate in the intervals comprised from –8.10 m to –2.50 m (–6.97‰to –2.05‰) and from +6.5 m to +11.4 m (–6.16‰ to –1.03‰). Less pronounced variations are recorded from –2.30 m to +6.30m where the δ^{18}O show a mean increase since values oscillate between –3.08‰ and –0.79‰.

4.4. Variation in Dissolution Proxies

The *F index* displays generally low background values close to 10%. A moderate increase in fragmented foraminiferal tests occurs within the MUs, up to ~29% (MU1 and MU2) and 25% (MU3), close to the negative peaks in δ^{13}C and the CaCO$_3$ % drops (Fig. 4 and Table S4). According to our qualitative evaluation, partly dissolved and fragmented planktic foraminiferal tests appear proportional to the genera percentages with no dominance of a particular genus. The *WPCF* at Terche varies between 1% and 8%. The most evident fluctuations are recorded within the MU1 where the *WPCF* shows the minimum value. The
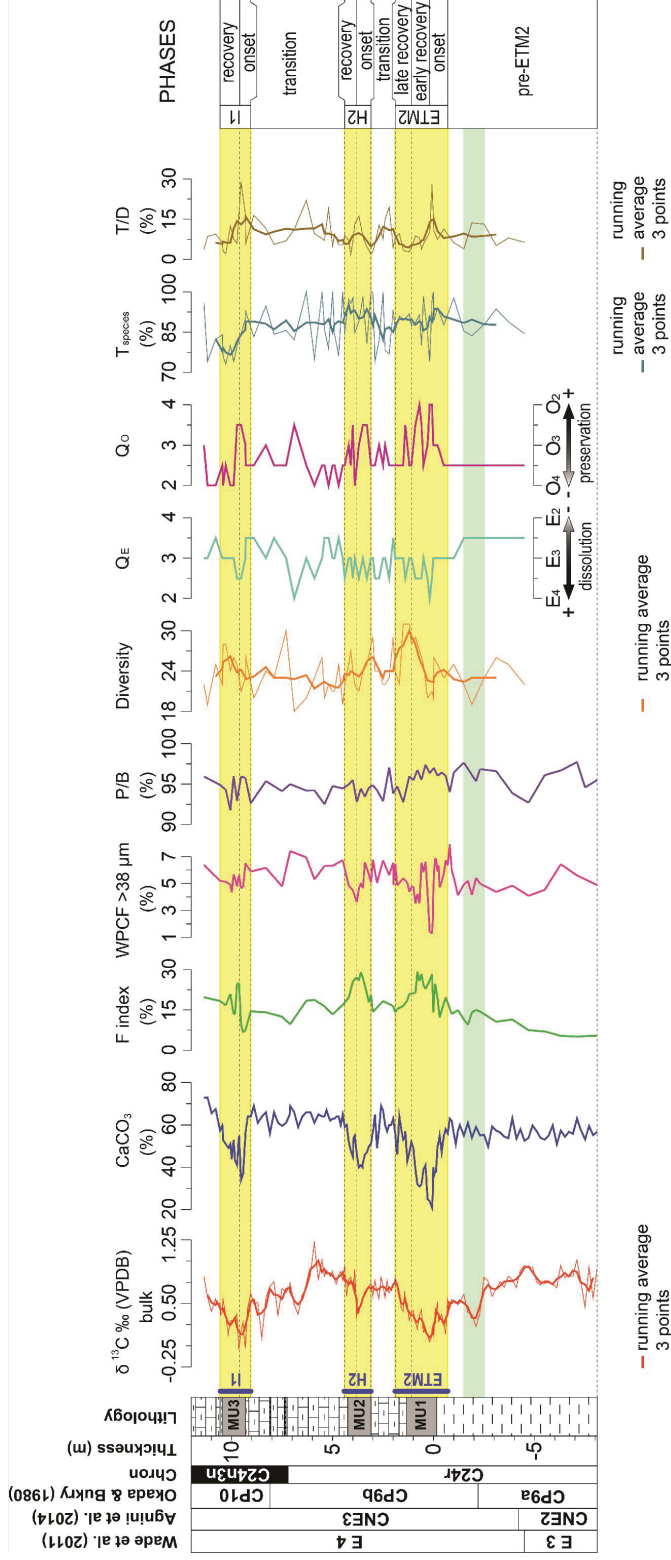
Figure 4. Curves showing the foraminiferal dissolution proxies and the calcareous nannofossil indices for dissolution and preservation (see text for adopted methods and discussion) plotted against the carbon stable-isotope record and the percentage of $CaCO_3$ at the Terche section. The foraminiferal dissolution proxies are the following: fragmentation index (*F index*), weight percent coarse fraction (*WPCF*), and plankton benthos ratio (*P/B*). The calcareous nannofossil dissolution indices are the following: species richness (*diversity*), qualitative estimation of etching (Q_E), relative percentage of the *Toweius* species with central area well preserved ($T_{species}$) versus all the species of *Toweius* (included the forms unrecognizable at species level), and *Toweius* (dissolution prone) *Discoaster* (dissolution resistant) ratio (*T/D*). The qualitative estimation of overgrowth (Q_O) is considered as a preservation proxy (see text). The yellow bands highlight the ETM2, H2, and I1 intervals as defined by the carbon cycle perturbations and expressed through the $\delta^{13}C$ shifts. We distinguish here 10 phases on the basis of the $\delta^{13}C$ curve variations. Pre-ETM2: interval below the negative CIE onset (from -8.1 m to -0.7 m). ETM2 onset: interval between the ETM2 CIE base and the level of the most negative $\delta^{13}C$ peak (from -0.7 m to $+0.2$ m). ETM2 early recovery: interval comprised between the ETM2 CIE peak to $+1.1$ m level. ETM2 late recovery: interval between $+1.1$ m level and ETM2 CIE top, i.e., the level where the $\delta^{13}C$ curve returns to the pre-excursion values ($+1.9$ m). Similarly, we identify the onset of the H2 and I1 as corresponding to the interval between the base of the H2 and I1 CIEs and the levels of the most negative peaks (respectively, from $+3.1$ m to $+3.8$ m and from $+9.0$ m to $+9.6$ m). Due to the lower thickness of the interval corresponding to the H2 and I1 CIEs, we distinguish a unique recovery phase for each event (from $+3.8$ m to $+4.4$ m and from $+9.6$ m to $+10.6$ m, respectively). Transitions between the ETM2-H2 and H2-I1: intervals of the $\delta^{13}C$ curve comprised between the negative shifts linked to the events (from $+1.9$ m to $+3.1$ m and $+4.4$ m to $+9.0$ m). The light green band underlines a pre-ETM2 minimum in carbon stable isotopes (see text). For lithological symbols see Figure 2.

38

P/B records minor fluctuations around the value of 95% ranging between 91% and 98.5% (Fig. 4 and Table S4). The calcareous nannofossil *diversity* index (Fig. 4 and Table S4) varies from 31 to 18 with a median of 24. Changes in the *diversity* curve are not directly correlated with the carbonate content and $\delta^{13}C$ curves. The lowest values (18–19 taxa) are indeed not associated with $CaCO_3$ and/or $\delta^{13}C$ minima (Fig. 4 and Table S4). The Q_E curve (Fig. 4) shows throughout values that generally correspond to moderately dissolved coccoliths ($Q_E \sim$ 3). A heavily etched assemblage (Q_E 2, Plate S1) has been observed at the MU1 in coincidence of *F index* and *WPCF* variations at the $\delta^{13}C$ negative peak. Overgrowth did not severely affect the Terche calcareous nannofossil assemblages that appear even best preserved within the MUs (Q_O; Fig. 4, Table 4, and Plate S1). A slight deterioration, though not steady, occurs in two segments of the upper part of the section (from +3.9 m to +5.9 m and from +9.9 m to +11.2 m). The $T_{species}$ curve shows high values fluctuating from 100% to ~75% with a mean of ~90%. In order to better highlight the general pattern a three-point running average of the $T_{species}$ has been performed (Fig. 4 and Table S4). Decreases of $T_{species}$ values are recorded within the MU1 and MU3 whereas across the MU2 the running average profile highlights a slight increase. The *T/D* curve displays mean values of 9% with peaks of ~ 30% at the MU1 and MU3.

4.5. Changes in Foraminiferal Assemblages and Radiolarian Abundance

The early Eocene genera typical of subtropical-temperate latitudes are represented at the Terche section (Fig. 5 and Table S5). The mixed-layer dwelling warm-index acarininids and morozovellids and the thermocline-dwelling cold-index subbotinids (e.g., Boersma et al., 1987; Pearson et al., 1993, 2006) are the most abundant forms with a mean respective abundance of 45%, 35%, and 20% (Fig. 5). The mean relative abundance of acarininids shows a long-term increase from the base to the top of the section. This is superimposed to the major fluctuations recorded within the MUs (Fig. 5). The acarininid highest abundance (68%) is recorded close to the top of the MU1 at +1.2 m. Prominent peaks are recorded also within the MU2 and MU3 (~56%). These marked increases are associated with a slight reduction in acarininid test size, with specimens becoming very rare to absent in the >300 μm size fraction. Subbotinid abundance fluctuates in antiphase with acarininids. Within this
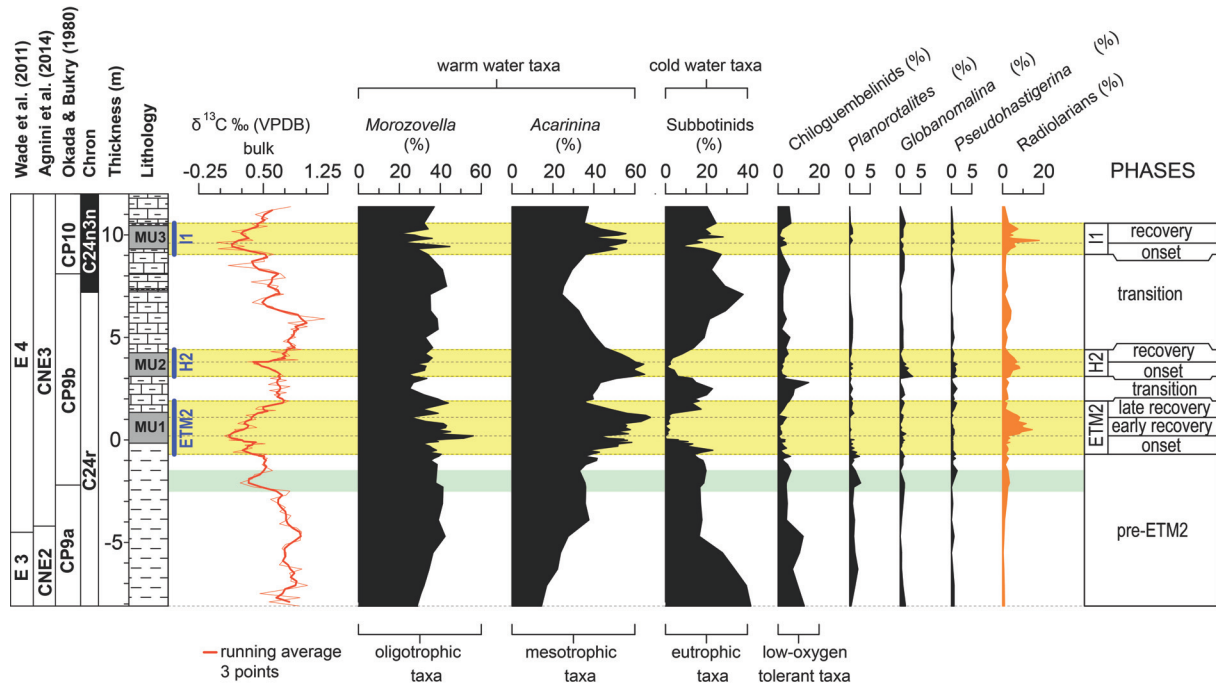
Figure 5. Changes in relative abundance of planktic foraminiferal genera (≥63 μm fraction) across the analyzed segment of the Terche section, plotted against carbon stable isotopes, biomagnetostratigraphy and radiolarian abundance. The *Subbotina* group includes, beside *Subbotina*, the ecologically similar genera *Parasubbotina*, *Paragloborotalia* and *Globorotaloides* (e.g., Pearson et al., 2006). Chiloguembelinids include the genera *Chiloguembelina* and *Zeauvigerina*. The yellow bands highlight the ETM2, H2, and I1 intervals expressed by the $\delta^{13}C$ negative shifts. We identify 10 phases on the basis of the $\delta^{13}C$ curve variations (see Fig. 4 and discussion in the text). The light green band underlines a minimum in carbon stable isotopes (see discussion in the text). For lithological symbols see Figure 2.

group, the genus *Subbotina* is dominant whereas *Parasubbotina*, *Paragloborotalia*, and *Globorotaloides* constitute all together minor components throughout. Subbotinid strong reductions in relative abundance or even virtual absence are recorded within the MUs (Fig. 5). Specifically, within the MU1 subbotinids record the lowest mean value of the entire section (~1.6%), and they temporarily disappear in coincidence of the maximum negative $\delta^{13}C$ peak recorded at + 0.2 m. A marked drop in subbotinids is documented within the MU2 as well, where their abundance is reduced to ~1%. The MU3 records a less pronounced decrease in subbotinids (8%), but their lowest percentages again coincide with the lowest $\delta^{13}C$ values. Morozovellid abundance records less marked changes. Within the MUs, this group displays brief positive peaks that are particularly evident at the base of MU1 and MU3 (56% and 45%, respectively), followed by moderate decreases in abundance. Their rapid increase at the base of MU1 coincides with a significant decrease in test size, with specimens becoming virtually absent in the >250 μm size fraction, while dominating the fraction comprised between 150 μm and 250 μm. Chiloguembelinids at Terche present generally low abundances, having mean values of ~4% throughout the section (Fig. 5 and Table S5) and are mostly represented by

Chiloguembelina with respect to *Zeauvigerina*. Relatively higher values (12%) characterize the basal portion of the section, up to –4.70 m, and a slight increase (up to 15%) is recorded below the MU2. Variations of chiloguembelinids, though characterized by small percentages, mimic the changes in the subbotinid abundance. *Planorotalites*, *Globanomalina*, and *Pseudohastigerina* are very rare in the assemblages throughout the section. Each of them never exceeds the 3% in abundance and does not display significant variations within the MUs (Fig. 5).

The benthic foraminiferal assemblage at the Terche section is strongly dominated by calcareous forms (~95% of the total). Preservation is generally good to moderate, and it improves within the marls cropping out between –8 and 0 m. Bolivinids are the most abundant forms throughout the studied interval, in particular, *Bolivinoides crenulata* (~30%) and smooth walled *Bolivina* (~20%), similarly to what is observed at the neighboring Farra, Alano, and Forada sections (Agnini et al., 2009; Boscolo Galazzo et al., 2013; Giusberti et al., 2016). *Cibicides* spp. are also common at Terche (15–20%) and are the dominant epifaunals.

Radiolarians are generally scarcely represented at the Terche section (mean value around 2%), except for temporary increases observed across the MUs (Fig. 5). Radiolarian peaks in abundance occur above the CIEs minima. Specifically, they reach the highest percentages within the MU1 (14.5%, +50 cm) and MU3 (17.9%, +9.73 m), while a minor peak (8.5%, +3.50 m) is recorded within the MU2 (Fig. 5). In the studied interval, radiolarians are generally represented by taxa belonging to the spumellarians; however, also nassellarians occur within the MU1 and MU3.

4.6. Changes in Calcareous Nannofossil Assemblages

Within the segment B of the Terche section, the calcareous nannofossil assemblage is dominated by *Toweius*, *Coccolithus pelagicus*, and *Sphenolithus* (mean abundance of ~20% for each taxon). *Prinsius* and *Zygrhablithus* account for the 8% and 15% respectively. The genera *Chiasmolithus*, *Discoaster*, *Ericsonia*, *Tribrachiatus*, and the calcareous dinocyst *Thoracosphaera* are minor components with an overall average abundance of ~8% (Fig. 6 and Table S6).

Calcareous nannofossil assemblages show four major transient and striking modifications that are constrained by the main negative $\delta^{13}C$ shift (Fig. 6). The lowest change is observed in coincidence to the negative $\delta^{13}C$ shift at –2.10 m. Specifically, a significant increase of *Prinsius*, *Sphenolithus*, *Zygrhablithus bijugatus*, and *Thoracosphaera* occurs along with a
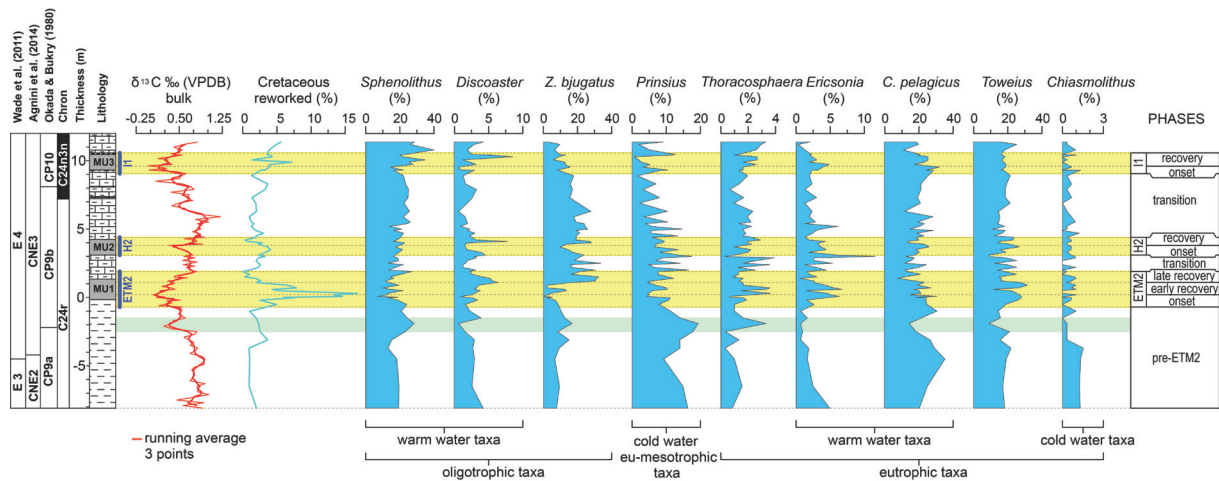
Figure 6. Changes in relative abundance of selected calcareous nannofossil genera and species across the studied segment of the Terche section plotted against carbon stable isotope curve, biomagnetostratigraphy, and percentage of reworked Cretaceous nannofossil taxa. The yellow bands highlight the ETM2, H2, and I1 intervals as expressed by the $\delta^{13}C$ negative shifts. We identify 10 phases on the basis of the $\delta^{13}C$ curve variations (see Figure 4 and discussion in the text). The light green band underlines a minimum in carbon stable isotopes (see discussion in the text). For lithological symbols see Figure 2.

drop of *Discoaster*, *Ericsonia*, *Toweius*, and *Coccolithus pelagicus* (Fig. 6). Across the three MUs are recorded the other marked modifications. These include an increase in the relative abundance of Cretaceous reworked taxa that is particularly marked at the MU1 (up to 17%). The distribution pattern of reworked forms mirrors the profile of the CaCO$_3$ % and $\delta^{13}C$ curves (Fig. 6). Concomitantly with the peaks in Cretaceous specimens, the taxa considered as oligotrophic, such as *Discoaster*, *Sphenolithus*, and *Z. bjiugatus* (e.g., Wei and Wise, 1990; Gibbs et al., 2004, 2006; Dunkley Jones et al., 2008; Kahn and Aubry, 2004; Tremolada and Bralower, 2004; Villa et al., 2008; Agnini et al., 2006, 2007a, 2009), decrease their abundance (Fig. 6). In parallel, the genera *Thoracosphaera*, *Ericsonia*, *Toweius*, and, subordinately, the species *C. pelagicus* increase significantly their percentage. These latter forms are known as meso/eutrophic indices (e.g., Perch-Nielsen, 1981; Fornaciari et al., 2007; Agnini et al., 2006, 2007a, 2009; Dedert et al., 2012; Tremolada and Bralower, 2004). The oligotrophic *Discoaster* and *Z. bijugatus* display a marked recovery in abundance in the upper MUs, with the exception of MU3 for *Z. bijugatus*. The genus *Prinsius* shows a slight general decrease throughout. *Sphenolithus* records minor changes throughout the section and displays a marked decline in abundance only within the MU1 (Fig. 6).

5. Discussion

5.1. Stable Isotopes at the Terche Section: Reliability and Stratigraphy

The carbon isotope signal shows general trends very similar to those previously recorded by coeval bulk δ^{13}C profiles (e.g., Cramer et al., 2003; Lourens et al., 2005; Nicolo et al., 2007; Stap et al., 2009, 2010a; Galeotti et al., 2010). This is a robust indication that the carbon isotope signature has not been considerably affected by meteoric or burial diagenesis (e.g., Marshall, 1992; Frank et al., 1999). Our biomagnetostratigraphic data allow us to correlate the negative CIEs associated with MU1, MU2, and MU3 to the three post-PETM events ETM2, H2, and I1. Note that the CIEs span stratigraphic intervals larger than the thickness of the MUs (Fig. 4). Here we consider the base of the ETM2, H2, and I1 events as coinciding with the onset of the respective negative δ^{13}C shifts. Similarly, the top of the events is related to the levels where the δ^{13}C profile returns to the pre excursion values (Fig. 4).

The absolute size of the ETM2 δ^{13}C negative shift is lower if compared to literature data (Cramer et al., 2003; Lourens et al., 2005; Nicolo et al., 2007; Stap et al., 2009, 2010a; Galeotti et al., 2010). We hypothesize that the original δ^{13}C signal was partially biased in our section by the huge input of reworked Cretaceous calcareous nannofossils (~17%), which presumably subdued the bulk sediment amplitude of the ETM2 CIE, and in a minor way, of the I1 CIE. A similar situation has been observed in the nearby Forada section where the CIE of the PETM is ~0.5‰ higher than other marine bulk carbonates (Giusberti et al., 2007). The interpretation of the bulk carbonate isotope data may also be compromised by variations in diagenetic alteration among lithologic levels. However, the δ^{13}C versus δ^{18}O cross plot (Fig. S4) displays a low correlation (R^2 = 0.014) between the two signals. This supports the hypothesis of a conservative behavior of the carbon isotope values in the studied samples that we consider as mainly reflecting changes in the isotopic composition of global oceanic carbon reservoir (e.g., Marshall, 1992).

Differently from the δ^{13}C curve, the δ^{18}O general profile is not consistent with the early Eocene oxygen isotope curves. Absolute δ^{18}O values, which scatter between –6.97‰ and –0.79‰ (Table S3), appear depleted by ~1‰ to 7‰ relatively to diagenetically unaltered marine calcite (e.g., Zachos et al., 2008). This offset can be explained as reflecting elevated
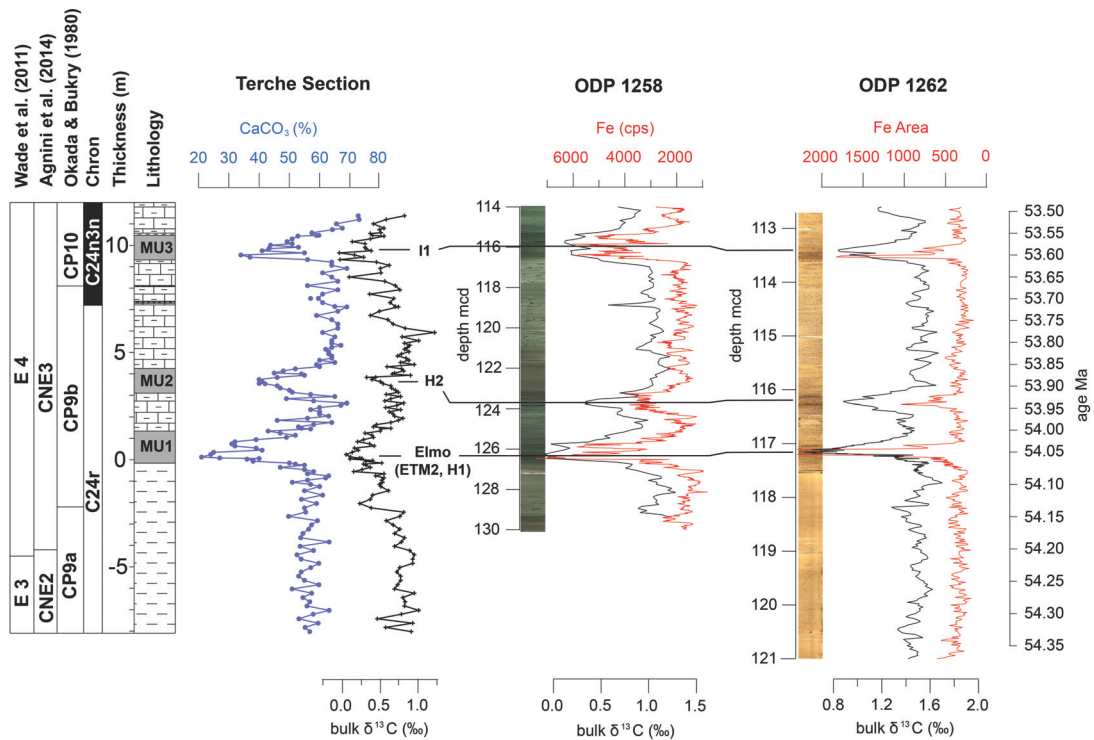
Figure 7. Correlation of the Terche section record to the ODP Site 1258 and 1262. From left to right, Terche section lithology with calcareous plankton biozonation and magnetostratigraphy; carbonate and stable carbon isotope data. For both Sites 1258 and 1262 bulk stable carbon isotope data (black line from Zachos et al., 2010; Littler et al., 2014; Kirtland-Turner et al., 2014; Westerhold et al., 2012), XRF core scanning Iron (Fe) intensity (Westerhold and Röhl, 2009; Littler et al., 2014), and the core images are plotted versus depth. The age model for Site 1258 and 1262 (Westerhold et al., 2015) is shown in the y axis on the very right; for reference the age model is given in Table 2b.

temperatures during lithification that usually enrich the isotopic composition in ^{16}O. Actually, when diagenetic processes occur well below the seafloor, where temperatures can exceed those of surface water, the $\delta^{18}O$ values of indurated limestones and marly limestone are significantly depleted in ^{18}O. Meteoric water might also have impacted our $\delta^{18}O$ record since rainwater generally has a $\delta^{18}O$ composition less than that of seawater (e.g., Marshall, 1992; Schrag et al., 1995; Frank et al., 1999).

5.2. Correlation to ODP Sites 1258 and 1262

After clear identification of the events ETM2, H2, and I1 by biomagnetostratigraphy the Terche section is correlated to the deep-sea reference records of ODP Site 1258 (Demerara Rise) and Site 1262 (Walvis Ridge), both South Atlantic. From these sites high-resolution XRF, isotopic records, and biomagnetostratigraphies are available for interbasinal correlations of the negative CIEs (Suganuma and Ogg, 2006; Agnini et al., 2007; Westerhold et al., 2007;

Table 2.1. Depth tie points Terche section to ODP 1258

Terche section level (m)	ODP 1258 depth (rmcd)
−10.90	136.42
−8.22	133.96
−5.44	131.40
−0.87	127.10
0.18	126.38
0.72	125.86
2.56	124.38
4.51	122.66
9.50	116.31
9.78	115.91
10.57	115.07
11.37	114.22

Westerhold and Röhl, 2009; Zachos et al., 2010; Kirtland-Turner et al., 2014; Littler et al., 2014). Correlation between ODP 1258 and Terche section is straightforward using the inverse XRF core scanning Fe intensity record and the CaCO$_3$ data (Fig. 7). The ETM2 event even shows the two prominent peaks with the first one having higher amplitude then the second peak. Tables 2a and 2b give the

Table 2.2. Age tie points ODP 1258

ODP 1258 depth (rmcd)	Age La2011	405-kyr Cycle ID	Source (Reference)
91.50	52.412	Ec 9	Westerhold et al. 2008; Westerhold & Röhl 2009
99.00	52.820	Ec 8	Westerhold et al. 2008; Westerhold & Röhl 2009
107.00	53.216	Ec 7	Westerhold et al. 2008; Westerhold & Röhl 2009
116.00	53.612	Ec 6	Westerhold et al. 2008; Westerhold & Röhl 2009
126.00	54.012	Ec 5	Westerhold et al. 2008; Westerhold & Röhl 2009
139.90	54.424	Ec 4	Westerhold et al. 2008; Westerhold & Röhl 2009

age-depth tie points for the correlation. Based on the depth correlation, the most up to date age model for the interval in ODP Sites 1258 and 1262 (Westerhold et al., 2015) can be transferred to the Terche section and enables to compare data on a global scale.

5.3. Paleodepth of the Terche Section

The values recorded by the *P/B* at the Terche section are greater than 90% throughout (Fig. 4). According to Van der Zwaan et al. (1990), these data suggest an average water depth of at least 1000 m. The common occurrence of *Nuttallides truempyi* and of deep-water agglutinants such as *Glomospira charoides*, *Karrerulina* spp., *Saccammina* spp., (upper depth limit at 300–500 m) (van Morkhoven et al., 1986; Speijer and Schmitz, 1998; Kaminski and Gradstein, 2005), and the common to rare occurrence of abyssal species such as *Clinapertina complanata*, *C. subplanispira*, and *Quadrimorphina profunda* (Tjalsma and Lohmann, 1983)

confirm a fully bathyal paleodepth (1000–1500 m) (van Morkhoven et al., 1986) for the entire Terche section. The occurrence of abundant cibicidids does not contrast with this interpretation, as these forms presently can live up to abyssal depths (e.g., Murray, 1991, 2006). The abundance of bolivinids in the study section is not related to the depositional depth, but it is a peculiar character of the successions deposited within the Belluno Basin. Specifically, this feature has been interpreted as an effect of lateral inputs of organic matter from the vicinity of lands and continental margins (Boscolo Galazzo et al., 2013; Giusberti et al., 2016).

5.4. Calcareous Plankton Preservation, Carbonate Dissolution, and Terrigenous Dilution linked to Enhanced Hydrological Cycle

The three foraminiferal dissolution proxies (*F index*, *WPCF*, and *P/B*; Fig. 4 and Table S4) adopted in our section ensure that the observed planktic foraminiferal changes mainly reflect responses to environmental modifications, even within the MUs, where the low $CaCO_3$ % might suggest severe carbonate dissolution. Specifically, the *F index* shows distinct lower values in correspondence to the MUs with respect to those observed in nearby sections of the Belluno Basin across the PETM and K/X event (Luciani et al., 2007; Agnini et al., 2009). The *P/B* index does not display any significant variation throughout the section, clearly indicating that there is no preferential dissolution of planktic tests with respect to the benthic shells. The *WPCF* shows as well minimum changes throughout the studied section. Based on our outcomes we can reasonably consider changes in calcareous nannoplankton assemblages as largely reflecting variations in paleoenvironmental conditions of the photic zone. All the adopted proxies for calcareous nannofossils point to a general scarce influence of dissolution and overgrowth. In the entire Terche section the specific *diversity*, the $T_{species}$ and *T/D* are constantly high (Fig. 4) even where dissolution is supposed to be present (the MUs). We attribute the minor decrease of $T_{species}$ and *T/D* values within the I1 recovery phase to a moderate increase in overgrowth rather than in carbonate dissolution. This is evident by a comparison with the Q_E and Q_O profiles (Fig. 4).

The aforementioned evidences allow us to interpret the MUs deposition as mainly related to dilution rather than increase in dissolution. According to our age model (Fig. 7), a distinct increase of the sedimentation rates occurred indeed across the investigated events. We infer the enhanced influence of terrigenous dilution within the MUs also by the associated Cretaceous reworking pulses (Fig. 6). A significant input of reworked Cretaceous nannofossils is a feature shared by Eocene hyperthermals and the middle Eocene Climatic

Optimum (MECO) in the Belluno Basin (Agnini et al., 2007a, 2009; Toffanin et al., 2011), an area influenced by a continental regime (e.g., Giusberti et al., 2007; Boscolo Galazzo et al., 2013). The reworking has been linked to enhanced discharge of terrigenous material to the ocean, as derived from strengthened hydrological cycle. A significant increase in Cretaceous reworked specimens may hence relate to transient enrichments in nutrients washed off from lands (Agnini et al., 2009). In the New Zealand slope marly beds coinciding with late Paleocene to early Eocene hyperthermals were interpreted by Nicolo et al. (2007) and Slotnick et al. (2012) as well as an effect of increased continental weathering and accelerated hydrological cycle.

Sedimentation rate and the Cretaceous reworking at Terche are considerably higher at the ETM2 with respect to H2 and I1. Therefore, the most significant perturbation of the hydrological cycle was linked to the climatic changes triggered by the ETM2.

5.5. Paleoenvironmental Scenarios across the ETM2, H2, and I1 at the Terche Section

We reconstruct below the paleoenvironmental changes that occurred across the ETM2, H2, and I1 events using the calcareous plankton variations recorded at the Terche section, assuming that the dissolution proxies exclude significant taphonomic bias as discussed above (Figs. 5 and 6).

The inferred interpretations are based on the known paleoecological affinities of planktic foraminifera and calcareous nannofossils, widely investigated in the past decades. There is indeed a general consensus that a number of calcareous nannofossil and planktic foraminiferal taxa are deeply sensitive to environmental variations reflecting climatic and oceanographic changes (e.g., Okada and Honjo, 1973; Gibbs et al., 2006; Villa et al., 2008; Kalb and Bralower, 2012; Berggren et al., 1978; Boersma et al., 1987; Premoli Silva and Boersma, 1988, 1989; Pearson et al., 2006). However, the role of environmental factors (e.g., temperature versus nutrient supply) on the fluctuations in Cenozoic calcareous plankton assemblages is not yet fully disentangled (e.g., Agnini et al., 2007a, 2009; Toffanin et al., 2011). It is worth to point out that we lack of the independent $\delta^{18}O$ temperature proxy at Terche (see section 5.1). Therefore, our interpretation on changes in water temperatures is indirect and entirely based on modifications in the calcareous plankton assemblages.
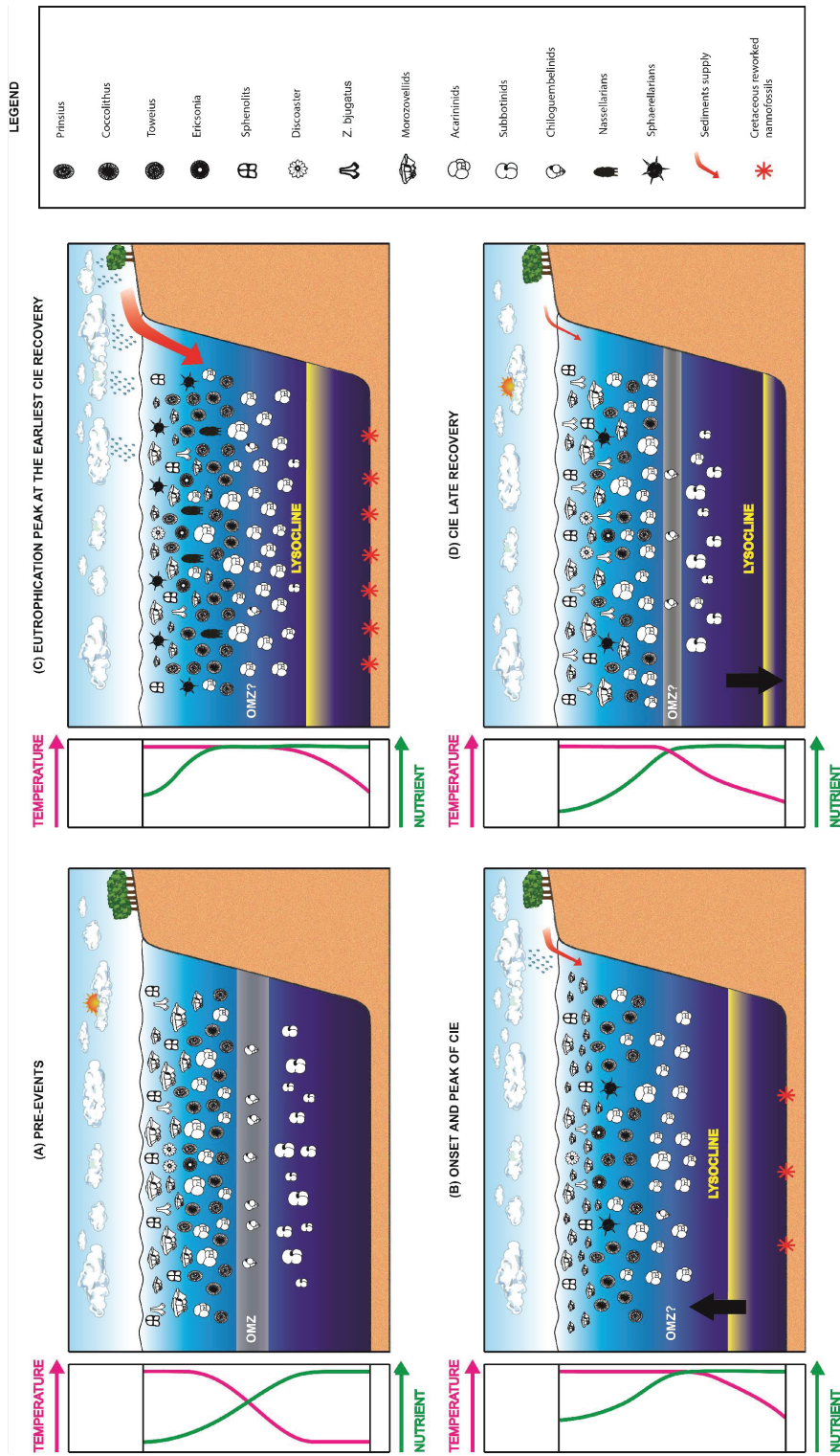
Figure 8. Cartoons illustrating the environmental scenarios across the ETM2 at the Tethyan Terche section deriving from the integrated record of changes in calcareous plankton and abiotic proxies. Similar sequences of environmental reconstructions, though less extreme, can be outlined for the H2 and I1 events (see more extensive discussions in the text). Depth is not in scale. (a) Pre-event: relatively warm, stable, and meso-oligotrophic conditions in the photic zone and structured water column with a relatively expanded OMZ. These conditions are similar to those observed during the ETM2-H2 and H2-I1 transition phases. (b) Onset and peak of the CIE: meso-eutrophic surface-water related to enhanced nutrient discharge induced by improved hydrological cycle coupled with collapse of thermal water-column stratification. (c) CIE early recovery: peak of eutrophic conditions relatively to the pre-event conditions in warm surface-water and still persistent weakening of thermal water-column stratification. (d) CIE late recovery: resume of relatively stable meso-oligotrophic environment in surface waters and of a stratified water column.

48

5.5.1. Pre-ETM2 Relatively Stable and Oligotrophic Environment

During the interval preceding the ETM2 onset, planktic foraminifera were dominated by warm surface-dweller morozovellids and acarininids with moderate percentages of cold thermocline-dweller subbotinids (Fig. 5). These features suggest a stable, thermally stratified water column, with a warm, oligotrophic surface layer and deeper cooler water rich in dissolved nutrient. The relatively common occurrence of low-oxygen tolerant chiloguembelinids (e.g., Boersma et al., 1987; Boersma and Premoli Silva, 1989) supports the existence of a stratified water column with a moderately expanded oxygen minimum zone (OMZ) (Fig. 8a). The sporadic occurrence of radiolarians, considered as eutrophy indicators (e.g., Hallock, 1987), confirms oligo-mesotrophic conditions at the surface waters. Nannofossils assemblages, during the pre-ETM2 interval, are well balanced in terms of average abundances of eutrophic (total of 55%) and oligotrophic (total of 45%) groups (Fig. 6), indicating evenly distributed nutrients within the euphotic zone and no input excess.

The calcareous nannofossil assemblage shows a distinct short-lived ecological turnover coinciding with the pre-ETM2 minor negative CIE identified at ~—2.10 m. Specifically, the cold-water index *Prinsius* and taxa with meso-oligotrophic affinities (*Sphenolitus* and *Z. bijugatus*) increase, while eutrophic taxa, such as *Ericsonia*, *Towieus*, and *Coccolithus* (with the only exception of *Thoracosphaera*) and the warm water index *Discoaster* drop (Fig. 6). These data suggest that the pre-ETM2 CIE was probably associated with a cooling and/or meso-oligotrophic episode. Planktic foraminifera do not display variations across this interval, possibly because this group was more sensitive to warming rather than cooling of the upper water column. A similar pre-ETM2 carbon-isotope feature has been recorded by Stap et al. (2009, 2010b) at ODP Site 1265 (Walvis Ridge). The pre-ETM2 δ^{13}C negative shift precedes at Terche the ETM2 minimum of circa 60 kyr. A comparable time interval can be estimated at Site 1265 (Stap et al., 2009, 2010b) between the ETM2 carbon isotope minimum and a positive peak in Acarinina δ^{18}O values that suggest a surface-water cooling episode preceding the ETM2. Colder temperatures just preceding the onset of the ETM2 are also reported in the Arctic Ocean (Lomonosov Ridge) by Krishnan et al. (2014).

All the adopted dissolution proxies (Fig. 4) point to a depositional environment above the lysocline during the interval preceding the ETM2 onset.

5.5.2. Environmental Changes at the ETM2, H2, and I1 Events

Coinciding with the CIEs, calcareous plankton records at Terche prominent change in the assemblage composition (Figs. 5 and 6). Such changes mainly reflect trends toward warmer and eutrophic conditions. The biotic and abiotic responses to the ETM2 largely replicate at the H2 and I1. Our results highlight, however, less intense perturbations across the H2, while the strongest disruption was at the ETM2. The amplitude of the biotic and environmental variations appears therefore somewhat proportional to the intensity of the carbon cycle perturbation as it has been documented globally.

5.5.2.1. Warming and Nutrient Enrichment in the Surface Waters at the CIE Onsets and following Recoveries

In the Terche section, the acarininids marked increase across the ETM2, H2, and I1 CIEs indicates that each of these events was associated with a rise in surface water temperature in the central western Tethys, since this group inhabited the warm surface layer of the Eocene oceans.

The greatest abundance of Cretaceous nannofossil reworking, sign of transient enrichments in nutrients washed off from lands, occurred across the CIE onsets (Figs. 6 and 8b) and ETM2 early recovery (Fig. 8c), and it coincides with nannofossil eutrophic taxa maxima (*Ericsonia*, *Towieus*, and *Coccolithus*). On the contrary, taxa with oligotrophic affinities, precisely *Z. bijugatus* and even the warm-oligotrophic *Discoaster*, drop within the same intervals. Similar features were observed across the PETM and other hyperthermals in the Belluno Basin (e.g., Agnini et al., 2007a, 2009). The increased input in radiolarians at the ETM2 early recovery and at the I1 recovery phases further supports a nutrient-rich surface waters environment.

Sphenoliths, thought to be adapted to oligotrophic warm-water conditions (e.g., Young, 1994; Aubry, 1998), do not show important changes except for a slight decrease at the ETM2 CIE onset. This suggests that sphenoliths were more influenced by trophic conditions than temperature in agreement with Agnini et al. (2007a) and Toffanin et al. (2011). The lack of a clear sphenoliths response to the H2 and I1 can be explained with the minor magnitude of these events, which led to environmental perturbations below the threshold of sphenoliths sensitivity.

The combined results from calcareous nannofossils and planktic foraminifera point to an increase in surface water eutrophication with respect to the pre-events conditions coupled with marked warmth at the CIE onsets and early recovery phases. The surface-dweller warm-index morozovellids, which largely shared the uppermost water-column habitat with acarininids (e.g., Pearson et al., 2006), show minor changes across the events consisting in transient declines in abundance (Fig. 5). Surface-water nutrient enrichment along with weak water column stratification is known to provide hostile ecological conditions for the highly specialized oligotrophic morozovellids (Boersma et al., 1987; Pearson et al., 2006; Premoli Silva and Boersma, 1989). Slight differences between the paleoecology of morozovellids and acarininids are known by minor variations in stable isotopes that generally indicate a shallower habitat for the former (Boersma et al., 1979; Pearson et al., 1993; 2006).

The variations, though not particularly marked, of four of the adopted dissolution proxies (*F index*, *WPCF*, *diversity*, and Q_E) imply that the lysocline may have intercepted to some extent the depositional environment of the Terche section during these phases (Fig. 8b and 8c).

Calcareous nannofossils suggest return to oligo-mesotrophic conditions within the photic zone only at the ETM2 CIE late recovery, and at the H2 and I1 recovery, where the Cretaceous reworking decreases implying a drop in terrigenous and nutrient supplies. The progressive reduction in radiolarian abundances, the recovery in oligotrophic indices (*Z. bjugatus*, *Discoaster* at ETM2 and H2; *Discoaster* at I1) and parallel decrease in eutrophic indicators toward the pre-event mean values (Figs. 6 and 8d) confirm the restoration of oligo-mesotrophy. Our record suggests that the major controlling factor driving *Discoaster* changes in abundance across the studied events was the excess in nutrient availability. Changes in temperature played a major role only when environmental conditions were meso-oligotrophic, as observed during the pre-ETM2 cooling episode where the drop of this genus is not paralleled by increase in Cretaceous reworked taxa, here adopted as proxy of enhanced nutrient availability. *Discoaster* displays actually low abundance when conditions became eutrophic and warmer and increases only when less eutrophic conditions coexisted with presumably still high temperatures, such as at ETM2 CIE late recovery, H2, and I1 recovery (Fig. 6). The dominance of warm-water indicators among planktic foraminifera, mainly acarininids, across these phases suggests indeed still warm surface-water conditions.

5.5.2.2. Weakening of the Thermal Water-Column Stratification

The switch in abundance between acarininids and subbotinids recorded at the CIE onsets and early recoveries may reflect the onset of a significant warming of sub-surface layer besides the ocean-surface warmth. The pronounced increase in temperature related to the studied events may have caused a regional reduction of the thermal stratification making the subsurface waters unsuitable for deeper dwellers cold-index subbotinids (Fig. 8b). These conditions favored the acarininids which might have been able to temporarily colonize warmer deep-waters previously occupied by subbotinids. The reduction in abundance of the chiloguembelinids within the whole CIE intervals (Fig. 5) might support warming of sub-surface waters since this group thrived at the cool mid-high latitudes (e.g., Boersma et al., 1987). On the other hand, chiloguembelinids are known to proliferate within OMZs (e.g., Boersma et al., 1987; Boersma and Premoli Silva, 1989), thus their reduction partly conflicts with our evidence of surface-water eutrophication that should in contrast induce an expansion of the OMZ. Altenatively, the thin-walled chiloguembelinids could have been partly lost during a rise of the lysocline. The rare chiloguembelinid fragments observed in coincidence to the F-index highest values, do not allow us to exclude that some of them may have been completely dissolved. The biserials chiloguembelinids can be considered among the most dissolution prone taxa as they have a thin-walled test and small size. Those features are considered as the most important factor controlling planktic foraminiferal dissolution (Nguyen et al., 2011). Moreover, experiments on benthic foraminifera highlight that taxa with biserial architecture are more fragile than trochospirals (Nguyen and Speijer, 2014).

A partial replacement of the pre-events water-column structures occurred during the late recovery phases as indicated by the initial resuming in thermocline-dweller subbotinid and chiloguembelinid abundance (Figs. 6 and 8d).

5.5.2.3. Reduced Size of Morozovellids at the ETM2 Onset

The morozovellid peak at the ETM2 onset is associated with significant reduction in their test size that involves, though at a lesser extent, also the acarininids. The morozovellid peak slightly precedes the eutrophication acme coinciding with the peak of nannofossil reworking and the highest radiolarian abundance (Figs. 5 and 6). We speculate that the occurrence of relatively small morozovellids, coupled with a pronounced increase in abundance, is the combined results of stressors such as extreme warmth and increased eutrophication. The first

phase of warming may have favored morozovellids until surface waters became exceedingly eutrophic for this group.

In the Holocene sediments size patterns are highly correlated with surface-water stratification, seasonality, and primary productivity on a regional scale (Schmidt et al., 2004). A negative effect of fertility on size is suggested by the distinctly smaller size of the upwelling Holocene assemblages (Schmidt et al., 2004). It is known that dwarfing in microfossils relates to extreme environmental stressors during biotic crisis or mass extinctions, even though it has been also observed as preceding the extinction level for some planktic foraminiferal species (e.g., Wade and Olsson, 2009; Keller and Abramovich, 2009). Causes explaining the reduced size in fossil organisms are manifold, and they may include a collapse in primary production, a loss of symbiotic relationship, changes in salinity and temperature, and decrease in oxygen levels (e.g., Hallam, 1965; Wade et al., 2008). It appears therefore that several different environmental, climatic, and ecological triggers may result in the same phenotypic response and it is problematic to determine precisely which factor is the main responsible for the transient dwarfing in the study case. We outline below a number of possible scenarios. Protists, both autotrophs and heterotrophs, reduce their cell size linearly with temperature (Atkinson et al., 2003), although direct laboratory tests on modern planktic foraminifera are lacking. The adaptation to reduce sinking rate within less dense warmer waters is one of the proposed causes invoked to explain the inverse temperature-size relationship for planktic protists (Atkinson, 1994). The metabolism of protists accelerates when temperature increases (e.g., O'Connor et al., 2009) thus requiring more resources, such as more oxygen. Since, in contrast, concentration of dissolved oxygen decreases in warm waters, a strategy to optimize resource uptake is to enlarge the ratio of surface area by reducing the cell mass (Atkinson et al., 2003). Enhanced planktic foraminiferal metabolic rates have been proposed to explain the decrease in planktic foraminiferal productivity across another interval of intense warmth, the MECO at the Atlantic Site 1263 (Boscolo Galazzo et al., 2014). The reduced sizes of morozovellids tests can also be explained as a consequence of a transient episode of photosymbionts loss (bleaching). The algal-symbiotic relationship is considered one of the most successful strategies adopted by morozovellids and acarininids during the earliest Paleogene (Norris, 1996; Quillévéré et al., 2001). A number of mechanisms considered to be responsible for bleaching are expected to have occurred at the ETM2, such as elevated sea surface temperatures, increased CO_2, lower sea-water pH, and changes in nutrient availability (e.g., Douglas, 2003; Wade et al., 2008). An episode of bleaching caused by global warming has been documented to explain the reduction in size of morozovelloidids

and acarininds across the MECO (Edgar et al., 2012). We cannot exclude the possibility that the loss of symbionts could have been the strategy adopted by morozovellids to temporarily adapt to eu-mesotrophic environments or to colonize relatively deeper habitats. Maximum size is normally achieved by planktic foraminifera within their preferred water mass, and it decreases away from such optimum environmental conditions (e.g., Schmidt et al., 2006). Growth rate of morozovellids may have been reduced under the stress deriving from temporarily inhabiting deeper or relatively more fertile waters.

5.5.3. ETM2-H2 and H2-I1 Transitions: Restoring of Relatively Stable and Meso-oligotrophic Environments

Across the ETM2-H2 and H2-I1 transitions, both radiolarians and reworked Cretaceous nannofossils are low in abundance, pointing to low rates of terrigenous nutrient supply (Fig. 8a). Calcareous plankton assemblages gradually recover toward pre-event conditions. The marked and possibly cyclic fluctuations in calcareous nannofossil abundances, particularly evident at the ETM2-H2 transition, suggest, however, still unstable conditions within the photic zone (Fig. 6). The substantial increase of nannofossil oligotrophic indices (sphenoliths and *Z. bijugatus*) points to a restoration of oligotrophic surface waters, while the increase of subbotinids to pre-ETM2 values suggests the upper water-column return to be well stratified (Figs. 5 and 8a).

5.6. Time Lag between the CIEs and Biotic-Paleoenvironmental Recoveries

The strongest surface-water eutrophication, relatively to the pre-event conditions, was reached just following the ETM2 δ^{13}C minimum, in the early recovery phase, as indicated by the greatest abundances in radiolarians, eutrophic calcareous nannofossils, and low values in oligotrophic indices, such as *Discoaster*, *Z. bijugatus* and *Morozovella* (Figs. 5, 6, and 8c). According to our age model, these conditions persisted over the circa 13–16 kyr long δ^{13}C early recovery phase. During this interval deep-dweller indices are still scarce among planktic foraminifera, while warm indices dominate thus implying a persistent weakening of the water-column thermal stratification (Fig. 8c). High rates of sedimentation and significant input in reworked Cretaceous nannofossils persisted during the ETM2 early recovery and I1 recovery phases, thus highlighting that the perturbation of the hydrological cycle was still strengthened. However, this delay is not observed at the H2 event.

We record therefore an offset between the rate of carbon cycle recovery and the rate of environmental and biotic restorations, which were somewhat slower. Even though it is beyond the aim of our work to provide models for the current scenario of anthropogenic CO_2 additions and related upcoming global climate change, our analysis can give insight on how marine biota and environments can react to rapid and drastic global warming. It appears clear that the immediately stopping of the massive anthropogenic release in greenhouse gases will be insufficient to instantly invert the disruption of marine biota and the strengthening of terrestrial hydrological cycle.

6. Summary and Conclusions

We provide a unique record that directly integrates changes in planktic foraminiferal and calcareous nannofossil assemblages across the post-PETM carbon cycle perturbations related to the ETM2, H2, and I1 at the central western Tethyan Terche section (northeastern Italy). Our study contributes to partially fill the gap of knowledge on the biotic response to the events following the PETM and characterizing the early Eocene climate. Differently from several deep-oceanic sites, our record displays only minimal evidences of carbonate dissolution making our results particularly relevant. Our records reveal the following:

1. During the studied events the calcareous plankton assemblages experienced significant changes indicating abrupt and transient episodes of environmental perturbations. Increased acarininid abundance, paralleled by subbotinid decline, suggests that each of the three carbon cycle disruptions was associated with upper water-column warming. Surface and subsurface waters warming may have led the weakening of the upper water column thermal stratification. This may have been the cause of the temporary decline in subbotinids. Changes in nannofossils assemblages along with increased radiolarian abundance point to surface-water nutrient enrichments and increased eutrophication relatively to the pre-event conditions.

2. We interpret surface-water eutrophication as forced by strengthening of the hydrological cycle and enhanced weathering. The enhanced discharge of terrigenous material is testified by increased sedimentation rates within the MUs, especially the MU1, and by peaks of reworked Cretaceous nannofossils. These features are also shared by PETM, X/K, and MECO events in the nearby areas influenced by a continental regime.

3. Across the studied events, calcareous nannofossils proved to be generally more susceptible to changes in nutrient supply, as can be expected for autotrophs, while planktic foraminiferal changes appear to have been mostly driven by warming rather than cooling of the upper water column.

4. Our data give insights on similarities and differences among the ETM2, H2, and I1 events from a Tethyan perspective, considering that the last two events are not unanimously regarded as hyperthermals. Calcareous plankton reacted in a similar way during all the events, with the most marked changes recorded at the ETM2. The ETM2 also records the most intense acceleration of the hydrological cycle. We can therefore conclude that ETM2 was the most prominent event. Nevertheless, the perturbations related to H2 and I1 were able to affect calcareous plankton, in particular, planktic foraminifera, and to induce changes in regional climate and oceanography.

5. The biotic changes and environmental perturbation at the ETM2 persisted after the CIE peaks for circa 13–16 kyr, during the early CIE recovery phase. Therefore, the recovery rates were slower for the environment and biota than for the carbon cycle. This has important implications in view of the modern human induced carbon cycle disruption.

References

Abels, H. A., W. C. Clyde, P. D. Gingerich, F. J. Hilgen, H. C. Fricke, G. J. Bowen, and L. J. Lourens (2012), Terrestrial carbon isotope excursions and biotic change during Palaeogene hyperthermals, Nat. Geosci., 5(5), 326–329, doi:10.1038/ngeo1427.

Adelseck, C. G., Jr., G. W. Geehan, and P. H. Roth (1973), Experimental evidence for the selective dissolution and overgrowth of calcareous nannofossils during diagenesis, Geol. Soc. Am. Bull., 84(8), 2755–2762, doi:10.1130/0016-7606(1973)84.

Agnini, C., G. Muttoni, D. V. Kent, and D. Rio (2006), Eocene biostratigraphy and magnetic stratigraphy from Possagno, Italy: The calcareous nannofossil response to climate variability, Earth Planet. Sci. Lett., 241, 815–830, doi:10.1016/j.epsl.2005.11.005.

Agnini, C., E. Fornaciari, D. Rio, F. Tateo, J. Backman, and L. Giusberti (2007a), Responses of calcareous nannofossil assemblages, mineralogy and geochemistry to the environmental perturbations across the Paleocene/Eocene boundary in the Venetian pre-Alps, Mar. Micropaleontol., 63, 19–38, doi:10.1016/j.marmicro.2006.10.002.

Agnini, C., E. Fornaciari, I. Raffi, D. Rio, U. Röhl, and T. Westerhold (2007b), High resolution nannofossil biochronology of middle Paleocene to early Eocene at ODP Site 1262: Implications for calcareous nannoplankton evolution, Mar. Micropaleontol., 64, 215–248, doi:10.1016/j.marmicro.2007.05.003.

Agnini, C., J. Backman, H. Brinkhuis, E. Fornaciari, L. Giusberti, V. Luciani, D. Rio, and A. Sluijs (2009), An early Eocene carbon cycle perturbation at similar to 52.5 Ma in the Southern Alps: Chronology and biotic response, Paleoceanography, 24, PA2209, doi:10.1029/2008PA001649.

Agnini, C., E. Fornaciari, I. Raffi, R. Catanzariti, H. Pälike, J. Backman, and D. Rio (2014), Biozonation and biochronology of Paleogene calcareous nannofossils from low and middle latitudes, Newslett. Stratigr., 47(2), 131–181, doi:10.1127/0078-0421/2014/0042.

Agnini, C., D. J. A. Spofforth, G. R. Dickens, D. Rio, H. Pälike, J. Backman, G. Muttoni, and E. Dallanave (2016), Stable isotope and calcareous nannofossil assemblage records for the Cicogna section: Toward a detailed template of late Paleocene and early Eocene global carbon cycle and nannoplankton evolution, Clim. Past, 12, 883–909, doi:10.5194/cp-12-883-2016.

Atkinson, D. (1994), Temperature and organism size—A biological law for ectotherms?, Adv. Ecol. Res., 25, 1–58.

Atkinson, D., B. J. Ciotti, and D. J. S. Montagnes (2003), Protists decrease in size linearly with temperature: Ca. 2.5%°C^{-1}, Proc. R. Soc. Lond. B., 270, 2605–2611, doi:10.1098/rspb.2003.2538.

Aubry, M.-P. (1998), Early Paleogene calcareous nannoplankton evolution: A tale of climatic amelioration, in Late Paleocene and Early Eocene Climatic and Biotic Evolution, edited by M.-P. Aubry et al., pp. 158–203, Columbia Univ. Press, New York.

Backman, J., and N. J. Shackleton (1983), Quantitative biochronology of Pliocene and early Pleistocene calcareous nannoplankton from the Atlantic, Indian and Pacific Oceans, Mar. Micropaleontol., 8, 141–170.

Bé, A. W. H., W. M. John, and M. H. Stanley (1975), Progressive dissolution and ultrastructural breakdown of planktic foraminifera, Cushman Found. Foraminiferal Res. Spec. Publ., 13, 27–55.

Berger, W. H. (1970), Planktonic foraminifera—Selective solution and lysocline, Mar. Geol., 8(2), 111–138.

Berger, W. H. (1973), Deep-sea carbonates: Pleistocene dissolution cycles, J. Foraminiferal Res., 3(4), 187–195.

Berger, W. H., M.-C. Bonneau, and F. L. Parker (1982), Foraminifera on the deep-sea floor: Lysocline and dissolution rate, Oceanol. Acta, 5(2), 249–258.

Berggren, W. A., M. C. Mckenna, J. Hardenbol, and J. D. Obradovich (1978), Revised Paleogene polarity time scale, J. Geol., 86(1), 67–81.

Boersma, A., and I. Premoli Silva (1989), Atlantic paleogene biserial heterohelicid foraminifera and oxygen minima, Paleoceanography, 4(3), 271–286, doi:10.1029/PA004i003p00271.

Boersma, A., N. J. Shackleton, M. A. Hall, and Q. C. Given (1979), Carbon and oxygen isotope variations at DSDP Site 384 (North Atlantic) and some paleotemperature and carbon isotope variations in the Atlantic Ocean, Init. Repts. DSDP, 43, 695–717.

Boersma, A., I. Premoli Silva, and N. J. Shackleton (1987), Atlantic Eocene planktonic foraminiferal paleohydrographic indicators and stable isotope paleoceanography, Paleoceanography, 2(3), 287–331, doi:10.1029/PA002i003p00287.

Bornemann, A., and J. Mutterlose (2008), Calcareous nannofossil and $\delta^{13}C$ records from the Early Cretaceous of the western Atlantic ocean: Evidence for enhanced fertilization across the Berriasian–Valanginian transition, Palaios, 23(12), 821–832, doi:10.2110/palo.2007.p07-076r.

Boscolo Galazzo, F., L. Giusberti, V. Luciani, and E. Thomas (2013), Paleoenvironmental changes during the Middle Eocene Climatic Optimum (MECO) and its aftermath: The benthic foraminiferal record from the Alano section (NE Italy), Palaeogeogr. Palaeoclimatol. Palaeoecol., 378, 22–35, doi:10.1016/j.palaeo.2013.03.018.

Boscolo Galazzo, F., L. M. Pagani, C. Warren, X. E. Thomas, V. Luciani, and L. Giusberti (2014), The middle Eocene climatic optimum (MECO): A multiproxy record of paleoceanographic changes in the southeast Atlantic (ODP Site 1263, Walvis Ridge), Paleoceanography, 29, 1143–1161, doi:10.1002/2014PA002670.

Bosellini, A. (1989), Dynamics of Tethyan carbonate platform, in Controls on Carbonate Platform and Basin Platform, Soc. Sediment. Geol. (SEPM) Spec. Publ., vol. 44, edited by P. D. Crevello et al., pp. 3–13. Univ. of California, Berkeley.

Chew, A. E. (2015), Mammal faunal change in the zone of the Paleogene hyperthermals ETM2 and H2, Clim. Past, 11, 1223–1237, doi:10.5194/cp-11-1223-2015.

Clementz, M., S. Bajpai, V. Ravikant, J. G. M. Thewissen, N. Saravanan, I. B. Singh, and V. Prasad (2011), Early Eocene warming events and the timing of terrestrial faunal exchange between India and Asia, Geology, 39(1), 15–18, doi:10.1130/G31585.1.

Coccioni, R., G. Bancalà, R. Catanzariti, E. Fornaciari, F. Frontalini, L. Giusberti, L. Jovane, V. Luciani, J. Savian, and M. Sprovieri (2012), An integrated stratigraphic record of the Palaeocene-lower Eocene at Gubbio (Italy), New insights into the early Palaeogene hyperthermals and carbon isotope excursions, Terra Nova, 24, 380–386, doi:10.1111/j.1365-3121.2012.01076.x.

Cramer, B. S., D. V. Kent, and M.-P. Aubry (2003), Orbital climate forcing of excursions in the late Paleocene–early Eocene (chrons C24n–C25n), Paleoceanography, 18(4), 1097, doi:10.1029/2003PA000909.

D'haenens, S., A. Bornemann, P. Stassen, and R. P. Speijer (2012), Multiple early Eocene benthic foraminiferal assemblage and δ^{13}C fluctuations at DSDP Site 401 (Bay of Biscay-NE Atlantic), Mar. Micropaleontol., 88–89, 15–35, doi:10.1016/j.marmicro.2012.02.006.

D'haenens, S., A. Bornemann, P. Claeys, U. Röhl, E. Steurbaut, and R. P. Speijer (2014), A transient deep-sea circulation switch during Eocene Thermal Maximum 2, Paleoceanography, 29, 370–388, doi:10.1002/2013PA002567.

Dallanave, E., C. Agnini, G. Muttoni, and D. Rio (2009), Magneto-biostratigraphy of the Cicogna section (Italy): Implications for the late Paleocene–early Eocene time scale, Earth Planet. Sci. Lett., 285, 39–51.

Dallanave, E., L. Tauxe, G. Muttoni, and D. Rio (2010), Silicate weathering machine at work: Rock magnetic data from the late Paleocene-early Eocene Cicogna section, Italy, Geochem. Geophys. Geosyst., 11, Q07008, doi:10.1029/2010GC003142.

Dallanave, E., C. Agnini, G. Muttoni, and D. Rio (2012a), Paleocene magneto-biostratigraphy and climate-controlled rock magnetism from the Belluno Basin, Tethys Ocean, Italy, Palaeogeogr. Palaeoclimatol. Palaeoecol., 337-338, 130–142.

Dallanave, E., G. Muttoni, C. Agnini, L. Tauxe, and D. Rio (2012), Is there a normal magnetic-polarity event during the Palaeocene-Eocene thermal maximum (~55 Ma)? Insights from the palaeomagnetic record of the Belluno Basin (Italy), Geophys. J. Int., 191, 517–529.

De Conto, R. M., S. Galeotti, M. Pagani, D. Tracy, K. Schaefer, T. Zhang, D. Pollard, and D. J. Beerling (2012), Past extreme warming events linked to massive carbon release from thawing permafrost, Nature, 484, 87–91, doi:10.1038/nature10929.

Dedert, M., H. M. Stoll, D. Kroon, N. Shimizu, K. Kanamaru, and P. Ziveri (2012), Productivity response of calcareous nannoplankton to Eocene Thermal Maximum 2 (ETM2), Clim. Past, 8(3), 977–993, doi:10.5194/cp-8-977-2012.

Dedert, M., H. Stoll, S. Kars, J. R. Young, N. Shimizu, D. Kroon, L. Lourens, and P. Ziveri (2014), Temporally variable diagenetic overgrowth on deep-sea nannofossil carbonates across Palaeogene hyperthermals and implications for isotopic analyses, Mar. Micropaleontol., 107, 18–31.

Dickens, G. R. (2011), Down the rabbit hole: Toward appropriate discussion of methane release from gas hydrate systems during the Paleocene-Eocene thermal maximum and other past hyperthermal events, Clim. Past, 7(3), 831–846, doi:10.5194/cp-7-831-2011.

Douglas, A. E. (2003), Coral bleaching—How and why?, Mar. Pollut. Bull., 46, 385–392.

Dunkley Jones, T., P. R. Bown, P. N. Pearson, B. S. Wade, H. K. Coxall, and C. H. Lear (2008), Major shifts in calcareous phytoplankton assemblages through the Eocene-Oligocene transition of Tanzania and their implications for low-latitude primary production, Paleoceanography, 23, PA4204, doi:10.1029/2008PA001640.

Edgar, K. M., S. M. Bohaty, S. J. Gibbs, P. F. Sexton, R. D. Norris, and P. A. Wilson (2012), Symbiont "bleaching" in planktic foraminifera during the Middle Eocene Climatic Optimum, Geology, 41, 15–18, doi:10.1130/G33388.1.

Fisher, R. (1953), Dispersion on a sphere, Proc. R. Soc. London, 217, 295–305.

Fornaciari, E., L. Giusberti, V. Luciani, F. Tateo, C. Agnini, J. Backman, M. Oddone, and D. Rio (2007), An expanded Cretaceous □Tertiary transition in a pelagic setting of the Southern Alps (central-western Tethys), Palaeogeor. Palaeoclimatol. Palaeoecol., 255, 98–131, doi:10.1016/j.palaeo.2007.02.044.

Frank, T. D., M. A. Arthur, and W. E. Dean (1999), Diagenesis of Lower Cretaceous pelagic carbonates, North Atlantic: Paleoceanographic signals obscured, J. Foraminiferal Res., 29, 340–351.

Galeotti, S., S. Krishnan, M. Pagani, L. Lanci, A. Gaudio, J. C. Zachos, S. Monechi, G. Morelli, and L. J. Lourens (2010), Orbital chronology of Early Eocene hyperthermals from the Contessa Road section, central Italy, Earth Planet. Sci. Lett., 290(1–2), 192–200, doi:10.1016/j.epsl.2009.12.021.

Gardin, S., and S. Monechi (1998), Palaeoecological change in middle to low latitude calcareous nannoplankton at the Cretaceous/Tertiary boundary, Bull. Soc. Geol. Fr., 169(5), 709–723.

Gibbs, S. J., N. J. Shackleton, and J. R. Young (2004), Orbitally forced climate signals in mid-Pliocene nannofossil assemblages, Mar. Micropaleontol., 51, 39–56.

Gibbs, S. J., T. J. Bralower, P. R. Bown, J. C. Zachos, and L. M. Bybell (2006), Shelf and open ocean calcareous phytoplankton assemblages across the Paleocene–Eocene thermal maximum: Implications for global productivity gradients, Geology, 34(4), 233–236.

Gibbs, S. J., P. R. Bown, B. H. Murphy, A. Sluijs, K. M. Edgar, H. Pälike, C. T. Bolton, and J. C. Zachos (2012), Scaled biotic disruption during early Eocene global warming events, Biogeosciences, 9(11), 4679–4688, doi:10.5194/bg-9-4679-2012.

Giusberti, L., D. Rio, C. Agnini, J. Backman, E. Fornaciari, F. Tateo, and M. Oddone (2007), Mode and tempo of the Paleocene–Eocene thermal maximum in an expanded section from the Venetian pre-Alps, Geol. Soc. Am. Bull., 119, 391–412, doi:10.1130/B25994.1.

Giusberti, L., F. Boscolo Galazzo, and E. Thomas (2016), Variability in climate and productivity during the Paleocene/Eocene thermal maximum in the Central-Western Tethys (Forada section), Clim. Past, 12, 1–28, doi:10.5194/cp-12-1-2016.

Hallam, A. (1965), Environmental causes of stunting in living and fossil marine benthonic invertebrates, Palaeontology, 8, 132–155.

Hallock, P. (1987), Fluctuations in the trophic resource continuum: A factor in global diversity cycles?, Paleoceanography, 2, 457–471, doi:10.1029/PA002i005p00457.

Hancock, H. J. L., and G. R. Dickens (2005), Carbonate dissolution episodes in Paleocene and Eocene sediment, Shatsky Rise, west-central Pacific, in Proceedings of the Ocean Drilling Program, Scientific Results, vol. 198, edited by T. J. Bralower, I. Premoli Silva, and M. J. Malone, 1-24, Texas A&M Univ., College Station. [Available at World Wide Web http://www-odp.tamu.edu/publications/198_SR/116/116.htm.].

Hollis, C. J., G. R. Dickens, B. D. Field, C. M. Jones, and C. P. Strong (2005), The Paleocene–Eocene transition at Mead Stream, New Zealand: A southern Pacific record of early Cenozoic global change, Palaeogeogr. Palaeoclimatol. Palaeoecol., 215(3), 313–343, doi:10.1016/j.palaeo.2004.09.011.

Hönisch, B., et al. (2012), The geological record of ocean acidification, Science, 335, 1058–1063, doi:10.1126/science.1208277.

Höntzsch, S., C. Scheibner, E. Guasti, J. Kuss, A. M. Marzouk, and M. W. Rasser (2011), Increasing restriction of the Egyptian shelf during the early Eocene? New insights from a southern Tethyan carbonate platform, Palaeogeogr. Palaeoclimatol. Palaeoecol., 302(3), 349–366, doi:10.1016/j.palaeo.2011.01.022.

Jennions, S. M., E. Thomas, D. N. Schmidt, D. Lunt, and A. Ridgwell (2015), Changes in benthic ecosystems and ocean circulation in the Southeast Atlantic across Eocene Thermal Maximum 2, Paleoceanography, 30, 1059–1077, doi:10.1002/2015PA002821.

Jones, C. H. (2002), User-driven integrated software lives: "Paleomag" paleomagnetics analysis on the Macintosh, Comput. Geosci., 28, 1145–1151.

Kahn, A., and M.-P. Aubry (2004), Provincialism associated with the Paleocene/Eocene thermal maximum: Temporal constraint, Mar. Micropaleontol., 52(1), 117–131, doi:10.1016/j.marmicro.2004.04.003.

Kalb, A. L., and T. J. Bralower (2012), Nannoplankton origination events and environmental changes in the late Paleocene and early Eocene, Mar. Micropaleontol., 92–93, 1–115.

Kaminski, M. A., and F. M. Gradstein (2005), in Atlas of Paleogene Cosmopolitan Deep-water Agglutinated Foraminifera, Gryzbowski Foundation Spec. Publ., vol. 10, edited by M. A. Kaminski and F. M. Gradstein, pp. 547, Krakow, Poland.

Keller, G., and S. Abramovich (2009), Lilliput Effect in late Maastrichtian Planktic Foraminifera: Response to Environmental Stress, Palaeogeogr. Palaeoclimatol. Palaeoecol., 284, 47–62.

Kennett, J. P., and L. D. Stott (1991), Abrupt deep-sea warming, palaeoceanographic changes and benthic extinctions at the end of the Palaeocene, Nature, 353, 225–229.

Kent, D. V., P. E. Olsen, and W. K. Witte (1995), Late Triassic-earliest Jurassic geomagnetic polarity sequence and paleolatitudes from drill cores in the Newark rift basin, eastern North America, J. Geophys. Res., 100, 14,965–14,998, doi:10.1029/95JB01054.

Kirschvink, J. L. (1980), The least-squares line and plane and the analysis of palaeomagnetic data, Geophys. J. R. Astron. Soc., 62, 699–718.

Kirtland-Turner, S., P. F. Sexton, C. D. Charles, and R. D. Norris (2014), Persistence of carbon release events through the peak of early Eocene global warmth, Nat. Geosci., 12, 1–17, doi:10.1038/ngeo2240.

Krishnan, S., M. Pagani, M. Huber, and A. Sluijs (2014), High latitude hydrological changes during the Eocene Thermal Maximum 2, Earth Planet. Sci. Lett., 404, 167–177, doi:10.1016/j.epsl.2014.07.029.

Lauretano, V., K. Littler, M. Polling, and J. C. Zachos (2015), Frequency, magnitude and character of hyperthermal events at the onset of the Early Eocene Climatic Optimum, Clim. Past, 11(3), 1795–1820, doi:10.5194/cpd-11-1795-2015.

Leon-Rodriguez, L., and G. R. Dickens (2010), Constraints on ocean acidification associated with rapid and massive carbon injections: The early Paleogene record at ocean drilling program site 1215, equatorial Pacific Ocean, Palaeogeogr. Palaeoclimatol. Palaeoecol., 298(3–4), 409–420, doi:10.1016/j.palaeo.2010.10.029.

Lirer, F. (2000), A new technique for retrieving calcareous microfossils from lithified lime deposits, Micropaleontology, 46, 365–369.

Littler, K., U. Röhl, T. Westerhold, and J. C. Zachos (2014), A high-resolution benthic stable isotope record for the South Atlantic: Implications for orbital-scale changes in late Paleocene–early Eocene climate and carbon cycling, Earth Planet. Sc. Lett., 401, 18–30, doi:10.1016/j.epsl.2014.05.054.

Lourens, L. J., A. Sluijs, D. Kroon, J. C. Zachos, E. Thomas, U. Röhl, J. Bowles, and I. Raffi (2005), Astronomical pacing of late Palaeocene to early Eocene global warming events, Nature, 435, 1083–1087.

Lowrie, W., and W. Alvarez (1977), Upper Cretaceous magnetic stratigraphy, in Upper Cretaceous–Paleocene Magnetic Stratigraphy at Gubbio, Italy, Geol. Soc. Am., vol. 88, edited by W. Lowrie, and W. Alvarez, 374–377, Geol. Soc. Am., Boulder, Colo., doi:10.1130/0016-7606.

Luciani, V., L. Giusberti, C. Agnini, J. Backman, E. Fornaciari, and D. Rio (2007), The Paleocene–Eocene Thermal Maximum as recorded by Tethyan planktonic foraminifera in the Forada section (northern Italy), Mar. Micropaleontol., 64(3), 189–214, doi:10.1016/j.marmicro.2007.05.001.

Luciani, V., G. R. Dickens, J. Backman, E. Fornaciari, L. Giusberti, C. Agnini, and R. D'Onofrio (2016), Major perturbations in the global carbon cycle and photosymbiont-bearing planktic foraminifera during the early Eocene, Clim. Past, 12, 981–1007, doi:10.5194/cp-12-981-2016.

Lunt, D. J., A. Ridgwell, A. Sluijs, J. C. Zachos, S. Hunter, and A. Haywood (2011), A model for orbital pacing of methan hydrate destabilization during the Paleogene, Nat. Geosci., 4, 775–778, doi:10.1038/ngeo1266.

MacKenzie, D. T., III, and S. W. Wise Jr. (1983), Paleocene and Eocene calcareous nannofossils from Deep Sea Drilling Project Legs 25 and 40, south and east of Africa, in Deep Sea Drilling Project, Initial Reports., 71, edited by W. J. Ludwig et al., pp. 1141-1180, U.S. Gov. Print. Off., Washington, D. C., doi:10.2973/dsdp.proc.71.147.1983.

Marshall, J. D. (1992), Climatic and oceanographic isotopic signals from the carbonate rock record and their preservation, Geol. Mag., 129(02), 143–160.

Martini, E. (1971), Standard Tertiary and Quaternary calcareous nannoplankton zonation, in Proceedings of the Second Planktonic Conference, vol. 1970, edited by A. Farinacci, pp. 739–785, Tecnoscienza, Roma.

McInerney, F. A., and S. L. Wing (2011), The Paleocene-Eocene Thermal Maximum: A perturbation of carbon cycle, climate, and biosphere with implications for the future, Annu. Rev. Earth Planet. Sci., 39(1), 489–516, doi:10.1146/annurev-earth-040610-133431.

Murray, J. W. (1976), A method of determining proximity of marginal seas to an ocean, Mar. Geol., 22, 103–119.

Murray, J. W. (Ed.) (1991), Ecology and Paleoecology of Benthic Foraminifera, pp. 398, Longman Scientific and Technical, Harlow Essex, U. K.

Murray, J. W. (Ed.) (2006), Ecology and Applications of Benthic Foraminifera, pp. 426, Cambridge Univ. Press, New York.

Nguyen, T. M. P., and R. P. Speijer (2014), A new procedure to assess dissolution based on experiments on Pliocene–Quaternary foraminifera (ODP Leg 160, Eratosthenes Seamount, Eastern Mediterranean), Mar. Micropaleontol., 106, 22–39, doi:10.1016/j.marmicro.2013.11.004.

Nguyen, T. M. P., M.-R. Petrizzo, and R. P. Speijer (2009), Experimental dissolution of a fossil foraminiferal assemblage (Paleocene–Eocene Thermal Maximum, Dababiya, Egypt): Implications for paleoenvironmental reconstructions, Mar. Micropaleontol., 73(3–4), 241–258, doi:10.1016/j.marmicro.2009.10.005.

Nguyen, T. M. P., M.-R. Petrizzo, P. Stassen, and R. P. Speijer (2011), Dissolution susceptibility of Paleocene–Eocene planktic foraminifera: Implications for palaeoceanographic reconstructions, Mar. Micropaleontol., 81(1–2), 1–21.

Nicolo, M. J., G. R. Dickens, C. J. Hollis, and J. C. Zachos (2007), Multiple early Eocene hyperthermals: Their sedimentary expression on the New Zealand continental margin and in the deep sea, Geology, 35(8), 699–702.

Norris, R. D. (1996), Symbiosis as an evolutionary innovation in the radiation of Paleocene planktic foraminifera, Paleobiology, 22(4), 461–480.

O'Connor, M., M. F. Piehler, D. M. Leech, A. Anton, and J. F. Bruno (2009), Warming and resource availability shift food web structure and metabolism, Plos Biol., 7(8), 1–6, doi:10.1371/journal.pbio.1000178.

Okada, H., and D. Bukry (1980), Supplementary modification and introduction of code numbers to the low latitude coccolith biostratigraphy zonation (Bukry, 1973, 1975), Mar. Micropaleontol., 51, 321–325.

Okada, H., and S. Honjo (1973), The distribution of oceanic coccolithophorids in the Pacific, Deep Sea Res. Oceanogr. Abstr., 20(4), 355–374, doi:10.1016/0011-7471(73)90059-4.

Olsson, R. K., C. Hemleben, W. A. Berggren, and B. T. Huber (1999), Atlas of Paleocene Planktonic Foraminifera, Smithsonian Contribution to Paleobiology, vol. 85, pp. 225, Smithsonian Institution Press, Washington D. C.

Pagani, M., K. Caldeira, D. Archer, and J. C. Zachos (2006), An ancient carbon mystery, Science, 314, 1556–57, doi:10.1126/science.1136110.

Pearson, P. N., N. J. Shackleton, and M. A. Hall (1993), Stable isotope paleoecology of middle Eocene planktonic foraminifera and multispecies isotope stratigraphy, DSDP Site 523, South Atlantic, J. Foraminiferal Res., 23, 123-140, doi:10.2113/gsjfr.23.2.123.

Pearson, P. N., R. K. Olsson, C. Hemblen, B. T. Huber, and W. A. Berggren (Eds.) (2006), Atlas of Eocene Planktonic Foraminifera, Cushman Special Publication, vol. 41, pp. 513, Department of Geology East Carolina Univ., Greenville.

Perch-Nielsen, K. (1981), Nouvelles observations sur les nannofossiles calcaires a la limite Cretace-Tertiaire pres de El Kef, Tunisie, Cahiers de Micropaléontol., 3, 25–36.

Petrizzo, M.-R., G. Leoni, R. P. Speijer, B. De Bernardi, and F. Felletti (2008), Dissolution susceptibility of some Paleogene planktonic foraminifera from ODP Site 1209 (Shatsky Rise, Pacific Ocean), J. Foraminiferal Res., 38(4), 357–371.

Premoli Silva, I., and A. Boersma (1988), Atlantic Eocene planktonic foraminiferal historical biogeography and paleohydrographic indices, Palaeogeogr. Palaeoclimatol. Palaeoecol., 67(3-4), 315–356, doi:10.1016/0031-0182(88)90159-9.

Premoli Silva, I., and A. Boersma (1989), Atlantic Paleogene planktonic foraminiferal bioprovincial indices, Mar. Micropaleontol., 14(4), 357–372, doi:10.1016/0377-8398(89)90019-4.

Quillévéré, F., R. D. Norris, I. Moussa, and W. A. Berggren (2001), Role of photosymbiosis and biogeography in the diversification of early Paleogene acarininids (planktonic foraminifera), Paleobiology, 27(2), 311–326, doi:10.1666/0094-8373(2001)027<0311:ROPABI>2.0.CO;2.

Rio, D., I. Raffi, and G. Villa (1990a), Pliocene-Pleistocene calcareous nannofossili distribution patterns in the western Mediterranean, in Proceedings of the Ocean Drilling Program, Scientific Results, edited by K. A. Kasterns et al., 107, 513-533, Ocean Drill. Program, College Station, Tex., doi:10.2973/odp.proc.sr.107.164.1990.

Rio, D., Fornaciari, E. and I. Raffi (1990b), Late Oligocene through early Pleistoene calcareous nannofossils from western equatorial Indian Ocean (Leg 115), in Proceedings of the Ocean Drilling Program, Scientific Results, 115, edited by R. A. Duncan et al., 175–235, Ocean Drilling Program, College Station, TX, USA, doi:10.2973/odp.proc.sr.115.152.1990.

Röhl, U., T. Westerhold, S. Monechi, E. Thomas, J. C. Zachos, and B. Donner (2005), The third and final early Eocene Thermal Maximum: Characteristics, timing, and mechanisms of the "X" event, Geol. Soc. Am. Abstr. Program, 37(7), 264.

Röhl, U., T. Westerhold, T. J. Bralower, and J. C. Zachos (2007), On the duration of the Paleocene-Eocene thermal maximum (PETM), Geochem. Geophys. Geosyst., 8, Q12002, doi:10.1029/2007GC001784.

Roth, P. H. (1983), Jurassic and Lower Cretaceous calcareous nannofossils in the western North Atlantic (Site 534): Biostratigraphy, preservation, and some observations on biogeography and paleoceanography, in Deep Sea Drilling Project, Initial Reports., 76, edited by R. E. Sheridan et al., 587-621, U.S. Gov. Print. Off., Washington, D. C., doi:10.2973/dsdp.proc.76.125.1983.

Roth, P. H., and H. Thierstein (1972), Calcareous nannoplankton: Leg 14 of the Deep Sea Drilling Project, in Deep Sea Drilling Project, Initial Reports., 14, edited by D. E. Hayes et al., 421-485, U.S. Gov. Print. Off., Washington, D. C., doi:10.2973/dsdp.proc.14.1972.

Schmidt, D. N., S. Renaud, J. Bollmann, R. Schiebel, and H. R. Thierstein (2004), Size distribution of Holocene planktic foraminifer assemblages: Biogeography, ecology and adaptation, Mar. Micropaleont., 50(3–4), 319–338, doi:10.1016/S0377-8398(03)00098-7.

Schmidt, D. N., D. Lazarus, J. R. Young, and M. Kucera (2006), Biogeography and evolution of body size in marine plankton, Earth Sci. Rev., 78, 239–266, doi:10.1016/j.earscirev.2006.05.004.

Schoon, P. L., A. Sluijs, J. S. Sinninghe Damsté, and S. Schouten (2011), High productivity and elevated carbon isotope fractionations in the Arctic Ocean during Eocene Thermal Maximum 2, Paleoceanography, 26, PA3215, doi:10.1029/2010PA002028.

Schrag, D. P., D. J. DePaolo, and F. M. Richter (1995), Reconstructing past sea surface temperatures: Correcting for diagenesis of bulk marine carbonate, Geochim. Cosmochim. Acta, 59, 2265–2278.

Sexton, P. F., R. D. Norris, P. A. Wilson, H. Pälike, T. Westerhold, U. Röhl, C. T. Bolton, and S. J. Gibbs (2011), Eocene global warming events driven by ventilation of oceanic dissolved organic carbon, Nature, 471(7338), 349–352, doi:10.1038/nature09826.

Slotnick, B. S., G. R. Dickens, M. J. Nicolo, C. J. Hollis, J. S. Crampton, and J. C. Zachos (2012), Large-amplitude variations in carbon cycling and terrestrial weathering during the latest Paleocene and earliest Eocene: The record at Mead Stream, New Zealand, J. Geol., 120(5), 487–505, doi:10.1086/666743.

Sluijs, A., S. Schouten, T. H. Donders, P. L. Schoon, U. Röhl, G.-J. Reichart, F. Sangiorgi, J. H. Kim, J. S. Sinninghe Damsté, and H. Brinkhuis (2009), Warm and wet conditions in the Arctic region during Eocene Thermal Maximum 2, Nat. Geosci., 2(11), 1–4, doi:10.1038/ngeo668.

Speijer, R. P., and B. Schmitz (1998), A benthic foraminiferal record of Paleocene sea level and trophic/redox conditions at Gebel Aweina, Egypt, Palaeogeogr. Palaeoclimatol. Palaeoecol., 137, 79–101.

Spötl, C., and T. W. Vennemann (2003), Continuous-flow isotope ratio mass spectrometric analysis of carbonate minerals, Rapid Commun. Mass Spectrom., 17(9), 1004–1006, doi:10.1002/rcm.1010.

Stap, L., A. Sluijs, E. Thomas, and L. J. Lourens (2009), Patterns and magnitude of deep sea carbonate dissolution during Eocene Thermal Maximum 2 and H2, Walvis Ridge, Southeastern Atlantic Ocean, Paleoceanography, 24, PA1211, doi:10.1029/2008PA001655.

Stap, L., L. J. Lourens, E. Thomas, A. Sluijs, S. Bohaty, and J. C. Zachos (2010a), High-resolution deep-sea carbon and oxygen isotope records of Eocene Thermal Maximum 2 and H2, Geology, 38, 607–610, doi:10.1130/G30777.1.

Stap, L., L. J. Lourens, A. van Dijk, S. Schouten, and E. Thomas (2010b), Coherent pattern and timing of the carbon isotope excursion and warming during Eocene Thermal Maximum 2 as recorded in planktic and benthic foraminifera, Geochem. Geophys. Geosyst., 11, Q11011, doi:10.1029/2010GC003097.

Stassen, P., E. Steurbaut, A.-M. M. Morsi, P. Schulte, and R. P. Speijer (2012), Biotic impact of Eocene Thermal Maximum 2 in a shelf setting (Dababiya, Egypt), Austrian J. Earth Sci., 105(1), 154–160.

Suganuma, Y., and J. G. Ogg (2006), Campanian through Eocene magnetostratigraphy of sites 1257–1261, ODP leg 207, Demerara rise (Western Equatorial Atlantic), in Proceedings of the Ocean Drilling Program, Scientific Results, 207, 1-48, Ocean Drill. Program, College Station, Texas. Available at http://www-odp.tamu.edu/publications/207_SR/102/102.htm.

Thierstein, H. R., K. R. Geitzenauer, and B. Molfino (1977), Global synchroneit of late Quaternary coccolith datum levels: Validation by oxygen isotopes, Geol. Soc. Am., 5, 400–404.

Thomas, E., J. C. Zachos, and T. J. Bralower (2000), Deep-sea environments on a warm earth: latest Paleocene–early Eocene, in Warm Climates in Earth History, edited by B. Huber, K. MacLeod, and S. Wing, pp. 132–160, Cambridge Univ. Press, Cambridge, U. K.

Thomas, E., H. Brinkhuis, M. Huber, and U. Röhl (2006), An ocean view of the early Cenozoic greenhouse world, Oceanography, 19, 63–72.

Thunell, R. C., and S. Honjo (1981), Calcite dissolution and the modification of planktonic foraminiferal assemblages, Mar. Micropaleontol., 6(2), 169–182.

Tjalsma, R. C., and G. P. Lohmann (1983), Paleocene-Eocene bathyal and abyssal benthic foraminifera from the Atlantic Ocean, Micropaleontol. Spec. Publ., 4, 1–90.

Toffanin, F., C. Agnini, E. Fornaciari, D. Rio, L. Giusberti, V. Luciani, D. J. A. Spofforth, and H. Pälike (2011), Changes in calcareous nannofossil assemblages during the Middle Eocene Climatic Optimum: Clues from the central-western Tethys (Alano section, NE Italy), Mar. Micropaleontol., 81(1), 22–31, doi:10.1016/j.marmicro.2011.07.002.

Tremolada, F., and T. J. Bralower (2004), Nannofossil assemblage fluctuations during the Paleocene-Eocene thermal maximum at Sites 213 (Indian Ocean) and 401 (North Atlantic Ocean): Palaeoceanographic implications, Mar. Micropaleontol., 52(1), 107–116, doi:10.1016/j.marmicro.2004.04.002.

Van der Zwaan, G. J., F. J. Jorissen, and H. C. De Stigter (1990), The depth dependency of planktic/benthonic foraminiferal ratios: Constraints and applications, Mar. Geol., 95, 1–16.

Van Hinsbergen, D. J. J., L. V. de Groot, S. J., van Schaik, W. Spakman, P. K. Bijl, A. Sluijs, C. G. Langereis, and H. Brinkhuis (2015), A Paleolatitude Calculator for Paleoclimate Studies, PLoS ONE, 10, e0126946, doi:10.1371/journal.pone.0126946.

Van Morkhoven, F. P. C. M., W. A. Berggren, and A. S. Edwards (1986), Cenozoic Cosmopolitan deep-sea benthic foraminifera, Bull. des Centres de Recherches Exploration-Production Elf-Aquitane, Mèmoire, 11, 11–421.

Villa, G., C. Fioroni, L. Pea, S. M. Bohaty, and D. Persico (2008), Middle Eocene–late Oligocene climate variability: Calcareous nannofossil response at Kerguelen Plateau, Site 748, Mar. Micropaleontol., 69, 173–192.

Wade, B. S., and R. K. Olsson (2009), Investigation of pre-extinction dwarfing in Cenozoic planktonic foraminifera, Palaeogeogr. Palaeoclimatol. Palaeoecol., 284, 39–46.

Wade, B. S., N. Al-Sabouni, C. Hemleben, and D. Kroon (2008), Symbiont bleaching in fossil planktonic foraminifera, Evol. Ecol., 22(2), 253–265, doi:10.1007/s10682-007-9176-6.

Wade, B. S., P. N. Pearson, W. A. Berggren, and H. Pälike (2011), Review and revision of Cenozoic tropical planktonic foraminiferal biostratigraphy and calibration to the geomagnetic polarity and astronomical time scale, Earth Sci. Rev., 104(1-3), 111–142, doi:10.1016/j.earscirev.2010.09.003.

Watson, G. (1983), Large sample theory of the Langevin distribution, J. Stat. Plan. Inference, 8, 245–256. Wei, W., and S. W. Wise Jr. (1990), Biogeographic gradients of middle Eocene–Oligocene calcareous nannoplankton in the South Atlantic Ocean, Palaeogeogr. Palaeoclimatol. Palaeoecol., 79, 29–61.

Westerhold, T., and U. Röhl (2009), High resolution cyclostratigraphy of the early Eocene—New insights into the origin of the Cenozoic cooling trend, Clim. Past, 5(3), 309–327, doi:10.5194/cp-5-309-2009.

Westerhold, T., U. Röhl, J. Laskar, I. Raffi, J. Bowles, L. J. Lourens, and J. C. Zachos (2007), On the duration of magnetochrons C24r and C25n and the timing of early Eocene global warming events: Implications from the Ocean Drilling Program Leg 208 Walvis Ridge depth transect, Paleoceanography, 22, PA2201, doi:10.1029/2006PA001322.

Westerhold, T., U. Röhl, I. Raffi, E. Fornaciari, S. Monechi, V. Reale, J. Bowles, and H. F. Evans (2008), Astronomical calibration of the Paleocene time, Palaeogeogr. Palaeoclimatol. Palaeoecol., 257, 377–403, doi:10.1016/j.palaeo.2007.09.016.

Westerhold, T., U. Röhl, and J. Laskar (2012), Time scale controversy: Accurate orbital calibration of the early Paleogene, Geochem. Geophys. Geosyst., 13, Q06015, doi:10.1029/2012GC004096.

Westerhold, T., U. Röhl, T. Frederichs, S. M. Bohaty, and J. C. Zachos (2015), Astronomical calibration of the geological timescale: Closing the middle Eocene gap, Clim. Past, 11(9), 1181–1195, doi:10.5194/cp-11-1181-2015.

Young, J. R. (1994), Functions of coccoliths, in Coccolithophores, edited by A. Winter and W. G. Siesser, pp. 63–82, Cambridge Univ. Press, Cambridge.

Zachos, J. C., et al. (2005), Rapid acidification of the ocean during the Paleocene-Eocene thermal maximum, Science, 308, 1611–1615, doi:10.1126/science.1109004.

Zachos, J. C., G. R. Dickens, and R. E. Zeebe (2008), An early Cenozoic perspective on greenhouse warming and carbon-cycle dynamics, Nature, 451(7176), 279-283, doi:10.1038/nature06588.

Zachos, J. C., H. K. McCarren, B. Murphy, U. Röhl, and T. Westerhold (2010), Tempo and scale of late Paleocene and early Eocene carbon isotope cycles: Implications for the origin of hyperthermals, Earth Planet. Sci. Lett., 299, 242–249, doi:10.1016/j.epsl.2010.09.004.

Zeebe, R. E., J. C. Zachos, and G. R. Dickens (2009), Carbon dioxide forcing alone insufficient to explain Palaeocene–Eocene Thermal Maximum warming, Nat. Geosci., 2(8), 576–580, doi:10.1038/ngeo578.

Zijderveld, J. D. A. (1967), A.C. demagnetization of rocks: analysis of results, in Methods in Paleomagnetism, vol. 3, edited by D. W. Collinson, K. M. Creer, and S. K. Runcorn, pp. 254–286, Elsevier, Amsterdam

CHAPTER III

Major perturbations in the global carbon cycle and photosymbiont-bearing planktic foraminifera during the early Eocene

Valeria Luciani[1], Gerald R. Dickens[2,3], Jan Backman[2], Eliana Fornaciari[4], Luca Giusberti[4], Claudia Agnini[4], and Roberta D'Onofrio[1]

[1]Department of Physics and Earth Sciences, Ferrara University, Polo Scientifico Tecnologico, Via G. Saragat 1, 44100 Ferrara, Italy

[2]Department of Geological Sciences, Stockholm University, 10691 Stockholm, Sweden

[3]Department of Earth Science, Rice University, Houston, TX 77005, USA

[4]Department of Geosciences, Padova University, Via G. Gradenigo 6, 35131 Padova, Italy

Abstract

A marked switch in the abundance of the planktic foraminiferal genera Morozovella and Acarinina occurred at low-latitude sites near the start of the Early Eocene Climatic Optimum (EECO), a multi-million-year interval when Earth surface temperatures reached their Cenozoic maximum. Stable carbon and oxygen isotope data of bulk sediment are presented from across the EECO at two locations: Possagno in northeast Italy and Deep Sea Drilling Project (DSDP) Site577 in the northwest Pacific. Relative abundances of planktic foraminifera are presented from these two locations, as well as from Ocean Drilling Program (ODP) Site 1051 in the northwest Atlantic. All three sections have good stratigraphic markers, and the $\delta^{13}C$ records at each section can be correlated amongst each other and to $\delta^{13}C$ records at other locations across the globe. These records show that a series of negative carbon isotope excursions (CIEs) occurred before, during and across the EECO, which is defined here as the interval between the J event and the base of *Discoaster sublodoensis*. Significant though ephemeral modifications in planktic foraminiferal assemblages coincide with some of the short-term CIEs, which were marked by increases in the relative abundance of *Acarinina*, similar to what happened across established hyperthermal events in Tethyan settings prior to the EECO. Most crucially, a temporal link exists between the onset of the EECO, carbon cycle changes during this time and the decline in *Morozovella*. Possible causes are manifold and may include temperature effects on photosymbiont bearing planktic foraminifera and changes in ocean chemistry.

1. Introduction

Cenozoic Earth surface temperatures attained their warmest long-term state during the Early Eocene Climatic Optimum (EECO). This was a 2–4 Myr time interval (discussed below) centered at ca. 51 Ma (Fig. 1), when average high-latitude temperatures exceeded those in the present day by at least10°C (Zachos et al., 2008; Bijl et al., 2009; Huber and Caballero, 2011; Hollis et al., 2012; Pross et al., 2012; Ingliset al., 2015). Several short-term (<200 kyr) global warming events (Fig. 1) occurred before the EECO. The Paleocene–Eocene Thermal Maximum (PETM) provides the archetypical example: about 55.9 Ma (Vandenberghe et al., 2012; Hilgen et al., 2015) temperatures soared an additional 5–6°C relative to background conditions (Sluijs et al., 2006, 2007; Dunkley Jones et al., 2013). Evidence exists for at least two other significant Eocene warming events (Cramer et al.,2003;

Lourens et al., 2005; Röhl et al., 2005; Thomas et al.,2006; Nicolo et al., 2007; Agnini et al., 2009; Coccioni et al., 2012; Lauretano et al., 2015; Westerhold et al., 2015): one ca. 54.1 Ma and named H1 or Eocene Thermal Maximum 2 (ETM2, also referred to as the Elmo event) and one at 52.8 Ma and variously named K, X or ETM3 (hereafter called K/X). However, additional brief warming events may have spanned the early Eocene (Cramer et al., 2003; Lourens et al., 2005; Röhl et al., 2005; Thomas et al., 2006; Nicolo et al., 2007; Agnini et al., 2009; Coccioni et al., 2012; Lauretano et al., 2015; Westerhold et al., 2015; Kirtland-Turner et al., 2014), and the EECO may comprise a series of successive events (Slotnick et al., 2012). Both long-term and short term intervals of warming corresponded to major changes in global carbon cycling, although the precise timing between these parameters remains insufficiently resolved.

In benthic foraminiferal stable-isotope records for the early Paleogene (Fig. 1), $\delta^{18}O$ serves as a proxy for deep-water temperature, while $\delta^{13}C$ relates to the composition of deep-water dissolved inorganic carbon (DIC). The highest $\delta^{13}C$ values of the Cenozoic occurred at ca. 58 Ma. From this Paleocene Carbon Isotope Maximum (PCIM), benthic foraminiferal $\delta^{13}C$ values plunge by approximately 2.5‰ to reach a near-Cenozoic minimum at or near the start of the EECO and subsequently rise by approximately 1.5‰ across this interval (Shackleton and Hall, 1984; Shackleton, 1986; Zachos et al., 2001, 2008; Cramer et al., 2009). Benthic foraminiferal 13C records also exhibit prominent negative carbon isotope excursions (CIEs) across the three hyperthermals mentioned above (Kennett and Stott, 1991; Littler et al., 2014; Lauretano et al., 2015). Crucially, at least from the late Paleocene to the start of the EECO, similar $\delta^{13}C$ records occur in other carbon-bearing phases, such as bulk marine carbonate, planktic foraminifera, and various marine and terrestrial organic carbon compounds (Shackleton, 1986; Schmitz et al., 1996; Lourens et al., 2005; Nicolo et al., 2007; Agnini et al., 2009, 2016; Leon-Rodriguez and Dickens, 2010; Abels et al., 2012; Coccioni et al., 2012; Sluijs and Dickens, 2012; Slotnick et al., 2012, 2015a; Clyde et al., 2013). This strongly suggests that observed changes in $\delta^{13}C$, both long-term trends as well as short-term perturbations, represent variations in the input and output of ^{13}C depleted carbon to the exogenic carbon cycle (Shackleton, 1986; Dickens et al., 1995; Dickens, 2000; Kurtz et al., 2003; Komar et al., 2013).

Significant biotic changes occur in terrestrial and marine environments during times when the early Paleogene $\delta^{18}O$ and $\delta^{13}C$ records show major variations. This has been recognized
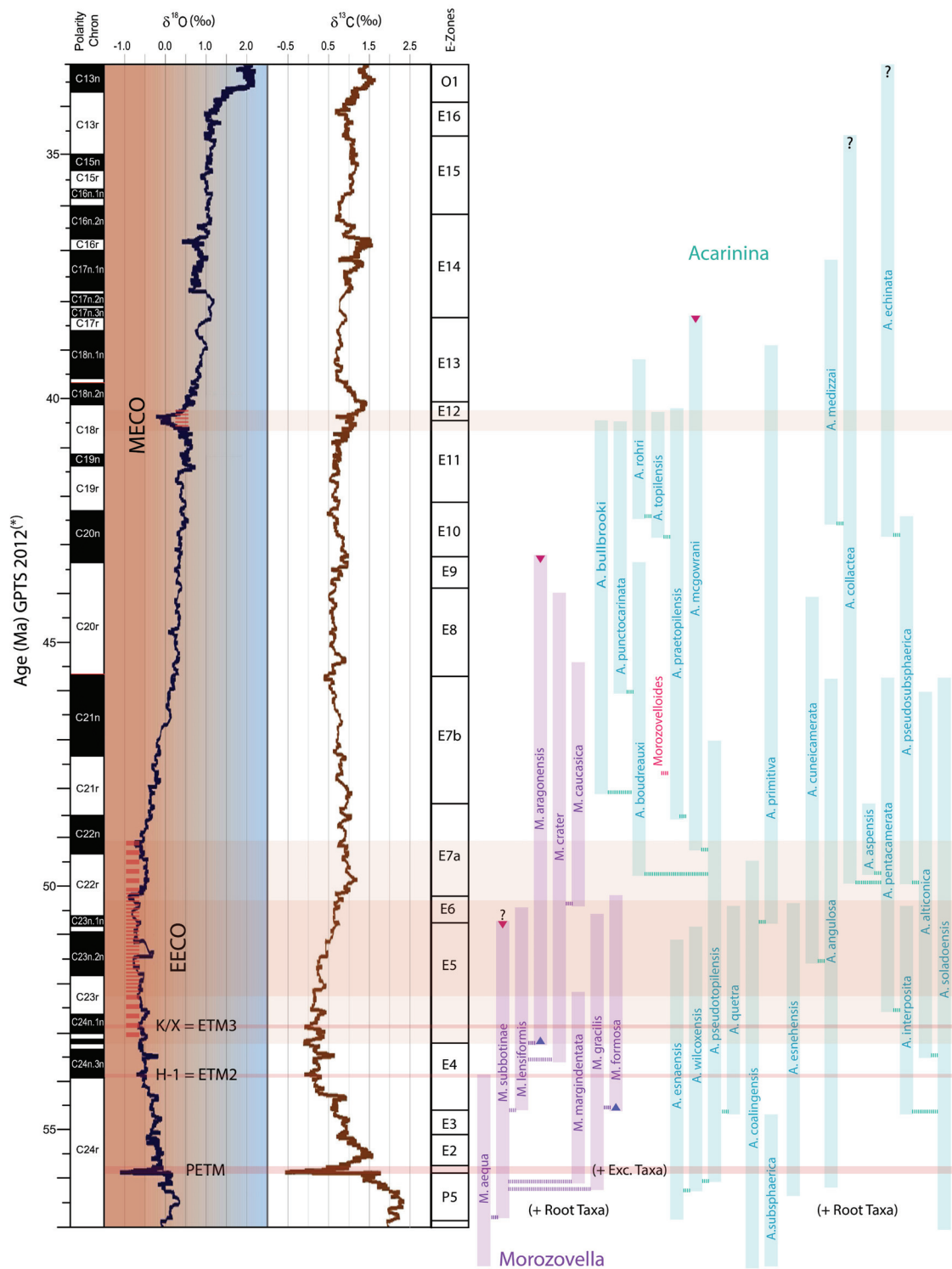
Figure 1. Evolution of climate, carbon cycling and planktic foraminifera across the middle Paleogene on the Geomagnetic Polarity Time Scale (GPTS) 2012 timescale. The left side shows polarity chrons and smoothed oxygen and carbon isotope records of benthic foraminifera, slightly modified from Vandenberghe et al. (2012). Oxygen and carbon isotope values come from compilations by Zachos et al. (2008) and Cramer et al. (2009). The middle of the figure indicates planktic foraminiferal biozones by Wade et al. (2011) with three modifications. The lower boundary for Zone E7a is now based on the first occurrence of *Astrorotalia palmerae* due to diachroneity in the first appearance of the previously selected marker *Acarinina cuneicamerata* (Luciani and Giusberti, 2014). The base of Zone E5, identified by the first appearance of *Morozovella aragonensis*,

70

occurs in the middle of C24n instead of lower C23r (see text). A question marks the top of *Morozovella subbotinae* because there is diachroneity for this occurrence (see text). Right side shows a partial view of *Morozovella* and *Acarinina* evolution as envisioned by Pearson et al. (2006) and Aze et al. (2011). It does not include several "root taxa" that disappear in the earliest Eocene (e.g., *M. velascoensis*) or "excursion taxa" that appear during the Paleocene–Eocene Thermal Maximum (PETM) (e.g., *M. allisonensis*). Superimposed on these records are key intervals of climate change, including the Early Eocene Climatic Optimum (EECO), the Middle Eocene Climatic Optimum (MECO) and the three well-documented early Eocene hyperthermal events. The extent of the EECO is not precise because of stratigraphic issues (see text). Red and blue triangles: top and base of the *Morozovella* and *Acarinina* zonal markers.

for the PETM, where land sections exhibit a prominent mammal turnover (Gingerich 2001, 2003; McInerney and Wing, 2011; Clyde et al., 2013) and where marine sections reveal a profound benthic foraminiferal extinction (Thomas, 1998), turnovers in calcareous nannoplankton, ostracods, corals and larger benthic foraminifera (Raffi and De Bernardi, 2008; Scheibner and Speijer, 2008; Yamaguchi and Norris, 2012; Agnini et al., 2014), and the appearance of excursion taxa in calcareous nannoplankton, dinoflagellates and planktic foraminifera (Kelly et al., 1996, 1998; Crouch et al., 2001; Sluijs et al., 2006; Self-Trail et al., 2012). Major plant and mammal turnovers also occurred on land during the longer EECO (Wing et al., 1991; Zonneveld et al., 2000; Wilf et al., 2003; Falkowski et al., 2005; Woodburne et al., 2009; Figueirido et al., 2012). In the marine realm, evolutionary trends across the EECO have been noted, in particular the inception of modern calcareous nannofossil community structure (Agnini et al., 2006, 2014; Schneider et al., 2011; Shamrock et al., 2012) and possibly of diatoms (Sims et al., 2006; Oreshkina, 2012). These observations, both from continents and the oceans, support an overarching hypothesis that climate change drives biotic evolution, at least in part (Ezard et al., 2011).

Planktic foraminiferal assemblages are abundant in carbonate-bearing marine sediments and display distinct evolutionary trends that can often be correlated to climate variability (Schmidt et al., 2004; Ezard et al., 2011; Fraass et al., 2015). This is especially true in the early Paleogene, even though the relationship between climate variability and planktic foraminiferal evolution remains insufficiently known. At the beginning of the Eocene, planktic foraminifera had evolved over ca. 10 Myr following the Cretaceous–Paleogene mass extinction event. Several early Paleogene phylogenetic lines evolved, occupying different ecological niches in the upper water column. Subsequently, a major diversification occurred during the early Eocene, which resulted in a peak of planktic foraminiferal diversity during the middle Eocene (Norris, 1991; Schmidt et al., 2004; Pearson et al., 2006; Aze et al., 2011; Ezard et al., 2011; Fraass et al., 2015).
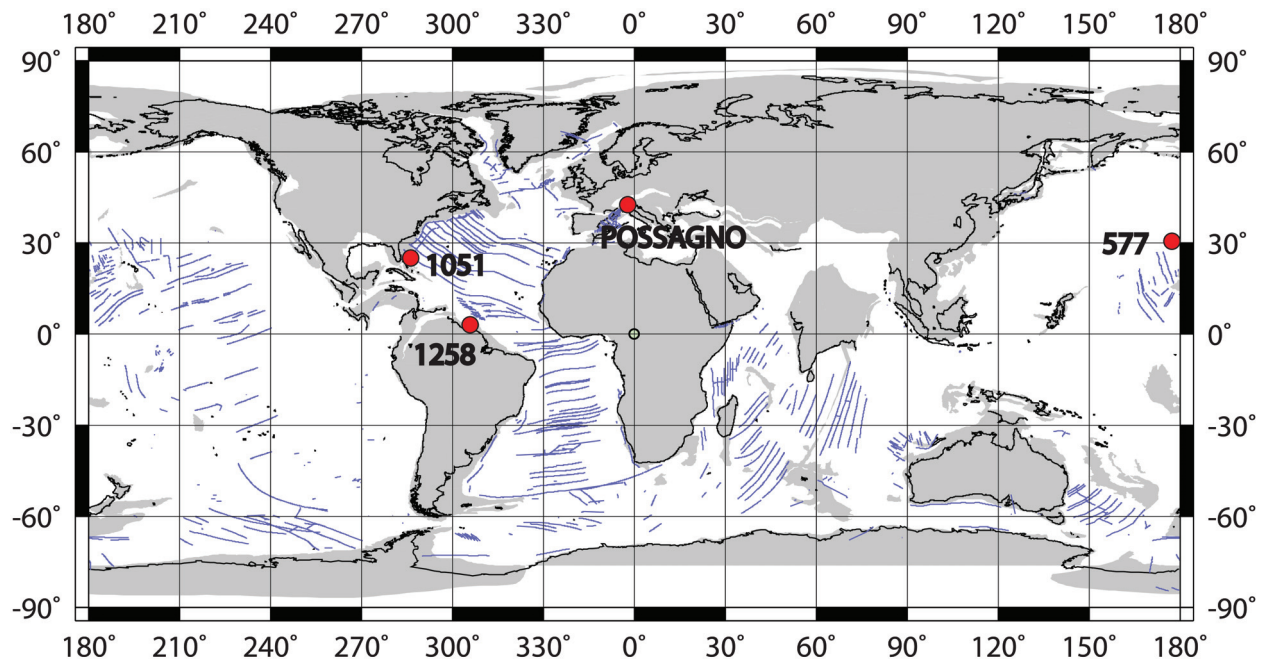
50 Ma Reconstruction

Figure 2. Approximate locations of the three sites discussed in this work during the early Eocene. Also shown is Site 1258, which has a bulk carbonate $\delta^{13}C$ record spanning the EECO. Base map is from http://www.odsn/de/services/paleomap.html with paleolatitudes modified for Sites 577, 1051 and 1258 according to www.paleolatitude.org model version 1.2 (Van Hinsbergen et al., 2015). Possagno paleolatitude is based on the http://www.odsn.de/odsn/services/paleomap/adv_map.html model since it is not yet available at http://www.odsn.de/services/paleomap.html.

In this study, we focus on the evolution of two planktic foraminiferal genera: *Morozovella* and *Acarinina* (Fig. 1). These two genera belong to the "muricate group", a term derived from the muricae that form layered pustules on the test wall. These two genera are of particular interest because of their dominance among tropical and subtropical assemblages of the early Paleogene oceans and because these genera show a major turnover in taxonomic diversity close to the beginning of the EECO, one that comprises species reduction among *Morozovella* and species diversification among *Acarinina* (Lu and Keller, 1995; Lu et al., 1998; Pearson et al., 2006; Aze et al., 2011).

Numerous lower Eocene sedimentary sections from lower latitudes contain well-recognizable (albeit often recrystallized) planktic foraminiferal tests. Changes in foraminiferal assemblages presumably reflect relationships between climate and carbon cycling across the EECO. The present problem is that no section examined to date provides counts of foraminiferal assemblages, detailed stable-isotope records and robust planktic foraminiferal biostratigraphies across the entire EECO. Indeed, at present, only a few sites have detailed and interpretable stable-isotope records across much of the EECO (Slotnick et al., 2012, 2015a; Kirtland-Turner et al., 2014). Furthermore, the EECO lacks formal definition. As a

consequence, any relationship between climatic perturbations during the EECO and the evolution of planktic foraminifera remains speculative. Here, we add new data from three locations: the Possagno section from the western Tethys, Deep Sea Drilling Project (DSDP) Site 577 from the tropical Pacific Ocean and Ocean Drilling Program (ODP) Site 1051 from the subtropical Atlantic Ocean (Fig. 2). These sections represent a wide longitudinal span of low-latitude locations during the early Paleogene. By comparing stable isotope and planktic foraminiferal records at these three locations, we provide a new foundation for understanding why the abundances of *Acarinina* and *Morozovella* changed during the EECO.

2. The Early Eocene Climatic Optimum

Evidence for extreme Earth surface warmth during a multimillion-year time interval of the early Eocene is overwhelming and comes from many studies, utilizing both marine and terrestrial sequences and both fossil and geochemical proxies (Huber and Caballero, 2011; Hollis et al., 2012; Pross et al., 2012). However, a definition for the EECO, including the usage of "optimum", endures as a perplexing problem. This is for several reasons, including the basic facts that (i) proxies for temperature should not be used to define a time increment, (ii) clearly correlative records across the middle of the early Eocene with a temporal resolution of less than 50 kyr remain scarce and (iii) absolute ages across the early Eocene have changed significantly (Berggren et al., 1995; Vandenberghe et al., 2102). As a consequence, various papers discussing the EECO give different ages and durations 2 to 4 Myr long sometime between circa 49 and 54Ma (e.g., Yapp, 2004; Lowenstein and Demicco, 2006; Zachos et al., 2008; Woodburne et al., 2009; Bijl et al., 2009; Smith et al., 2010; Hollis et al., 2012; Slotnick et al., 2012; Pujalte et al., 2015).

The EECO, at least as presented in many papers, refers to the time of minimum $\delta^{18}O$ values in "stacked" benthic foraminifera stable-isotope curves (Fig. 1). These curves were constructed by splicing together multiple $\delta^{18}O$ records generated at individual locations onto a common age model (originally Berggren et al., 1995). However, the stacked curves (Zachos et al., 2001, 2008; Cramer et al., 2009), while they can be adjusted to different timescales, show significant variance in $\delta^{18}O$ across the middle to late early Eocene. Some of this variance is due to imprecisely calibrated records at individual sites, where cores do not align properly in the depth domain (Dickens and Backman, 2013). Some of this variance probably reflects a dynamic early Eocene climate regime, where average temperatures and atmospheric $p\mathrm{CO}_2$ across Earth changed significantly, perhaps on orbital timescales (Smith et al., 2010; Slotnick et al., 2012, 2015a; Kirtland-Turner et al., 2014).

There is also the root problem as to where EECO starts and ends. At a basic level, the interval characterized by the lowest Cenozoic benthic foraminiferal $\delta^{18}O$ values begins at a time that closely corresponds with a long-term minimum in $\delta^{13}C$ values (Fig. 1). This is important for stratigraphic reasons because the two stable-isotope curves were generated using the same benthic foraminiferal samples, but $\delta^{13}C$ records at different locations should necessarily correlate in the time domain (unlike $\delta^{18}O$ and temperature). The rationale for such a carbon isotope stratigraphy lies in the rapid cycling of carbon across Earth's surface (Shackleton, 1986; Dickens, 2000).

The Eocene minimum in $\delta^{13}C$ corresponds to the K/X event (Fig. 1), which happened in polarity Chron C24n.1n and approximately 3 Myr after the PETM (Agnini et al., 2009; Leon-Rodriguez and Dickens, 2010; Slotnick et al., 2012; Dallanave et al., 2015; Lauretano et al., 2015; Westerhold et al., 2015). However, in several detailed studies spanning the early Eocene, changes in long-term trends appear to have occurred about 400 kyr before the K/X event and at an event called "J" (after Cramer et al., 2003), which happened near the boundary of polarity chrons C24n.2r and C24n.3n (Slotnick et al., 2015a; Lauretano et al., 2015). Notably, the long-term late Paleocene–early Eocene decrease in detailed benthic foraminiferal $\delta^{18}O$ records at Site 1262 on Walvis Ridge ceases at the J event (Lauretano et al., 2015).

The end of the EECO has received limited attention from a stratigraphic perspective. Indeed, the termination of the EECO may not be a recognizable global "event" because it may relate to ocean circulation and gateways expressed mostly in the Southern Ocean and deep-ocean records (Pearson et al., 2007; Bijl et al., 2013). In Paleogene continental slope sections now uplifted and exposed in the Clarence River valley, New Zealand, a major lithologic change from limestone to marl coincides with the J event (Slotnick et al., 2012, 2015a; Dallanave et al., 2015). The marl-rich unit, referred to as "Lower Marl", has been interpreted to reflect enhanced terrigenous supply to a continental margin because of greater temperature and enhanced seasonal precipitation. It has been suggested further that Lower Marl indicates the EECO (Slotnick et al., 2012; Dallanave et al., 2015). The top of Lower Marl, and a return to limestone deposition, lies within the upper part of polarity Chron C22n (Dallanave et al., 2015). This is interesting because it approximates the time when general long-term Cenozoic cooling is initiated at several locations that have records of polarity chrons and proxies for temperature (Bijl et al., 2009; Hollis et al., 2012; Pross et al., 2012). It is also useful from a stratigraphic perspective because the end of the EECO thus lies close to a well-documented and widespread calcareous nannofossil biohorizon, the base of *Discoaster sublodoensis*. This

marks the base of CP10, NP12 or CNE4, depending on the chosen calcareous nannofossil zonal scheme (Okada and Bukry, 1980; Martini, 1971; Agnini et al., 2014).

Without an accepted definition in the literature, we tentatively present the EECO as the duration of time between the J event and the base of *D. sublodoensis*. This interval thus begins at about 53 Ma and ends at about 49 Ma on the 2012 Geologic Time Scale (GTS; Vandenberghe et al., 2012). However, while the EECO was characterized by generally warm conditions, numerous fluctuations in average temperature likely occurred during the 4 Myr interval.

3. Sites and Stratigraphy

3.1. Possagno, Venetian Prealps, Tethys

An Upper Cretaceous through Miocene succession crops out at the bottom of the Monte Grappa massif in the Possagno area, about 60 km northwest of Venice. The lower to middle Eocene, of primary focus in this study, is represented by the Scaglia beds. These sedimentary rocks represent pelagic and hemipelagic sediment that accumulated at middle to lower bathyal depths (Cita, 1975; Thomas, 1998) in the western part of the Belluno Basin, a Mesozoic–Cenozoic paleogeographic unit of the European Southern Alps (Bosellini, 1989). The basin very likely was an embayment connected to the western Tethys, with a paleolatitude of ca. 42° during the early Eocene (Fig. 2).

A quarry at 45°51.0′ N and 11°51.60′ E exposed a 66 m thick section of the Scaglia beds in 2002–2003 (Fig. 3), although it is at present largely covered and inaccessible. This section was examined for its stratigraphy (Agnini et al., 2006; Luciani and Giusberti, 2014) and shown to extend from just below the PETM to within lower Chron C20r in the lower middle Eocene. Like other lower Paleogene sections of the Venetian Prealps (Giusberti et al., 2007; Agnini et al., 2016), a clay marl unit (CMU) with a prominent negative CIE marks the PETM.

The Possagno section appears to be continuous, but with an important decrease in sedimentation rate (to below 1.4 m Myr^{-1}) between 14.66 and 15.51 m (Agnini et al.,2006). This interval lies within Chron C23r and near the startof the EECO and predates the onset of a major increase in *Discoaster* abundance (Agnini et al., 2006).
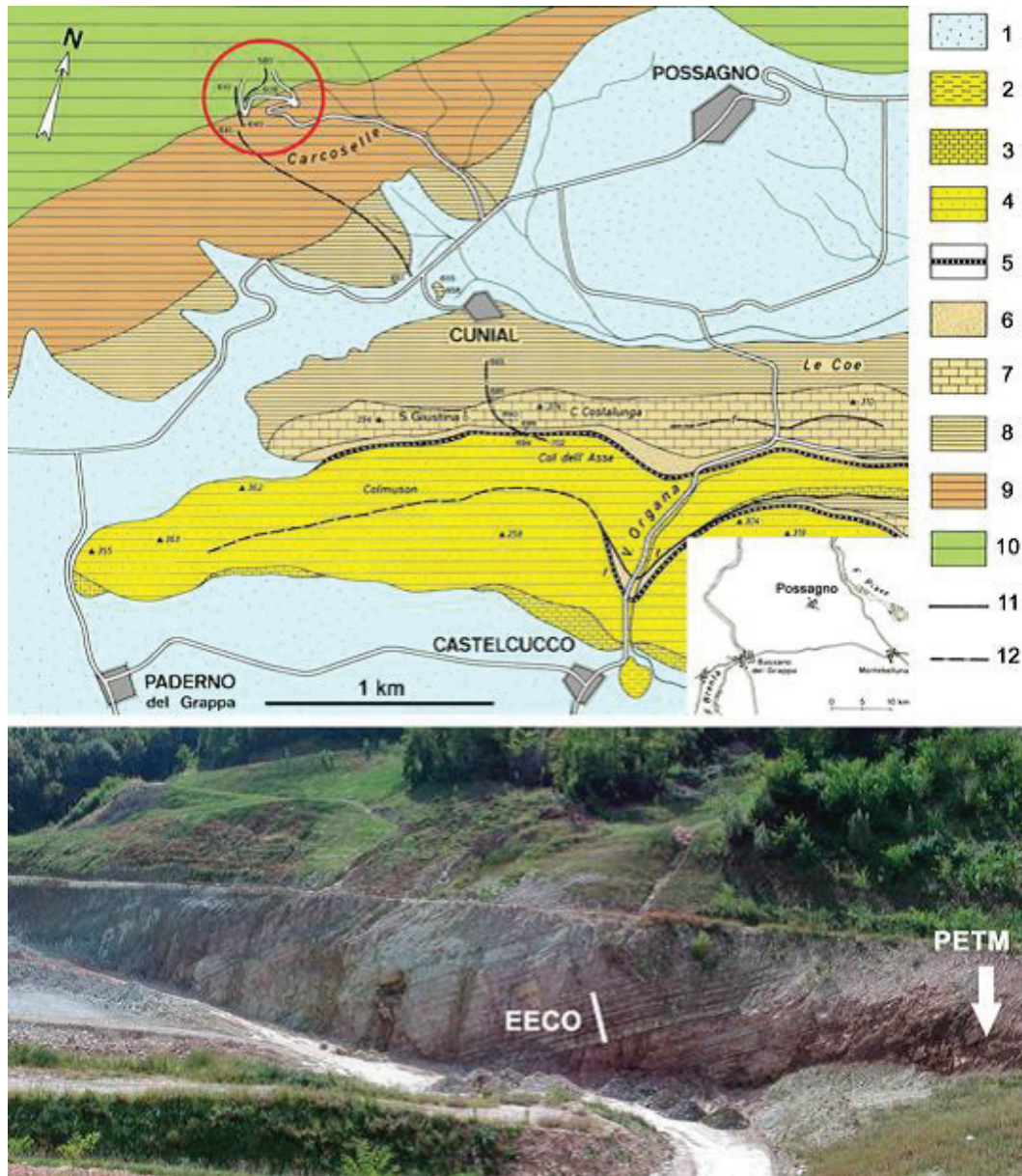
Figure 3. The Possagno section. Upper panel: geological map (modified from Braga, 1970). 1: Quaternary deposits; 2, 3: Calcarenite di Castelcucco (Miocene); 4: glauconitic arenites (Miocene); 5: siltstones and conglomerates (upper Oligocene–lower Miocene); 6: Upper Marna di Possagno (upper Eocene); 7: Formazione di Pradelgiglio (upper Eocene); 8: Marna di Possagno (upper Eocene); 9: Scaglia Cinerea (middle–upper Eocene); 10: Scaglia Rossa (Upper Cretaceous–lower Eocene); 11: faults; 12: traces of stratigraphic sections originally studied by Bolli (1975); red circle: the Carcoselle quarry. Lower panel: the exposed quarry face during Summer 2002 (Photo by Luca Giusberti).

3.2. Site 577, Shatsky Rise, Western Pacific

DSDP Leg 86 drilled Site 577 at 32°26.50´ N, 157°43.40´ E and 2680 m water depth on Shatsky Rise, a large igneous plateau in the NW Pacific with a relatively thin veneer of sediment (Shipboard Scientific Party, 1985). During the early Eocene, this site was located closer to 30° N (Fig. 2), and probably at a slightly shallower water depth (Ito and Clift, 1998).

Two primary holes were drilled at Site 577. Both Hole 577* and Hole 577A recovered portions of a nominally 65 m thick section of Upper Cretaceous through lower Eocene nannofossil ooze. Similar to the Possagno section, the lower Paleogene interval has biomagnetostratigraphic information (Bleil, 1985; Monechi et al., 1985; Backman, 1986; Lu and Keller, 1995; Dickens and Backman, 2013). Stable-isotope records of bulk carbonate have been generated for sediment from several cores at low sample resolution (Shackleton, 1986) and for much of cores 577*-9H and 577*-10H at a fairly high sample resolution (Cramer et al., 2003).

The composition and relative abundances of planktic foraminifera were nicely documented at Site 577 (Lu, 1995; Lu and Keller, 1995) and show a marked turnover between *Morozovella* and *Acarinina* during the early Eocene. These data, however, relied on an outdated view of the stratigraphy at this location, where cores were not originally aligned to account for gaps and overlaps (Dickens and Backman, 2013). As will become obvious later, the main phase of the EECO spans cores 577*-8H and 577A-8H, where detailed stable isotope records have not been generated previously.

3.3. Site 1051, Blake Nose, Western Atlantic

The Blake Nose is a gentle ramp extending from 1000 to 2700 m water depth east of Florida (Norris et al., 1998). The feature is known for a relatively thick sequence of middle Cretaceous through middle Eocene sediment with minimal overburden. ODP Leg 171B drilled and cored this sequence at several locations, including Site 1051 at 30°03.20′ N, 76°21.50′ W and 1994 m water depth (Shipboard Scientific Party, 1998). The site was located slightly to the south during the early Eocene (Fig. 2). Benthic foraminiferal assemblages indicate a lower bathyal depth (1000–2000 m) during the late Paleocene and middle Eocene (Norris et al., 1998), although Bohaty et al. (2009) estimated a paleodepth of about 2200 m for sedimentation at ca. 50 Ma.

Sediments from 452.24 to 353.10 m below the sea floor (mbsf) at Site 1051 consist of lower to middle Eocene carbonate ooze and chalk (Shipboard Scientific Party, 1998).The site comprises two holes (1051A and 1051B), with core gaps and core overlaps existing at both (Shipboard Scientific Party, 1998). However, the impact of these depth offsets upon age is less than at Site 577 because of higher overall sedimentation rates.

The Eocene section at Site 1051 has good sediment recovery, except in an interval between 382 and 390 mbsf, which contains significant chert. Stratigraphic markers across the Eocene interval include polarity chrons (Ogg and Bardot, 2001), calcareous nannofossil

biohorizons (Mita, 2001) and planktic foraminiferal biohorizons (Norris et al., 1998; Luciani and Giusberti, 2014). As first noted by Cramer et al. (2003), though, there is a basic stratigraphic problem with the labeling of the polarity chrons. The intervals of normal polarity between approximately 388 and 395 mbsf and between approximately 412 and 420 mbsf were tentatively assigned to C22n and C23n, respectively (Ogg and Bardot, 2001). This age assignment was assumed to be correct by Luciani and Giusberti (2014), who therefore considered the last occurrence of *Morozovella subbotinae* as happening near the top of C23n, an assumption that was also made for the revision of Eocene foraminiferal biozones (Wade et al., 2011).

These age assignments, however, cannot be correct because calcareous nannofossil biohorizons that lie below or within C22n (top of *T. orthostylus*, top of *Toweius*, base of *D. sublodoensis*) occur above 388 mbsf (Mita, 2001). Instead, there must be a significant hiatus or condensed interval at the chert horizon, and the intervals of normal polarity noted above are C23n and C24n.1n.

4. Methods

4.1. Samples for Isotopes and Foraminifera

The three sites provide a good stratigraphic background and the key existing data for understanding the temporal link between the EECO, carbon isotope perturbations and planktic foraminiferal evolution. Our analytical aim was to obtain comparable data sets across the sites. More specifically, a need existed to generate stable-isotope and planktic foraminiferal assemblage records at the Possagno section, to generate stable-isotope records at DSDP Site 577, and to generate planktic foraminiferal assemblage records at ODP Site 1051.

In total, 298 samples were collected from the originally exposed Possagno section in 2002–2003 for isotope analyses. The sampling interval was 2 to 5 cm for the basal 0.7 m and varied between 20 and 50 cm for the interval between 0.7 and 66 m. Bulk sediment samples were previously examined for their calcareous nannofossil assemblages (Agnini et al., 2006). One hundred and ten of these samples were selected for the foraminiferal study.

Aliquots of the 110 samples were weighed and then washed to obtain foraminifera using two standard procedures, depending on lithology. For the indurated marly-limestones and limestones, the cold-acetolysis technique was used (Lirer, 2000; Luciani and Giusberti, 2014). This method disaggregates strongly lithified samples, in which foraminifera can otherwise

only be analyzed in thin sections (Fornaciari et al., 2007; Luciani et al., 2007). For the marls, samples were disaggregated using 30% hydrogen peroxide and subsequently washed and sieved at 63 μm. In most cases, gentle ultrasonic treatment (e.g., low-frequency at 40 kHz for30–60 s) improved the cleaning of the tests.

Relative abundance data of planktic foraminiferal samples were generated for 65 samples at Site 577 (Lu, 1995; Lu and Keller, 1995). We collected new samples for stable-isotope measurements that span their previous effort.

Fifty samples of Eocene sediment were obtained from Hole 1051A between 452 to 353 mbsf Sample spacing varied from 2.0 to 0.5 m. As the samples are ooze and chalk, they were prepared using disaggregation using distilled water and washing over 38 and 63 μm sieves. Washed residues were dried at <50°C.

4.2. Stable Isotopes

Carbon and oxygen stable-isotope data of bulk sediment samples from the Possagno section and Site 577 were analyzed using a Finnigan MAT 252 mass spectrometer equipped with a Kiel device at Stockholm University. Precision is within –0.06‰ for carbon isotopes and within –0.07‰ for oxygen isotopes. Stable-isotope values were calibrated to the Vienna Pee Dee Belemnite standard (VPDB) and converted to conventional delta notation ($\delta^{13}C$ and $\delta^{18}O$).

4.3. Foraminiferal Analyses

The mass percent of the > 63 μm size fraction relative to the mass of the bulk sample, typically 100 g sample^{-1}, was calculated for the 110 Possagno samples. This is referred to as the weight percent coarse fraction (WPCF), following many previous works. Due to the consistent occurrence of radiolarians at Site 1051, the WPCF cannot give information on foraminiferal productivity.

Relative abundances for both Possagno and Site 1051 have been determined from about 300 complete specimens extracted from each of the 110 samples investigated in the >63 μm size fraction from random splits.

The degree of dissolution, expressed as the fragmentation index (F-index) was evaluated according to Petrizzo et al. (2008) on ca. 300 elements by counting planktic foraminiferal fragments or partially dissolved tests versus complete tests. These data are expressed in percentages. Fragmented foraminifera include specimens showing missing chambers and

substantial breakage. The taxonomic criteria for identifying planktic foraminifera follow the work by Pearson et al. (2006).

5. Results

5.1. Carbon Isotopes

5.1.1. Possagno

Carbon isotopes of bulk carbonate at Possagno vary between +1.8 and −0.3‰ (Fig. 4, Supplement Table S1). Overall, $\delta^{13}C$ decreases from 1.8‰ at the base of the section to about 0.6‰ at 14 m. Generally, values then increase to 1.5‰ at 24 m and remain between 1.5 and 0.8‰ for the remainder of the studied interval.

Superimposed on these trends are a series of negative CIEs. The most prominent of these (~1.5‰) occurs at the 0 m level, and marks the PETM (Agnini et al., 2009). However, other negative CIEs lie above this marker and within the lowermost 21.4 m, although some are only defined by one data point (Fig. 4, Table S1). The lower two, at ~8 and ~12.5 m, probably represent the H1/ETM2 and J event, respectively, as they lie at the appropriate stratigraphic horizons in relation to polarity chrons. The K/X event may lie at 14.8 m, although this height marks the start of the condensed interval.

The complex interval between 15.5 and 24 m broadly corresponds to all of Chron C23n and the bottom half of Chron C22r. A series of CIEs occur in that interval on the order of 1.4‰, superimposed on a background trend of increasing $\delta^{13}C$ values (about 0.7 ‰). We tentatively label these CIEs with even numbers for internal stratigraphic purposes (Fig. 4), as will become obvious below; their magnitudes range between 0.9 and 0.3‰ (Table S1). However, the samples pacing through this interval varies from 20 to 50 cm. The precise magnitudes and positions certainly could change with higher sample resolution, given the estimated compacted sedimentation rate of ~0.5 cm kyr^{-1} for this part of the section (Agnini et al., 2006).

Above Chron C22r, the Possagno $\delta^{13}C$ record contains additional minor CIEs (Fig. 4). The most prominent of these CIEs, at least relative to baseline values (~1.2 ‰), occurs within Chron C21n. More important to understanding the EECO, a ~0.6‰ CIE nearly coincides with the base of *D. sublodoensis* within the lower part of Chron C22n.
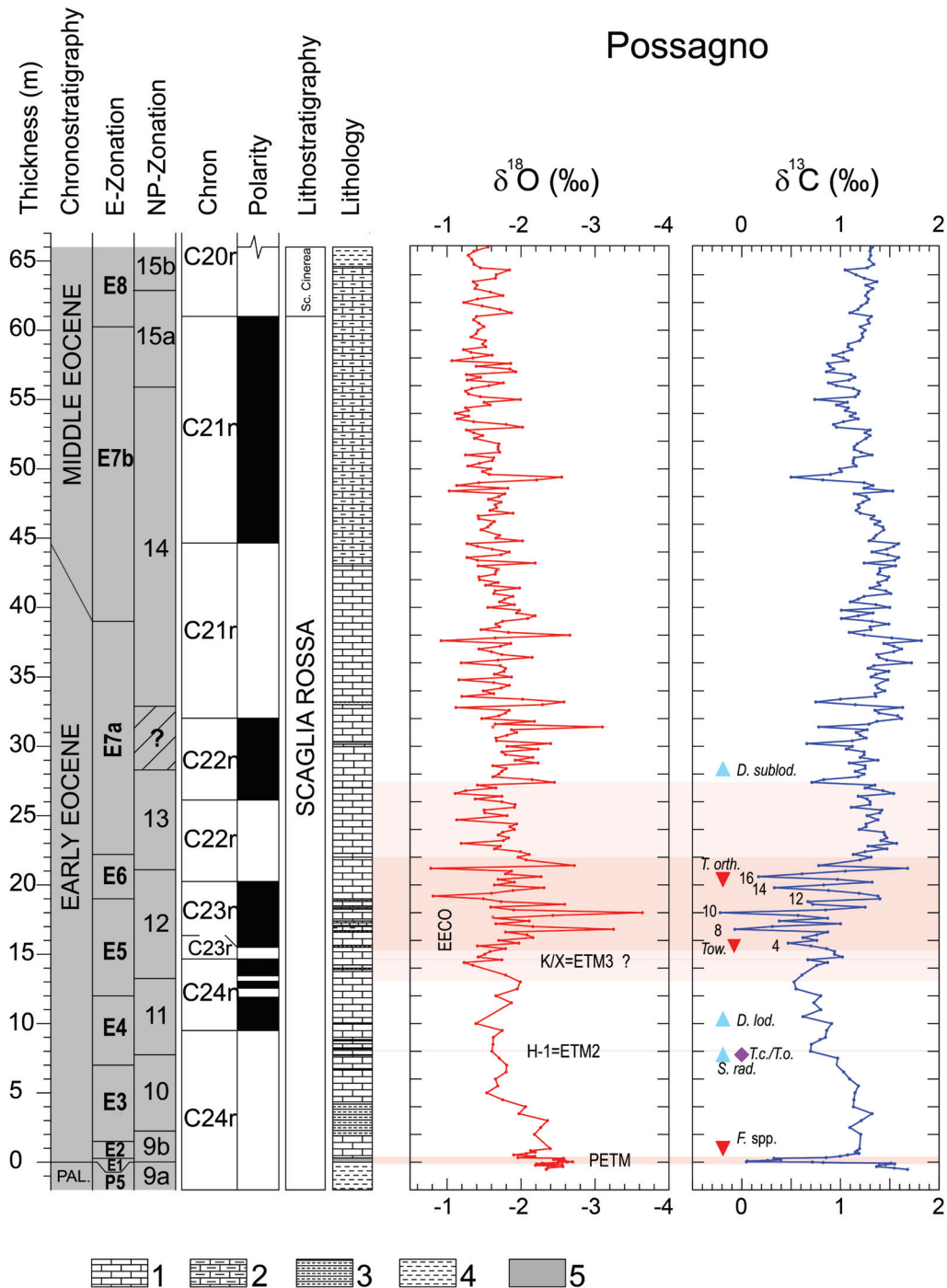
Figure 4. Lithology, stratigraphy and bulk sediment stable-isotope composition of the Possagno section aligned according to depth. Lithololologic key: 1 – limestone; 2 – marly limestone and calcareous marl; 3 – cyclical marl–limestone alternations, 4 – marl; 5 – clay marl unit (CMU). Planktic foraminiferal biozones follow those of Wade et al. (2011), as modified by Luciani and Giusberti (2014). Magnetostratigraphy and key calcareous nannofossil events come from Agnini et al. (2006); NP-zonation is from Martini (1971). Nannofossil events are shown as red triangles (tops), blue triangles (bases) and purple diamonds (evolutionary crossovers); *S. rad.*: *Sphenolithus radians*; *T.c./T.o.*: *Tribrachiatus contortus/Tribrachiatus orthostylus*; *D. lod.*: *Discoaster lodoensis*; *Tow.*: *Toweius*; *T. orth.*: *Tribrachiatus orthostylus*; *D. sublod.*: *Discoaster sublodoensis*. Stable-isotope records determined in this study. Established early Eocene "events" are superimposed in light red; suggested carbon isotope excursions (CIEs) within the EECO are shown with numbers.

5.1.2. DSDP Site 577

The δ^{13}C record of bulk-carbonate at DSDP Site 577 from just below the PETM through Chron C22n ranges between 2.3 and 0.6‰ (Fig. 5; Table S2). Overall, δ^{13}C decreases from 1.4‰ at 84.5 meters composite depth (mcd) to about 0.6‰ at ~76 mcd. Values then generally increase to 2.1‰ at ~68 mcd and remain between 2.3 and 1.6‰ for the rest of the studied interval. Thus, the ranges and general trends in δ^{13}C for the two sections are similar but skewed at DSDP Site 577 relative to Possagno by about +0.6‰.

Like at Possagno, the early Eocene δ^{13}C record at DSDP Site 577 exhibits a series of CIEs (Fig. 5). The portion of this record from the PETM through the K/X event has been documented and discussed elsewhere (Cramer et al., 2003; Dickens and Backman, 2013). The new portion of this record, from above the K/X event through Chron C22n, spans the remainder of the EECO. Within this interval, where background δ^{13}C values rise by ~1.5 ‰, there again occurs a series of minor CIEs with magnitudes between 0.3 and 0.5‰ (Table S2). Here, however, multiple data points define most of the CIEs. We again give these an internal numerical labelling scheme. A ~0.4‰ CIE also nearly coincides with the base of *D. sublodoensis* within the lower part of C22n.

5.2. Oxygen Isotopes

5.2.1. Possagno

Oxygen isotopes of bulk carbonate at Possagno range between –3.3 and 0.8‰, with a mean value of –1.7‰ (Fig. 4, Table S1). In general, considerable scatter exists across the data set with respect to depth, as adjacent samples often display a difference in δ^{18}O that exceeds 0.5 ‰. Nonetheless, some of the more prominent lows in δ^{18}O show a clear correspondence with negative δ^{13}C values (CIEs) and vice versa. This correspondence occurs across the PETM and other known hyperthermals, as well as within and after the EECO. Indeed, the main phase of the EECO corresponds to an interval with the lowest δ^{18}O values.

5.2.2. DSDP Site 577

The δ^{18}O record at Site 577 noticeably deviates from that at Possagno (Fig. 5, Table S2). This is because values range between –1.1‰ and 0.2, with an average value of –0.4 ‰. Thus, relative to Possagno, the record at Site 577 has less scatter and an overall shift of about –3‰.
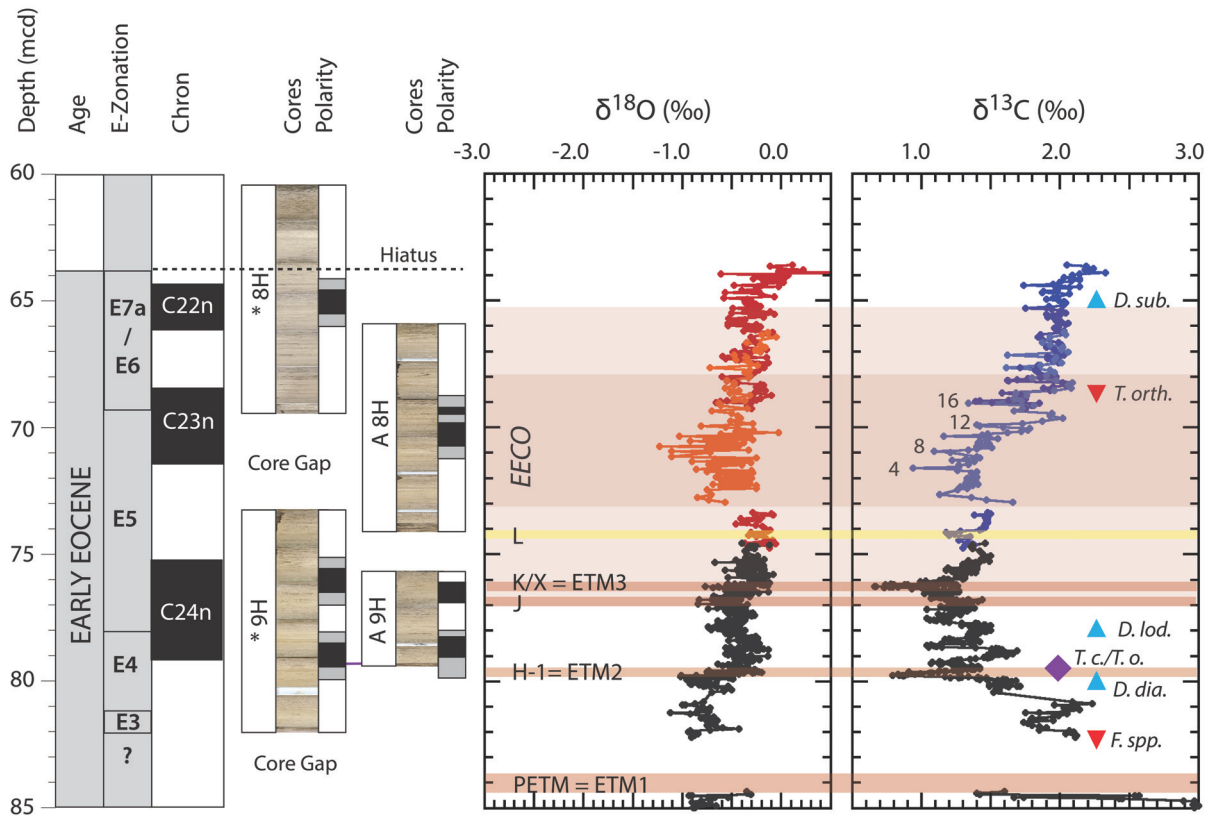
Figure 5. Cores, stratigraphy and bulk sediment stable-isotope composition for the early Eocene interval at Deep Sea Drilling Project (DSDP) Site 577 aligned according to composite depth (Dickens and Backman, 2013). Note the increased length for the gap between Core 577*-8H and Core 577*-9H (see text). The Wade et al. (2011) E-zonation, partly modified by Luciani and Giusberti (2014), has been applied to Site 577, given assemblages presented by Lu (1995) and Lu and Keller (1995). Note that (i) the base of Zone E3 (top of *Morozovella velascoensis*) lies within a core gap; (ii) the E4–E5 zonal boundary (base of *M. aragonensis*) occurs within C24n, in agreement with Luciani and Giusberti (2014); (iii) the E5–E6 zonal boundary is problematic because the top of *M. subbotinae* occurs in the middle of C24n, much earlier than the presumed disappearance in the upper part of C23n (Wade et al., 2011), and we have therefore positioned the E5–E6 boundary at the lowest occurrence of *Acarinina aspensis*, according to the original definition of Zone E5 (Berggren and Pearson, 2005); and (iv) we cannot differentiate between Zone E6 and Zone E7a due to the absence of *Astrorotalia palmerae* and to the diachronous appearance of *A. cuneicamerata* (Luciani and Giusberti, 2014). Magnetostratigraphy and key calcareous nannofossil events are those summarized by Dickens and Backman (2013). These events noted in Fig. 4 are abbreviated as follows here and in the following figures: *F:* spp. – *Fasciculithus* spp.; *D. dia.* – *Discoaster diastypus*. Stable-isotope records: black – Cramer et al. (2003); red and blue – this study. Early Eocene events are the same as those in Fig. 4.

There is again a modest correlation between decreases in $\delta^{18}O$ and negative $\delta^{13}C$ values, as well as a general low in $\delta^{18}O$ across the main phase of the EECO.

5.3. Coarse Fraction

The coarse fraction of samples from Possagno shows two distinct trends (Fig. 6, Table S3). Before the EECO, values are 10.4 % ± 2.67 %. However, from the base of the EECO and up through the section, values decrease to 5.3 % ± 1.3 %.

5.4. Foraminiferal Preservation and Fragmentation

Planktic foraminifera are consistently present and diverse throughout the studied intervals at Possagno and at ODP Site 1051. Preservation of the tests at Possagno varies from moderate to fairly good (Luciani and Giusberti, 2014). However, planktic foraminiferal tests at Possagno are recrystallized and essentially totally filled with calcite. Planktic foraminifera from samples at Site 1051 are readily recognizable throughout the studied interval. Planktic foraminifera from Site 577, at least as illustrated by published plates (Lu and Keller, 1995), show a very good state of preservation (albeit possibly recrystallized).

The F-index record at Possagno (Fig. 6, Table S3) displays large-amplitude variations throughout the investigated interval. The highest values, up to 70 %, were observed between 16 and 22 m. In general, highs in F-index values correspond to lows in the δ^{13}C record.

The F-index record at Site 1051 (Fig. 8, Table S4) shows less variability compared to that at Possagno, although some of this may reflect the difference in the number of samples examined at the two locations. A maximum value of 60% is found in Zone E5, just below an interval of uncertain magnetostratigraphy (Norris et al., 1998) but corresponding to the J event (Cramer et al., 2003). Relatively high F-index values, around 50 %, also occur in several samples below this horizon. The interval across the EECO generally displays low F-index values (<20 %).

5.5. Planktic Foraminiferal Quantitative Analysis

5.5.1. Possagno

Planktic foraminiferal assemblages at Possagno show significant changes across the early to early middle Eocene (Fig. 6, Table S3). Throughout the entire section, the mean relative abundance of *Acarinina* is about 46 % of the total assemblage. However, members of this genus exhibit peak abundances of 60–80 % of the total assemblage across several intervals,
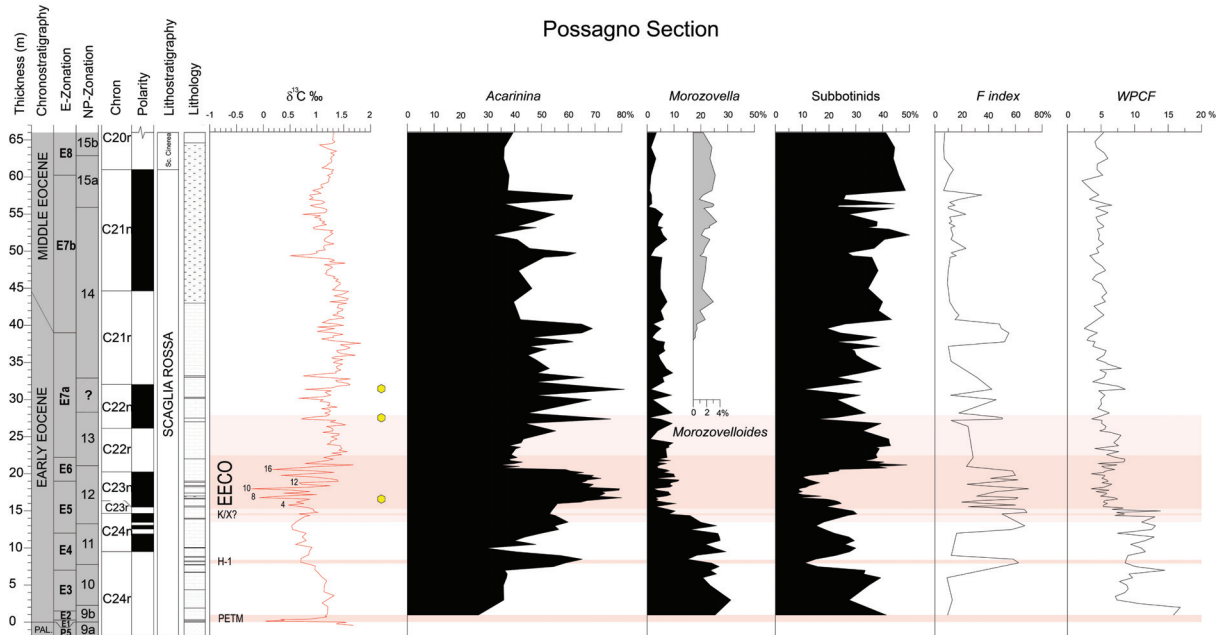
Figure 6. The Possagno section and its δ^{13}C record (Fig. 4) with measured relative abundances of primary planktic foraminiferal genera, fragmentation index (*F-index*) and coarse fraction (*WPCF*). The subbotinid abundance includes both *Subbotina* and *Parasubbotina* genera. Note that a significant increase in *Acarinina* abundance marks the EECO and several carbon isotope excursions (CIEs). Note also the major decline in abundance of *Morozovella* at the start of the EECO. Filled yellow hexagons show occurrences of abundant radiolarians. Lithological symbols and early Eocene events are the same as those in Fig. 4.

often corresponding to CIEs. Particularly prominent is the broad abundance peak of *Acarinina* coincident with the main phase of the EECO.

The increases in *Acarinina* relative abundance typically are counterbalanced by transient decreases in subbotinids (which include both *Subbotina* and *Parasubbotina* genera; Fig. 6). This group also shows a general increase throughout the section. Below the EECO the relative abundances of subbotinids average ~24 %. Above the EECO, this average rises to ~36 %.

The trends in *Acarinina* and subbotinids contrast with that in *Morozovella* (Fig. 6), which exhibits a major and permanent decline within Zone E5. This group collapses from mean abundances ~24 % in the 0–15 m interval to <6 % above 15 m. Qualitative examination of species shows that, in the lower part of Zone E5, where relatively high *Morozovella* abundances are recorded, there is no dominance of any species. *M. marginodentata*, *M. subbotinae* and *M. lensiformis* are each relatively common, and *M. aequa*, *M. aragonensis*, *M. formosa* and *M. crater* are each less common. By contrast, in the upper part of Zone E5, where low abundances of *Morozovella* occur, *M. aragonensis*, *M. formosa*, *M. crater* and *M. caucasica* are the most common species. The general decrease in Morozovella abundances appears unrelated to the disappearance of a single, dominant species.

At Possagno, *Morozovella* never recover to their pre-EECO abundances. This is true even if one includes the morphologically and ecologically comparable genus *Morozovelloides* (Pearson et al., 2006), which first appears in samples above 36 m.

Other planktic foraminiferal genera are always less than 15 % of the total assemblages throughout the studied interval at Possagno (Supplement Fig. S1, Table S3).
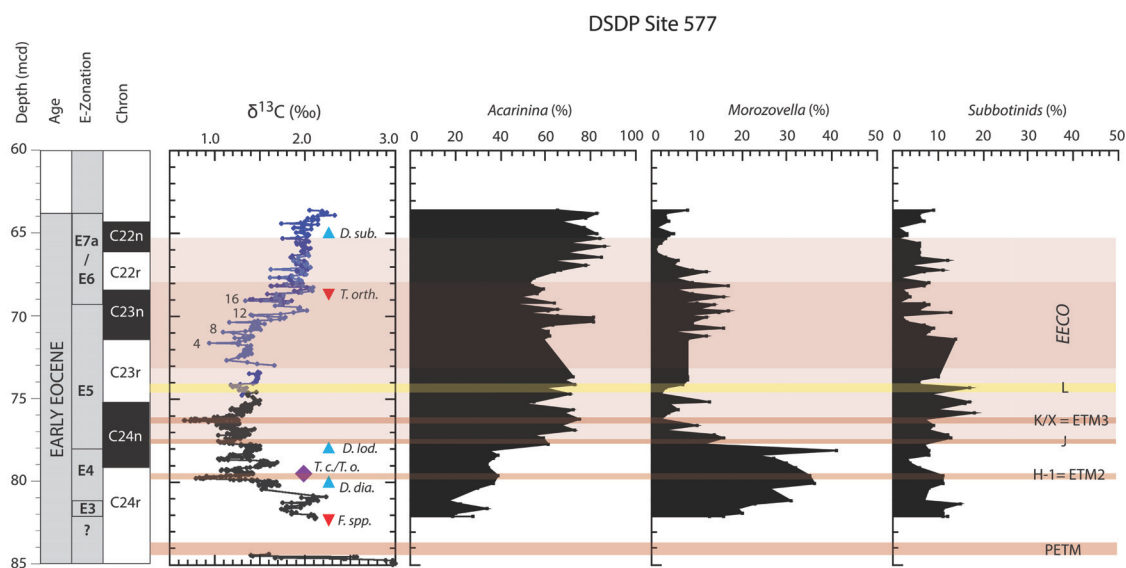
5.5.2. ODP Site 577

Samples from Site 577 were disaggregated in water and washed through a > 63 sieve (Lu, 1995; Lu and Keller, 1995). Lu and Keller determined relative abundances of planktic foraminifera from random splits of about 300 specimens (Lu, 1995; Lu and Keller, 1995). The resulting data are shown in Fig. 7, placed onto the composite depth scale of Dickens and Backman (2013). Major changes in planktic foraminiferal assemblages are comparable to those recorded at Possagno. Indeed, such changes include a distinct decrease in *Morozovella* within Zone E5. The decrease at Site 577 is from mean values of 26.6 to 6.7 % (Table S4). This marked drop occurs at ca. 78 mcd, close to the J event and at the start of the EECO. Like at Possagno, *Morozovella* never recover to their pre-EECO abundances.

The *Morozovella* decrease is counterbalanced by the trend in *Acarinina* abundances that increase from mean values of 30.4 to 64.8 %, corresponding to the level of the *Morozovella* collapse. Subbotinids fluctuate in abundance throughout the interval investigated from 1 to 18 %, with a mean value of ca. 8 %.
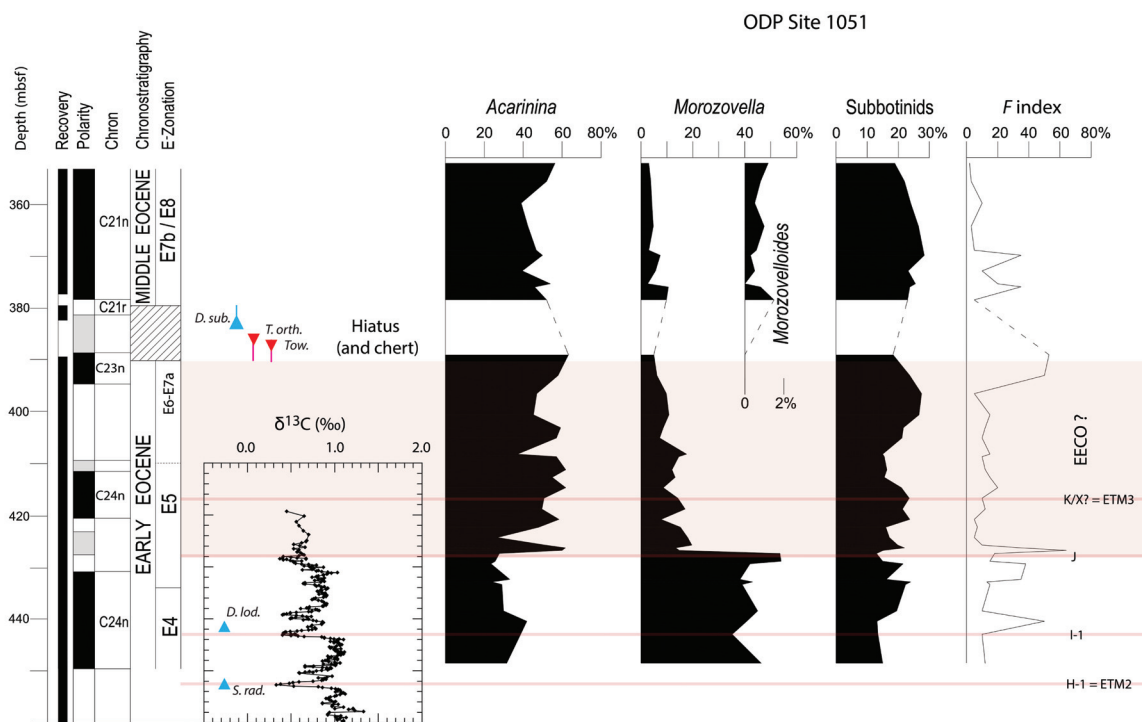
5.5.3. ODP Site 1051

Planktic foraminifera show distinct changes in abundance at Site 1051 (Fig. 8, Table S5). The changes in the main taxa are similar to the variations observed at Possagno. The genus *Acarinina* displays an increase in mean relative abundance from 35 % (base to ca. 450 mbsf) to around 50 % (ca. 430 mbsf), with maximum values of about 60 %. The relatively low esolution used here does not permit comparison to the early Eocene CIEs at Site 1051 (Cramer et al., 2003) or determining how the relative abundance of planktic foraminiferal genera varies with respect to CIEs.

The abundance of subbotinids shows small variations around mean values of 20 % at Site 1051. Like at Possagno, samples from Site 1051 also record a slight increase in abundance toward the end of the EECO and above.

DSDP Site 577

Figure 7. The early Eocene succession at DSDP Site 577 and its δ¹³C record (Fig. 5) with relative abundances of primary planktic foraminiferal genera (Lu, 1995; Lu and Keller, 1995). Note that the major switch in *Morozovella* and *Acarinina* abundances approximately coincides with the J event, the top of polarity Chron C24n and the start of the EECO. Calcareous nannofossil horizons are the same as in previous figures. Early Eocene events are the same as those in Fig. 4.

ODP Site 1051

Figure 8. Stratigraphy, bulk sediment δ¹³C composition, relative abundances of primary planktic foraminiferal genera and fragmentation index (*F-index*) for the early Eocene interval at ODP Site 1051. Planktic foraminiferal biozones follow those of Wade et al. (2011), as modified by Luciani and Giusberti (2014; see Fig. 1 caption). Magnetostratigraphy and positions of key calcareous nannofossil events come from Ogg and Bardot (2001) and Mita (2001), but with an important modification to polarity chron labeling (see text and Cramer et al., 2003). Calcareous nannofossil horizons are the same as in previous figures. Foraminferal information comes from this study; subbotinids include both *Subbotina* and *Parasubbotina*. Early Eocene events are the same as those in Fig. 4.

The major change in planktic foraminiferal assemblages at Site 1051 includes a distinct decrease in *Morozovella*, from mean values around 40 to 10 % in the middle part of Zone E5 (Fig. 7). Similar to Possagno, the lower part of Zone E5 with the higher percentages of *Morozovella* does not record the dominance of selected species, but at Site 1051 *M. aragonensis* and *M. formosa* as well as *M. subbotinae* are relatively common, whereas *M. marginodentata* is less frequent. Within the interval of low *Morozovella* abundances, M. *aragonensis* and *M. formosa* are the most common taxa. The general decline in *Morozovella* does not therefore appear to be related, neither at Possagno nor at Site 1051, to the extinction or local disappearance of a dominant species.

6. Discussion

6.1. Dissolution, Recrystallization and Bulk Carbonate Stable Isotopes

The bulk carbonate stable-isotope records within the lower Paleogene sections at Possagno and at Site 577 need some reflection, considering how such records are produced and modified in much younger strata dominated by pelagic carbonate. In open-ocean environments, carbonate preserved on the seafloor principally consists of calcareous tests of nannoplankton (coccolithophores) and planktic foraminifera (Bramlette and Riedel, 1954; Berger, 1967; Vincent and Berger, 1981). However, the total amount of carbonate and its microfossil composition can vary considerably across locations because of differences in deep-water chemistry and in test properties (e.g., ratio of surface area to volume, mineralogical composition). For regions at mid to low latitudes, a reasonable representation of carbonate components produced in the surface water accumulates on the seafloor at modest (< 2000 m) water depth. By contrast, microfossil assemblages become heavily modified in deeper water because of increasingly significant carbonate dissolution (Berger, 1967).Such dissolution preferentially affects certain tests, such as thin-walled, highly porous planktic foraminifera (Berger,1970; Bé et al., 1975; Thunell and Honjo, 1981).

The stable-isotope composition of modern bulk carbonate ooze reflects the mixture of its carbonate components, which mostly record water temperature and the composition of dissolved inorganic carbon (DIC) within the mixed layer (< 100m water depth). The stable-isotope records are imperfect, though, because of varying proportions of carbonate constituents and "vital effects", which impact stable-isotope fractionation for each component (Anderson and Cole, 1975; Reghellin et al., 2015). Nonetheless, the stable-isotope

composition of bulk carbonate ooze on the seafloor can be related to overlying temperature and chemistry of surface water (Anderson and Cole, 1975; Reghellin et al., 2015).

Major modification of carbonate ooze occurs during sediment burial. This is because, with compaction and increasing pressure, carbonate tests begin to dissolve and recrystallize (Schlanger and Douglas, 1974; Borre and Fabricus, 1998). Typically within several hundred meters of the seafloor, carbonate ooze becomes chalk and, with further burial, limestone (Schlanger and Douglas, 1974; Kroenke et al., 1991; Borre and Fabricus, 1998). Carbonate recrystallization appears to be a local and nearly closed-system process, such that mass transfer occurs over short distances (i.e., less than a few meters) (Schlanger and Douglas, 1974; Matter et al.,1975; Arthur et al., 1984; Kroenke et al., 1991; Borre and Fabricus, 1998; Frank et al., 1999).

In pelagic sequences with appreciable carbonate content and low organic carbon content, bulk carbonate $\delta^{13}C$ records typically give information of paleoceanographic significance (Scholle and Arthur, 1980; Frank et al., 1999). Even when transformed to indurated limestone, the $\delta^{13}C$ value for a given sample should be similar to that originally deposited on the seafloor. This is because, for such sediments, almost all carbon in small volumes exists as carbonate. Bulk carbonate $\delta^{18}O$ records are a different matter, especially in indurated marly-limestones and limestones (Marshall, 1992; Schrag et al., 1995; Frank et al., 1999). This is because pore water dominates the total amount of oxygen within an initial parcel of sediment, and oxygen isotope fractionation depends strongly on temperature. Thus, during dissolution and recrystallization of carbonate, a significant exchange of oxygen isotopes occurs. At first, carbonate begins to preferentially acquire ^{18}O because shallowly buried sediment generally has lower temperatures than surface water. However, with increasing burial depth along a geothermal gradient, carbonate begins to preferentially acquire ^{16}O (Schrag et al., 1995; Frank etal., 1999).

6.2. Carbon Isotope Stratigraphy through the EECO

Stratigraphic issues complicate direct comparison of various records from Possagno and Site 577. The two sections have somewhat similar multi-million-year sedimentation rates across the early Eocene. However, the section at Possagno contains the condensed interval, where much of C23r spans a very short distance (Agnini et al., 2006), and the section at Site 577 has a series of core gaps and core overlaps (Dickens and Backman, 2013).

An immediate issue to amend is the alignment of cores 8H and 9H in Hole 577* and Core 8H in Hole 577A (Fig. 5). On the basis of Gamma Ray Porosity Evaluator (GRAPE) density

records for these cores, Dickens and Backman (2013) initially suggested a 2.6 m core gap between cores 8H* and 9H*. However, a 3.5 m core gap also conforms to all available stratigraphic information. The newly generated δ^{13}C (and δ^{18}O) records across these three cores show the latter to be correct.

Once sedimentation rate differences at Possagno are recognized and coring problems at Site 577 are rectified, early Eocene δ^{13}C records at both locations display similar trends and deviations in relation to polarity chrons and key microfossil events (Figs. 4, 5). Moreover, the δ^{13}C variations seemingly can be correlated in time to those found in bulk carbonate δ^{13}C records at other locations, including Site 1051(Fig. 8) and Site 1258 (Fig. 9). As noted previously, such correlation occurs because the bulk carbonate δ^{13}C signals reflect past global changes in the composition of surface water DIC, even after carbonate recrystallization.

For the latest Paleocene and earliest Eocene, nominally the time spanning the period from the base of C24r through the middle of C24n, detailed stable carbon isotope records have been generated at more than a dozen locations across the globe (Cramer et al., 2003; Agnini et al., 2009, 2016; Galeotti et al., 2010; Zachos et al., 2010; Slotnick et al., 2012; Littleret al., 2014). These records can be described consistently as a long-term drop in δ^{13}C superimposed with a specific sequence of prominent CIEs that include those corresponding to the PETM, H1 and J events. In continuous sections with good magnetostratigraphy and biostratigraphy, there is no ambiguity in the assignment of CIEs (Zachos et al., 2010; Littler et al., 2014; Slotnick et al., 2012, 2105a; Lauretano et al., 2015). This "13C template" can be found at the Possagno section and at Site 577 (Fig. 9); it is found at Site 1051 for the depth interval where carbon isotopes have been determined (Fig. 8).

For the period after the J event and across the EECO, very few detailed δ^{13}C records have been published (Slotnick et al., 2012, 2015a; Kirtland-Turner et al., 2014). Moreover, the available records are not entirely consistent. For example, the K/X event in Clarence River valley sections manifests as a prominent CIE within a series of smaller δ^{13}C excursions (Slotnick et al., 2012, 2015a), whereas the event has limited expression in the δ^{13}C record at Site 1258 (Kirtland-Turner et al., 2014; Fig. 9).

The new records from Possagno and Site 577 emphasize an important finding regarding bulk carbonate δ^{13}C records across the EECO. Between the middle of C24n and the upper part of C23r, there appears to be a sequence of low amplitude, low-frequency CIEs (note that this portion of the record is missing at Possagno because of the condensed interval; Fig. 9.).
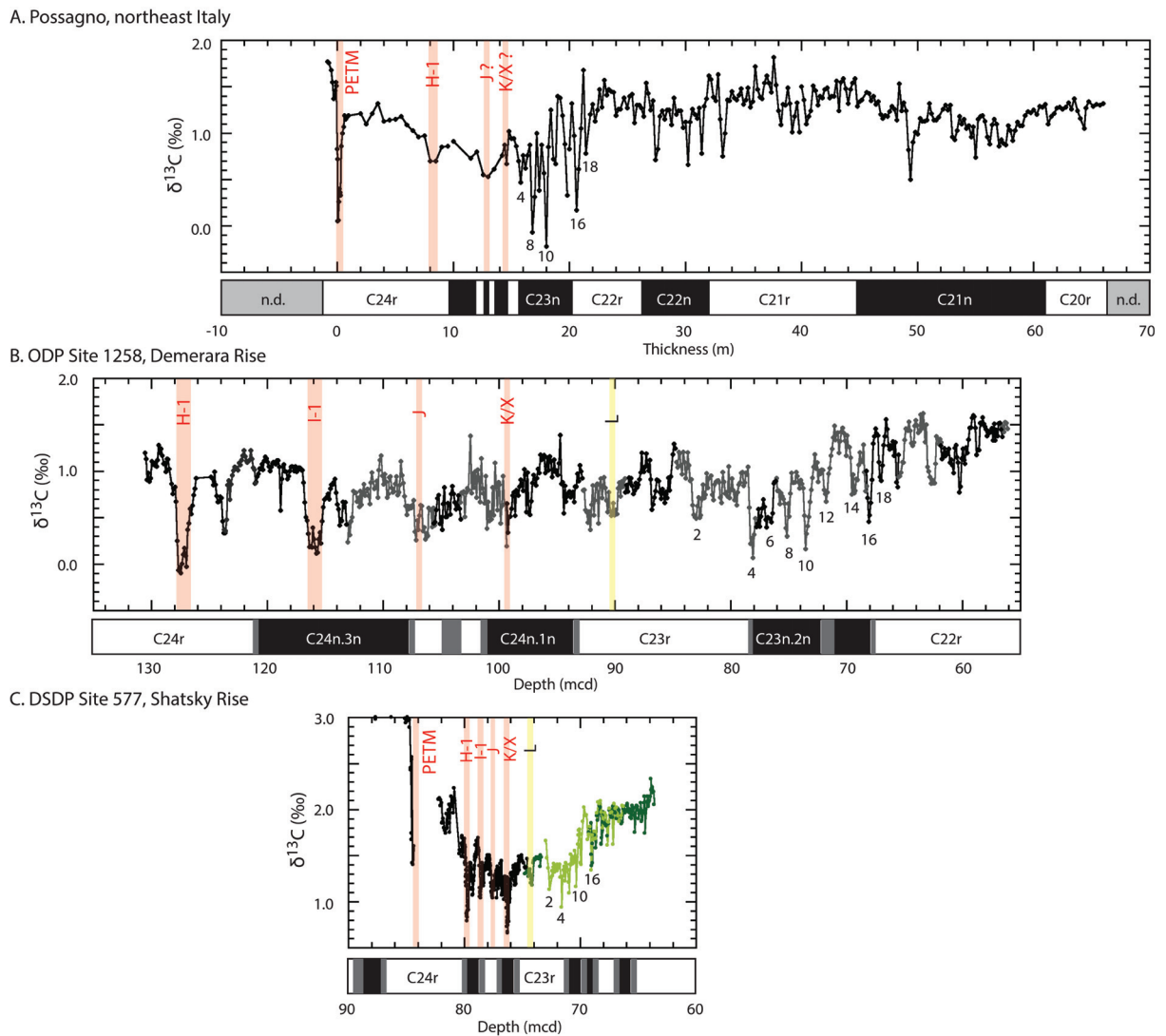
Figure 9. Carbon isotope and paleomagnetic records across the early Eocene for the Possagno section, DSDP Site 577 and ODP Site 1258 (Kirtland-Turner et al., 2014). This highlights the overall framework of carbon cycling in the early Eocene but also stratigraphic problems across the EECO at each of the three sites. At Possagno, the coarse resolution of $\delta^{13}C$ records and the condensed interval make correlations difficult. At ODP Site 1258 the prominent K/X event seems missing. At DSDP Site 577, the entire record is compressed in the depth domain. Nonetheless, a major shift in frequency and amplitude of carbon isotope excursions (CIEs) appears to have happened during the EECO. CIEs that may correlate within the EECO are shown with numbers.

However, near the C23r–C23n boundary, a long-term rise in $\delta^{13}C$ begins but with a series of relatively high-amplitude, high-frequency CIEs (Kirtland-Turner et al., 2014; Slotnick et al., 2014). The number, relative magnitude and precise timing of CIEs within this interval remain uncertain. For example, the CIE labeled "4" appears to occur near the top of C23r at Site 577 but near the bottom of C23n.2n at Site 1258 and at Possagno. Additional $\delta^{13}C$ records across this interval are needed to resolve the correct sequence of CIEs and to derive an internally consistent labelling scheme for these perturbations. It is also not clear which of these CIEs

during the main phase of the EECO specifically relate to significant increases in temperature, as is clear for the "hyperthermals" in the earliest Eocene. Nonetheless, numerous CIEs, as well as an apparent change in the mode of these events, characterize the EECO (Kirtland-Turner et al., 2014; Slotnick et al., 2014).

The causes of $\delta^{13}C$ changes during the early Paleogene lie at the heart of considerable research and debate (Dickens et al., 1995, 1997; Zeebe et al., 2009; Dickens, 2011; Lunt et al., 2011; Sexton et al., 2011; DeConto et al., 2012; Lee et al., 2013; Kirtland-Turner et al., 2014). Much of the discussion has revolved around three questions. (1) What are the sources of ^{13}C-depleted carbon that led to prominent CIEs, especially during the PETM? (2) Does the relative importance of different carbon sources vary throughout this time interval? (3) Are the geologically brief CIEs related to the longer secular changes in $\delta^{13}C$? One may see in several papers, a convergence of thought on how carbon cycled across Earth's surface during the early Paleogene, at least between the late Paleocene and the K/X event (Cramer et al., 2003; Lourens et al., 2005; Galeotti et al., 2010; Hyland et al., 2013; Zachos et al., 2010; Lunt et al., 2011; Littler et al., 2014; Lauretano et al., 2015; Westerhold et al., 2015). Changes in, tectonism, volcanism and weathering drove long-term changes in atmospheric pCO$_2$ (Vogt, 1979; Raymo and Ruddiman, 1992; Sinton and Duncan, 1998;Demicco, 2004; Zachos et al., 2008), which was generally high throughout the early Paleogene but further increased toward the EECO (Pearson and Palmer, 2000; Fletcher et al.,2008; Lowenstein and Demicco, 2006; Smith et al., 2010; Hyland and Sheldon, 2013). However, as evident from the large range in $\delta^{13}C$ across early Paleogene stable-isotope records, major changes in the storage and release of organic carbon must have additionally contributed to variability in atmospheric pCO$_2$ and ocean DIC concentrations (Shackleton, 1986; Kurtz et al., 2003; Komar et al., 2013). When long-term increases in pCO$_2$, perhaps in conjunction with orbital forcing, pushed temperatures across some threshold, such as the limit of sea-ice formation (Lunt et al., 2011), rapid inputs of ^{13}C-depleted organic carbon from the shallow geosphere served as a positive feedback to abrupt warming (Dickens et al., 1995; Bowen et al., 2006; DeConto et al., 2012).

Our new $\delta^{13}C$ records do not directly address the above questions and narrative concerning early Paleogene carbon cycling. However, they do highlight two general and related problems when such a discussion includes the EECO. First, surface temperatures appear to stay high across an extended time interval when the $\delta^{13}C$ of benthic foraminifer (Fig. 1) and bulk carbonate (Fig. 9) increase. Second, numerous brief CIEs mark this global long-term rise in $\delta^{13}C$. Whether the aforementioned views need modification or reconsideration (Kirtland-Turner et al., 2014) is an issue as yet unresolved and one that

depends on how long-term and short-term δ^{13}C changes relate across the entire early Paleogene.

The overall offset between bulk carbonate δ^{13}C values at Possagno and Site 577 may hint at an important constraint to any model of early Paleogene carbon cycling. Throughout the early Eocene, δ^{13}C values at Site 577 exceed those at Possagno by nominally 0.8‰ (Fig. 9). This probably does reflect recrystallization or lithification because similar offsets appear across numerous records independent of post depositional history but dependent on location (Schmitz et al., 1996; Cramer et al., 2003; Slotnick et al., 2012, 2015a; Agnini et al., 2016). In general, absolute values of bulk carbonate δ^{13}C records increase from the North Atlantic and western Tethys (low), through the South Atlantic and eastern Tethys and the Indian Ocean, to the Pacific (high), although, significantly, with a latitudinal component to this signature.

6.3. Stable Oxygen Isotope Stratigraphy across the EECO

Bulk carbonate δ^{18}O values for Holocene sediment across the eastern equatorial Pacific relate to average temperatures in the mixed layer (Shackleton and Hall, 1995; Reghellin etal., 2015). Indeed, values are close to those predicted from water chemistry (δ^{18}O$_w$) and equilibrium calculations for calcite precipitation (e.g., Bemis et al., 1998) if vital effects in the dominant nannoplankton increase δ^{18}O by nominally 1 ‰ (Reghellin et al., 2015).

Site 577 was located at about 30°N latitude in the eastern Pacific during the early Paleogene. Given that sediment of this age remains "nannofossil ooze" (Shipboard Scientific Party, 1985), one might predict past mixed layer temperatures from the δ^{18}O values with three assumptions: early Paleogene δ^{18}O was 1.2 ‰ less than that in the present day to account for an ice-free world; local δ^{18}O$_w$ was equal to average seawater, similar to modern chemistry at this off-Equator location (LeGrande and Schmidt, 2006); and, Paleogene nannoplankton also fractionated δ^{18}O by 1.0 ‰. With commonly used equations that relate the δ^{18}O of calcite to temperature (Bemis et al., 1998), these numbers render temperatures of between 16 and 21°C for the data at Site 577. Such temperatures seem too cold by at least 10°C, given other proxy data and modelling studies (e.g., Pearson et al., 2007; Huber and Caballero, 2011; Hollis et al., 2012; Pross et al., 2012; Inglis et al., 2015). At low latitudes, bottom waters are always much colder than surface waters. Even during the EECO, deep waters probably did not exceed 12°C (Zachos et al., 2008). The calculated temperatures likely indicate partial recrystallization of bulk carbonate near the sea-floor. Examinations of calcareous nannofossils in Paleogene sediment at Site 577 show extensive calcite overgrowths (Shipboard Scientific Party, 1985; Backman, 1986). Relatively low δ^{18}O values mark the H1 and K/X events, as

well as the main phase of the EECO (Fig. 5). Both observations support the idea that the bulk carbonate $\delta^{18}O$ at Site 577 represents the combination of a primary surface water $\delta^{18}O$ signal and a secondary shallow pore water $\delta^{18}O$ signal.

Lithification should further impact bulk carbonate $\delta^{18}O$ records (Marshall, 1992; Schrag et al., 1995; Frank et al., 1999). Because this process occurs well below the seafloor, where temperatures approach or exceed those of surface water, the $\delta^{18}O$ values of pelagic marls and limestones should be significantly depleted in ^{18}O relative to partially recrystallized nannofossil ooze. This explains the nominal 2‰ offset in average $\delta^{18}O$ between correlative strata at Possagno and at Site 577. While temperature calculations using the $\delta^{18}O$ record at Possagno render reasonable surface water values for a mid-latitude location in the early Paleogene (26–31°C, using the aforementioned approach), any interpretation of these terms more than likely reflects happenstance. The fact that planktic foraminifera are completely recrystallized and totally filled with calcite at Possagno supports this inference.

One might suggest, at least for the Possagno section, that meteoric water might also have impacted the happenstance record. This is because rainwater generally has a $\delta^{18}O$ composition less than that of seawater. However, samples were collected from fresh quarry cuts at Possagno in 2002–2003.

As observed at Site 577, however, horizons of lower $\delta^{18}O$ at Possagno may represent times of relative warmth in surface water. This includes the broad interval between 16 and 22.5 m, which marks the main phase of the EECO, as well as many of the brief CIEs, at least one that clearly represents the PETM (Fig. 4). That is, despite obvious overprinting of the original $\delta^{18}O$ signal, early to early middle Eocene climate variations appear manifest in the data.

6.4. The EECO and Planktic Foraminiferal Abundances

Bulk carbonate $\delta^{13}C$ records, especially in conjunction with other stratigraphic markers, provide a powerful means to correlate early Paleogene sequences from widely separated locations (Fig. 9). They also allow for the placement of planktic foraminiferal assemblage changes into a broader context.

The most striking change in planktic foraminiferal assemblages occurred near the start of the EECO. Over a fairly short time interval and at multiple widespread locations, the relative abundance of *Acarinina* increased significantly, whereas the relative abundance of
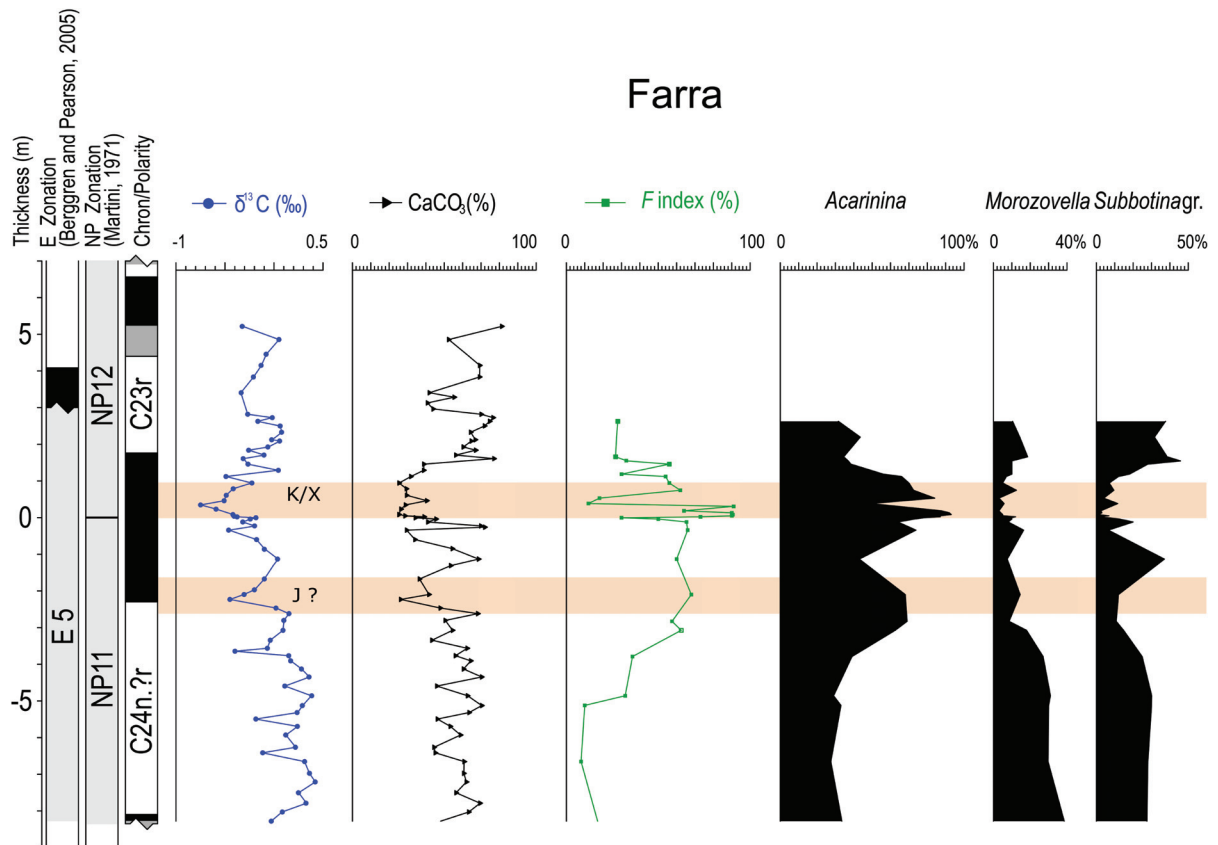
Figure 10. Records of magnetostratigraphy, bulk sediment δ¹³C, CaCO₃ content, *F-index* and abundance patterns for primary planktic foraminiferal taxa at the Farra section, which crops out 50 km NE of Possagno. All data are from Agnini et al. (2009). Note that the switch in abundance between *Morozovella* and *Acarinina* occurs close to the J event.

Morozovella decreased significantly. This switch, best defined by the decline in *Morozovella*, happened just before the condensed interval at Possagno (Fig. 6), just above the J event at Site 577 (Fig. 7,Table S4) and during the J event at Site 1051 (Fig. 8). At the Farra section, cropping out in the same geological setting of Possagno at 50 km NE of the Carcoselle quarry, it also appears to have occurred close to the J event (Fig. 10). Indeed, the maximum turnover in relative abundances may have been coincident with the J event at all locations. Importantly, the relative abundance of subbotinids only changed marginally during this time.

The *Morozovella* decline across the start of the EECO did not rebound afterward. At Possagno, at Site 1051 and at Site577, it was coupled with the gradual disappearances of several species, including *M. aequa*, *M. gracilis*, *M. lensiformis*, *M. marginodentata* and *M. subbotinae*. Furthermore, the loss of *Morozovella* was not counterbalanced by the appearance of the *Morozovelloides* genus, which shared the same ecological preferences with *Morozovella*. This latter genus appeared in C21r, near the Ypresian–Lutetian boundary, and well after the EECO (Pearson et al., 2006; Aze et al., 2011), including at Possagno (Luciani

and Giusberti, 2014; Fig. 6). Though *Morozovelloides* were morphologically similar to *Morozovella*, they probably evolved from *Acarinina* (Pearson et al., 2006; Aze et al., 2011; Fig. 1).

At Possagno, higher abundances of *Acarinina* also correlate with pronounced negative $\delta^{13}C$ perturbations before and after the EECO (Fig. 6). This includes the H1 event, as well as several unlabelled CIEs during C22n, C21r and C21n. Such increases in the relative abundances of *Acarinina* have been described for the PETM interval at the nearby Forada section (Luciani et al., 2007) and for the K/X event at the proximal Farra section (Agnini et al., 2009). Unlike for the main switch near the J event, however, these changes are transient, so that relative abundances in planktic foraminiferal genera are similar before and after the short-term CIEs.

6.5. The Impact of Dissolution

Carbonate dissolution at or near the seafloor presents a potential explanation for observed changes in foraminiferal assemblages. Some studies of latest Paleocene to initial Eocene age sediments, including laboratory experiments, suggest a general ordering of dissolution according to genus, with *Acarinina* more resistant than *Morozovella* and the latter more resistant than subbotinids (Petrizzo et al., 2008; Nguyen et al., 2009, 2011).

Carbonate solubility horizons that impact calcite preservation and dissolution on the seafloor (i.e., the carbonate compensation depth (CCD) and lysocline) also shoaled considerably during various intervals of the early Eocene. The three most prominent hyperthermals that occurred before the main phase of the EECO (PETM, H1, K/X) were clearly marked by pronounced carbonate dissolution at multiple locations (Zachos et al., 2005; Agnini et al., 2009; Stap et al.,2009; Leon-Rodriguez and Dickens, 2010). A multi-million year interval characterized by a relatively shallow CCD also follows the K/X event (Leon-Rodriguez and Dickens, 2010; Pälike et al., 2012; Slotnick et al., 2015b).

Should changes in carbonate preservation primarily drive the observed planktic foraminiferal assemblages, it follows that the dominance of *Acarinina* during the EECO and multiple CIEs could represent a taphonomic artifact. Limited support for this idea comes from our records of fragmentation (F-index). In general, intervals with relatively high abundances of *Acarinina* (and low $\delta^{13}C$) correspond to intervals of fairly high fragmentation at Possagno and at Site 1051 (Figs. 6, 8). This may suggest carbonate dissolution because this process breaks planktic foraminifera into fragments (Berger, 1967; Hancock and Dickens, 2005).

Carbonate dissolution can cause the coarse fraction of bulk sediment to decrease (Berger et al., 1982; Broecker et al., 1999; Hancock and Dickens, 2005). This happens because whole planktic foraminiferal tests typically exceed 63 μm, whereas the resulting fragments often do not exceed 63 μm. The decrease in *WPCF* values at the start of the EECO at Possagno (Fig. 6) may therefore further indicate loss of foraminiferal tests. However, relatively low *WPCF* values continue to the top of the section, independent of changes in the *F-index*. The *WPCF* record parallels the trend in *Morozovella* abundance and thus might also suggest a loss of larger *Morozovella* rather than carbonate dissolution.

The cause of the long-term rise in carbonate dissolution horizons remains perplexing but may relate to increased inputs of ^{13}C-depleted carbon into the ocean and atmosphere (Leon-Rodriguez and Dickens, 2010; Komar et al., 2013). Should the *Morozovella* decline and amplified *F-index* at the Possagno section mostly represent dissolution, it would imply considerable shoaling of these horizons in the western Tethys, given the inferred deposition in middle to lower bathyal setting. As with open-ocean sites (Slotnick et al., 2015b), further studies on the Eocene lysocline and CCD are needed from Tethyan locations. One idea is that remineralization of organic matter intensified within the water column, driven by augmented microbial metabolic rates at elevated temperatures during the EECO; this may have decreased pH at intermediate water column depths (Brown et al., 2004; Olivarez Lyle and Lyle, 2006; O'Connor et al., 2009; John et al., 2013, 2014).

Despite evidence of carbonate dissolution, this process probably only amplified primary changes in planktic foraminiferal assemblages. The most critical observation is the similarity of the abundance records for major planktic foraminiferal genera throughout the early Eocene at multiple locations (Figs. 6–8). This includes the section at Site1051, where carbonate appears only marginally modified by dissolution according to the *F-index* values (Fig. 7). Subbotinid abundance also remains fairly high throughout the early Eocene. One explanation is that, in contrast to the results from laboratory experiments (Nguyen et al., 2009, 2011), subbotinids are more resistant to dissolution than *Morozovella* (Boersma and Premoli Silva, 1983; Berggren and Norris, 1997), at least once the EECO has transpired. In the proximal middle–upper Eocene section at Alano, Luciani et al. (2010) documented a dominance of subbotinids within intervals of high fragmentation (*F-index*) and enhanced carbonate dissolution. The degree of dissolution across planktic foraminiferal assemblages may have varied through the early Paleogene, as distinct species within each genus may respond differently (Nguyen et al., 2011). So far, data on dissolution susceptibility for different species and genera are limited for early and early middle Eocene times (Petrizzo et al., 2008).

There is also recent work from the Terche section (ca. 28 km NE of Possagno) to consider. This section is located in the same geological setting as Possagno, but across the H1, H2 and I1 events, there are very low F-index values and marked increases in *Acarinina* coupled with significant decreases in subbotinids (D'Onofrio et al., 2014). Therefore, although the Possagno record may be partially altered by dissolution, an increase in warm water *Acarinina* concomitant with a decrease in subbotinids seems to be a robust finding during early Paleogene warming events in Tethyan settings.

6.6. A Record of Mixed Water Change

The switch in abundance between *Morozovella* and *Acarinina* at the start of the EECO supports a hypothesis whereby environmental change resulted in a geographically widespread overturn of planktic foraminiferal genera. During the PETM and K/X events, *Acarinina* became dominant over *Morozovella* in a number of Tethyan successions. This has been interpreted as signifying enhanced eutrophication of surface waters near continental margins (Arenillas et al., 1999; Molina et al., 1999; Ernst et al., 2006; Guasti and Speijer, 2007; Luciani et al., 2007; Agnini et al., 2009), an idea consistent with evidence for elevated (albeit more seasonal) riverine discharge during these hyperthermals (Schmitz and Pujalte, 2007; Giusberti et al., 2007; Schulte et al., 2011; Slotnick et al., 2012; Pujalte et al., 2015). Increased nutrient availability may also have occurred at Possagno during the early part of the EECO, given the relatively high concentration of radiolarians, which may reflect eutrophication (Hallock, 1987).

However, the fact that the major switch at the start of the EECO can be found at Sites 1051 (western Atlantic) and Site 577 (central Pacific) suggests that local variations in oceanographic conditions, such as riverine discharge, were not the primary causal mechanism. Rather, the switch must be a consequence of globally significant modifications related to the EECO, most likely sustained high temperatures, elevated pCO_2 or both. Given model predictions for our Earth in the coming millennia (IPCC, 2014), indirect effects could also have contributed, especially including increased ocean stratification and decreased pH.

An explanation for the shift may lie in habitat differences across planktic foraminiferal genera. Although both *Morozovella* and *Acarinina* likely had photosymbionts, *Morozovella* may have occupied a shallower surface habitat than the latter genus as indicated by minor variations in their stable-isotope compositions (Boersma et al., 1987; Pearson et al., 1993, 2001).

One important consideration for any interpretation is the evolution of new species that progressively appear during the post-EECO interval. In good agreement with studies of lower Paleogene sediment from other low-latitude locations (Pearson et al., 2006), thermocline dwellers such as subbotinids and parasubbotinids seem to proliferate at Possagno (Luciani and Giusberti, 2014). These include *Subbotina corpulenta*, *S. eocaena*, *S. hagni*, *S. senni*, *S. yeguanesis*, *Parasubbotina griffinae* and *P. pseudowilsoni*. The appearance of the radially chambered *Parasubbotina eoclava*, considered to be the precursor of the truly clavate chambered *Clavigerinella* (Coxall et al., 2003; Pearson and Coxall, 2014), also occurs at 19.8 m and in the core of the EECO (Luciani and Giusberti, 2014). Clavigerinella is the ancestor of the genus *Hantkenina*, which successfully inhabited the subsurface and surface waters during the middle through late Eocene (Coxall et al., 2000).

A second consideration is the change in planktic foraminiferal assemblages during the Middle Eocene Climate Optimum (MECO), another interval of anomalous and prolonged warmth at ca. 40 Ma (Bohaty et al., 2009). At Alano (Fig. 11) and other locations (Luciani et al., 2010; Edgar et al., 2012), the MECO involved the reduction in the abundance and test size of large *Acarinina* and *Morozovelloides*. This has been attributed to "bleaching", i.e., the loss of photosymbionts, resulting from global warming (Edgar et al., 2012), although related factors, such as a decrease in pH, a decrease in nutrient availability or changes in salinity, may have been involved (Douglas, 2003; Wade et al., 2008). The symbiotic relationship with algae is considered an important strategy adopted by muricate planktic foraminifera during the early Paleogene (Norris, 1996; Quillévéré et al., 2001). Considering the importance of this relationship in extant species (Bé, 1982; Bé et al., 1982; Hemleben et al., 1989), the loss of photosymbionts may represent a crucial mechanism to explain the relatively rapid decline in foraminifera utilizing this strategy, including *Morozovella* at the start of the EECO.

Available data suggest that the protracted conditions of extreme warmth and high pCO$_2$ during the EECO were the key elements inducing a permanent impact on planktic foraminiferal evolution and the decline in *Morozovella*. Even the PETM, the most pronounced hyperthermal, did not adversely affect the genus *Morozovella* permanently. While excursion taxa appeared, *Morozovella* seem to have increased in abundance in open-ocean settings (Kelly et al., 1996, 1998, 2002; Lu and Keller, 1995; Petrizzo, 2007); only in some continental margin settings did a transient decrease in abundance occur (Luciani et al., 2007).
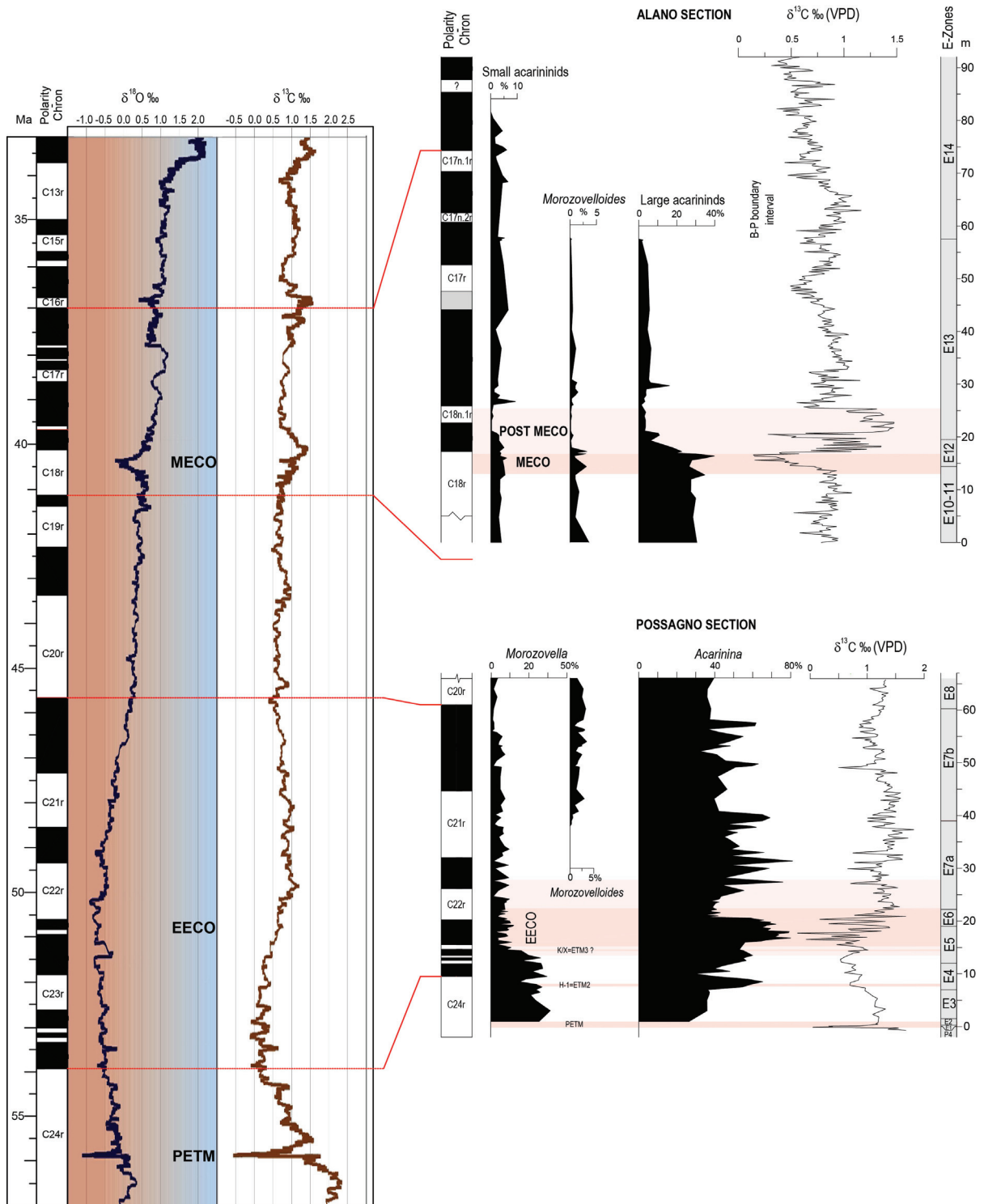
Figure 11. Records of *Morozovella* and large *Acarinina* (> 200 μm) in the western Tethyan setting from the Possagno section (this paper) and the Alano section (Luciani et al., 2010), plotted with generalized δ¹³C and δ¹⁸O curves for benthic foraminiferal on the GTS2012 (as summarized by Vandenberghe et al. (2012); slightly modified). These records suggest that the long-lasting EECO and MECO intervals of anomalous warmth mark two main steps in the decline in *Morozovella*, *Morozovelloides* and *Acarinina*. The planktic foraminiferal biozones follow those presented by Wade et al. (2011), as partly modified by Luciani and Giusberti (2014).